IDŐJÁRÁS

QUARTERLY JOURNAL
OF THE HUNGARIAN METEOROLOGICAL SERVICE

CONTENTS

VOL. 124 * NO. 4 * OCTOBER – DECEMBER 2020

IDŐJÁRÁS

Quarterly Journal of the Hungarian Meteorological Service

Editorial Office: Kitaibel P.u. 1, H-1024 Budapest, Hungary
P.O. Box 38, H-1525 Budapest, Hungary
E-mail: journal.idojaras@met.hu
Fax: (36-1) 346-4669

Indexed and abstracted in Science Citation Index Expanded™ and Journal Citation Reports/Science Edition
Covered in the abstract and citation database SCOPUS®
Included in EBSCO's databases

Subscription by mail:
IDŐJÁRÁS, P.O. Box 38, H-1525 Budapest, Hungary
E-mail: journal.idojaras@met.hu

DOI:10.28974/idojaras.2020.4.1

IDŐJÁRÁS

Quarterly Journal of the Hungarian Meteorological Service
Vol. 124, No. 4, October – December, 2020, pp. 427–445

Projected temperature changes in Kolašin (Montenegro) up to 2100 according to EBU-POM and ALADIN regional climate models

Dragan Burić * and **Miroslav Doderović**

Department of Geography
Faculty of Philosophy, Niksic
University of Montenegro
Cetinjski put 2, 81000 Podgorica, Montenegro

**Corresponding author E-mail: buric.d@ucg.ac.me (dragan.buric@meteo.co.me)*

(Manuscript received in final form January 30, 2020)

Abstract— This paper deals with the temperature projections of two regonal climate models, actually three scenarios by 2100: the A2 scenario of the EBU-POM model and the RCP4.5 and RCP8.5 scenarios, the latest projections of the ALADIN model. Kolašin was chosen, because the altitude of the place is the average height of the northern region of Montenegro (about 1000 m). A total of 22 temperature parameters for the period 2011–2100 were analyzed. The upward trend of projected seasonal and annual (TY, TYx, and TYn) mean, mean maximum, and mean minimum temperatures by 2100 is very significant. According to the RCP4.5 and RCP8.5 scenarios, in 2011-2100, the trend of projected mean winter (TW) temperatures will be from 0.2 to 0.37 °C per decade, and the trend of projected mean summer (TSu) temperatures will be from 0.24 to 0.54 °C per decade. Compared to the base period (1981–2010), the average annual temperature in 2071–2100 is expected to be higher than 2.2 (RCP4.5) to 3.6 °C (A2 and RCP8.5). Also, by the end of the 21st century, a significant increase in the number of summer and tropical days (SD and TD) together with a decrease in the number of frost and ice days (FD and ID) are expected. During the instrumental period, a temperature higher than 37 °C was not recorded. According to projections, in the late 21st century, in summer, maximum temperatures of 40 °C are possible, even in the milder variant (RCP4.5) scenario. According to projections of the used models, Kolašin and the northern region of Montenegro expect a warmer future with more frequent extreme temperatures in a positive direction.

Key-words: temperature, projections, EBU-POM, ALADIN, scenarios A2, RCP4.5, RCP8.5, Kolašin, Montenegro

1. Introduction

Since the mid-20th century, the Mediterranean region has recorded a significant rise in air temperature. Also the Mediterranean Sea registers an increase in the surface water temperature. Satellite data indicate that from 1985 to 2006, the increase in surface water temperature was slightly more intense in the eastern than in the western regions of the Mediterranean Sea. The maximum increase in water temperature, 0.16 °C per year, was recorded in June in the Adriatic, Ligurian, and Tyrrhenian Seas (*Nykjaer,* 2009). The increase in temperature has led to greater evaporation causing an increase in dryness in the Iberian Peninsula in the last five decades (*Vicente-Serrano et al.,* 2014).

Projections for the 21st century indicate that the Mediterranean (*Mostafa et al.,* 2019) and southeastern parts of Europe (*Hochman et al.,* 2018a) will be affected by significant warming and precipitation. According to the RCP8.5 scenario for the Eastern Mediterranean, it is projected that at the end of the 21st century, the duration of the synoptic summer will be 49% longer, and the synoptic winter will be shorter by 56% (*Hochman et al.,* 2018b). As a result of the many contrasts (the collision of air masses from the north and the south, land-sea-atmosphere interactions, relief disaggregation), the Mediterranean region is often chosen to test new regional climate modeling tools (*Sevault et al.,* 2014; *Nabat et al.,* 2015).

Based on the model ensemble, both scenarios (RCP4.5 and RCP8.5) predict that Mediterranean Europe and the northeastern parts of the continent will heat up most intensively during the 21st century. In the Mediterranean area, annual rainfall is expected to decrease by up to 25% (*Jacob et al.,* 2014). However, studies show that in Western Europe, the trend of temperature rise in 1950-2008 was much faster than projected by individual models (*Van Oldenborgh et al.,* 2009). The expected rise in temperature and the likely increase in dryness in the Mediterranean region are thought to have serious consequences on ecosystems and local populations (*Lelieveld et al.,* 2016; *Bucchignani et al.,* 2018).

The Intergovernmental Panel on Climate Change (*IPCC,* 2014) points out that the human impact on climate is clear, primarily in the form of increased concentrations of greenhouse gases in the atmosphere. The fifth IPCC report, as previous reports, says that many regions of the world have recorded changes in the intensity and frequency of extreme weather events such as: droughts, floods, extreme temperatures, heat waves, stormy weather followed by the hail, heavy short-term rains, etc. It is also noted that the increased incidence of extreme weather events should also be possible during the 21st century, but significant regional variations are expected, especially with regard to precipitation. According to the IPCC, among other things, the entire Mediterranean region, the southeastern parts of Europe, and the Middle East are considered potential hotspots of climate change in the future.

According to an extensive study by the French National Alliance for the Environment (Alliance nationale de recherche pour l'environnement – AllEnvi), the Mediterranean is one of the most vulnerable regions to climate change in the world. GCM and RCM simulations for the Mediterranean region indicate that the trend of warming and drying is likely to continue in the future, but that there are uncertainties in the spatial distribution, especially in precipitation (*AllEnvi*, 2016). That is why the mentioned study emphasizes the importance of research on smaller spatial units – subregions and individual locations of the Mediterranean. A similar observation is made in the study by *Giorgi* (2006) and *Adloff et al*. (2015).

The first four reports of the Intergovernmental Panel on Climate Change (IPCC) used SRES emission scenarios (*Nakicenovic et al*., 2000). The IPCC Fifth Assessment Synthesis Report (*IPCC*, 2014) uses the results of regional climate models. RCMs use the so-called representative concentration pathways (RCPs), which take climate change mitigation and adaptation into account and define the increase in radiation energy depending on the CO2 concentration trend by 2100 (*Moss et al*., 2010).

RCPs take into account different mixtures of greenhouse gas and aerosol emissions on the one hand and climate protection measures on the other. Scenarios RCP2.6, RCP4.5, RCP6.0, and RCP8.5 are in use, and the number in the suffix indicates the radiation sensitivity with respect to the pre-industrial period. RCP2.6 is a scenario indicating a slight variant of energy gain (2.6 W/m2), RCP4.5 is a moderate scenario (energy increase of 4.5 W/m²), RCP6.0 is a moderately high variant (6.0 W/m²), and RCP8 .5 is an extreme or very high variant that takes into account the heating of an 8.5 W/m² air-conditioning system. The main difference between the extreme scenarios is that the RCP8.5 variant implies economic growth based on fossil fuel combustion, while the RCP2.6 is optimistic as it takes into account global climate protection efforts. According to the RCP4.5 scenario, which is in line with the 2015 Paris Agreement, the average global temperature will rise by 1.6 °C by the end of the century (range between 1.1 and 2.6 °C), and according to RCP8.5, which takes into account the current trend CO2, the average rise in global temperature will be around 3.7 °C (2.6 – 4.8 °C). A comparative overview of the SRES and RCP emission scenarios is in *Table 1* (*Chimani et al.*, 2016).

The main objective of this research is to analyze several temperature parameters according to the projections of two regional climate models (RCMs), the EBU-POM and ALADIN models for scenarios A2, RCP4.5, and RCP8.5. The used models will be discussed in more detail in subtitle 2.2. After the introductory part (Section 1), the research area, databases, and methodology (Section 2) are described, the results of the EBU-POM model for A2 scenario and of the ALADIN model for RCP4.5 and RCP8.5 simulations are presented in Section 3, followed by the discussion (Section 4) and conclusion (Section 5).

Table 1. Comparison of SRES and RCP emission scenarios (Source: *Chimani et al.*, 2016)

SRES	RCP	Description (by 2100):
A2	RCP8.5	**A2:** Constant population increase, further economic growth, regional, slower technological change than in other scenarios.
		RCP8.5: Over 1370ppm CO_2 equivalent concentration by 2100.
A1B	RCP6.0	**A1B:** Increased economic growth, slower population growth, usage of new and more efficient technologies, reduction of regional income disparities, balanced usage of all energy sources (not too dependent on a particular energy source), etc.
		RCP6.0: Slower greenhouse radiation effect growth, around 850 ppm CO_2 equivalent concentration by 2100
B1	RCP4.5	**B1:** Global population peak in the mid-21st century, followed by a decrease, rapid change in economic structures towards the development of services and information technologies, introduction of a clean economy and clean energy sources**,** global environmental**,** economic, and social sustainability, etc.
		RCP4.5: The rise in CO_2 emissions peaks around 2040, then the emission decreases, and in 2100 the atmospheric concentration of greenhous gases will be about 650 ppm CO_2-equivalent.

2. Research area, models used, databases and methodology

2.1. Research area

Montenegro is a Mediterranean country. Covering an area of 13 812 km^2 it belongs to Southeastern Europe (Western Balkans), extending over 100 km (air distance) to the Adriatic Sea. The study covers the area of Kolašin, a town which belongs to the northern region of Montenegro. The main factors that influence the formation of the Kolašin climate are: its latitude, air currents, and relief.

The urban area is located at 1000 m above sea level while the weather station is at 944 m above sea level (*Burić et al.*, 2013). According to the Köppen climate classification, the urban areas and lower terrains have characteristics of moderately continental climate (climate formula Csbx '), while higher mountain areas have characteristics of moderately cold climate(climate formula D) (*Burić et al.*, 2014). Kolašin is located in the upper part of the Tara River valley, surrounded by mountain ranges of Sinjajevina and Bjelasica, whose peaks exceed 2000 m (*Fig. 1*).

Fig. 1. Location of Montenegro in the Mediterranean region and Kolašin in Montenegro (Kolašin: latitude = $42^0$49'22"N, longitude = $19^0$31'4"E, altitude = 944 m)

2.2. Models used

Djurdjevic and *Rajkovic* (2010) developed a dynamically adapted RCM for the Mediterranean region of Europe, EBU-POM model. It is a fully coupled atmospheric-ocean model. The atmospheric part of the model is a version of the state-of-the-art atmospheric model ETA of tje National Centers for Environmental Protection (NCEP), and the ocean part is the Princeton Ocean Model (POM). Based on the results of future climate change scenarios obtained by EBU-POM, a database was created for individual parts and locations for Mediterranean Europe. The oceanic part of the model covers the area of the Mediterranean Sea, but without the Black Sea. The horizontal resolution of EBU-POM model is 25 km, while in the vertical direction the model has 32 levels. The EBU-POM model for initial and boundary simulation conditions uses the results of the ECHAM5 global climate model (GCM) (*Roeckner et al*., 2003), together with the MPI-OM ocean model. Professor Đurđević completed the correlation for the A2 scenario and gave us the data for the grid field to which Kolašin belongs.

The Institute of Meteorology and Climatology of the University of Natural Resources and Life Sciences, Vienna (BOKU-Met) evaluated the available regional climate change projections (EURO-CORDEX, MED-CORDEX) comparing them with observational data, and generated an ensemble of bias-corrected climate change scenarios for the Western Balkan Region. For bias

correction BOKU-Met developed and used a program called ICC-OBS Tool (*Formayer et al.,* 2019). Bias correction algorithms are based on observations, and the model data is modified so that its statistical properties become the same as those of observations. The climate change signals are calculated with reference to the period 1981–2010. After numerous corrections, from June 2019, data for the Western Balkans National Meteorological Services are available through the Climate Change Center Austria (CCCA).

Studies have shown that ALADIN-Climat v5, developed in CNRM/Météo-France, can be successfully used for Central and Eastern Europe, and for temperature and precipitation simulations in the Balkans, where Bulgaria were considered as an evaluation area (*Farda et al.,* 2010). It can also be used for the Balkans and the Apennines (*Spiridonov* and *Valcheva*, 2019), as well as for the Morocco area (*Tramblay et al.,* 2013). Related to that and for the purposes of this study, RCM ALADIN data, which uses the GCM CNRM-CM5 results as boundary and lateral conditions, were also analyzed. The resolution of the Aladin model is 0.11° (about 12.5 km).

2.3. Database and methodology

For the purposes of this study, the data of two RCMs and three scenarios were considered. The data for Kolašin's EBU-POM model for scenario A2 were obtained from Professor Djurdjevic (author of the model).The ALADIN model data for RCP4.5 and RCP8.5 scenarios for Kolašin were obtained from the Climate Change Center Austria (CCCA). Based on historical observational data for Kolasin, simulations were made for the base period 1981–2010, and projections were given for the period 2011–2100 based on these simulations. In accordance with the horizontal resolution of the models used, the projected data refer to the grid field to which Kolašin belongs.

The trend was calculated by the Sen method, and its significance was tested by the Mann-Kendall test. Importance of tendency was tested at the risk level of $p<0.001$, $p<0.01$, $p<0.05$, and $p<0.1$ (the degree of accuracy of the hypothesis of 99.9%, 99%, 95% and 90%). A total of 22 temperature parameters were considered in this study (*Table 2*).

The climatic period 1981–2010 was taken as reference (base) period, and the results of simulation of the projected temperature in Kolašin were given for the period 2011–2100. The 30-year periods for the 21st century were separated, and for each the mean value, i.e., the deviation from the base period (1981–2010) was calculated. In addition the trend for the period 2011–2100 was also calculated.

Table 2. Abbreviations, definitions, and units of the used temperature parameters

No.	Index	Definition	Unit
1.	TY	Mean annual temperature	°C
2.	TW	Average winter temperature	°C
3.	TSp	Mean spring temperature	°C
4.	TSu	Mean summer temperature	°C
5.	TA	Average autumn temperature	°C
6.	TYx	Mean annual maximum temperature	°C
7.	TWx	Mean winter maximum temperature	°C
8.	TSpx	Mean spring maximum temperature	°C
9.	TSux	Mean summer maximum temperature	°C
10.	TAx	Mid-autumn maximum temperature	°C
11.	TYn	Mean annual minimum temperature	°C
12.	TWn	Mid-winter minimum temperature	°C
13.	TSpn	Mean spring minimum temperature	°C
14.	TSun	Mean summer minimum temperature	°C
15.	TAn	Mid-autumn minimum temperature	°C
16.	FD	Total number of frost days - daily Tn <0 °C	number of days
17.	ID	Total number of ice days - daily Tx <0 °C	number of days
18.	SU	Total number of summer days - daily Tx≥25 °C	number of days
19.	TD	Total Tropical Days - Daily Tx≥30 °C	number of days
20.	TR	Total tropical nights - daily Tn> 20 °C	number of days
21.	35+	Total number of days with a maximum temperature of 35 degrees or higher (Tx≥35 °C)	number of days
22.	40+	Total number of days with a maximum temperature of 40 degrees or higher (Tx≥40 °C)	number of days

Tx (n) - daily maximum (minimum) temperature

3. Results

3.1. Results of the EBU-POM model for A2 scenario

According to the A2 projections of the EBU-POM model scenario, the mean annual temperature (TY) will be higher by 0.5 °C in the period 2011–2040, by 1.7 °C in 2041–2070, and by 3.6 °C in 2071–2100 compared to the base period (1981–2010). At the seasonal level, the most intense increase of mid-winter (TW) and mid-summer (TSu) temperatures is expected. In qualitative terms, the same results were obtained for both the annual mean maximum (TYx) and minimum (TYn) temperatures. According to these projections, a more intense increase of the maximum than the minimum temperature is expected. It is noted that the further the future goes, the more intensively the temperature increases.

Thus, the most intense increase in temperature is expected for the last 30-year period (2071–2100). Compared to the base period (1981–2010), projections indicate that TYn will be 3.8 °C higher, while TYx will be 5.0 °C higher in 2071–2100. The expected increase in the summer temperature parameters in Kolašin in the period 2071–2100, according to the A2 scenario, will be the following: TSu will be higher by 3.6 °C, TSun by 3.5 °C, and TSux by 5.4 °C (*Table 3*). If these projections do come true, by the end of the 21st century, Kolašin will be extremely hotter than nowadays.

Table 3. Projections of mean annual and seasonal temperatures (°C) for 2100 in Kolašin, relative to the 1981–2010 base period, based on the A2 scenario of the EBU-POM model

T (°C)	**Base period**	**A2 scenario**		
Avg.T	1981–2010	2011–2040	2041–2070	2071–2100
TY	7.4	+0.5	+1.7	+3.6
TW	–1.1	+1.1	+2.1	+3.8
TSp	6.5	+0.6	+1.2	+3.0
TSu	14.9	+0.8	+1.6	+3.6
TA	7.7	+0.4	+1.4	+3.2
Avg.Tn	1981–2010	2011–2040	2041–2070	2071–2100
TYn	2.3	+0.6	+1.8	+3.8
TWn	–5.0	+1.3	+2.5	+4.2
TSpn	1.3	+0.5	+1.1	+2.9
TSun	8.5	+0.9	+1.6	+3.5
TAn	2.8	+0.5	+1.6	+3.5
Avg.Tn	1981–2010	2011–2040	2041–2070	2071–2100
TYx	14.0	+0.6	+2.2	+5.0
TWx	3.5	+1.3	+2.3	+4.3
TSpx	12.7	+0.8	+1.6	+4.1
TSux	22.9	+1.1	+2.3	+5.4
TAx	14.7	+0.6	+1.8	+4.4

Avg.T – average; Avg.Tn(Tx) – average max (min) temperature

Also, days with characteristic temperatures indicate a warmer future. In 2011–2040, the annual number of summer days (SU) will be 9.1 days higher than in the base period. During 2041–2070, the projected average annual number of SUs will be 29.2 days higher than in 1981–2010. According to projections, in 2071–2100 Kolašin will have an average of 66.9 SU annually, more than in the

base period. In the last 30-year period (2071–2100), there will be about 50 tropical days (50.3 TD), more than in the base period. After 2070, tropical nights (TR) are possible in Kolašin, which is 1 tropical night in certain years. During the instrumental period, days with a maximum temperature above 35 °C were rarely recorded. However, the projected number of days with a maximum temperature above 35 °C (35+) in 2071–2100 is about 12–13 days a year. During the instrumental measurement period (1949–present), no temperature of 40 °C or higher (40+) was recorded in Kolašin. However, projections show that after 2070, summer maximum daily temperatures above 40 °C will be possible, one day per year. On the other hand, frost and ice days (FD and ID) will occur less frequently by 2100. In the average year, Kolašin registers about 122 FD, and projections for the period 2071–2100 indicate that this number will decrease by as much as 59.5 days (*Table 4*).

Table 4. Projections of the annual number of days with temperatures above fixed thresholds by 2100 in Kolašin, relative to the 1981–2010 base period, based on the A2 scenario of the EBU–POM model

Number	Base period	A2 scenario		
days	1981–2010	2011–2040	2041–2070	2071–2100
SU	44.3	+9.1	+29.2	+66.9
TD	5.1	+4.6	+17.7	+50.3
TR	0.0	0.0	0.0	+0.5
ID	17.6	–0.4	–7.4	–12.7
FD	122.1	–14.0	–29.9	–59.5
35+	0.2	0.0	+1.4	+12.7
40+	0.0	0.0	0.0	+0.5

The trend component is the basic direction of movement of a given climate element and an excellent indicator of changes over a longer period of time. Therefore, the trend of individual air temperature parameters was calculated for the purposes of the study. The calculations show that the trend of temperature increase is fairly uniform: from 0.46 °C (TSp) to 0.52 °C (TSu and TA) per decade. The tendency for an increase in projected mean temperature during the 21st century is significant at the highest level of confidence ($p<0.001$): 99.9% of the level of acceptance of the hypothesis, both annually and seasonally (*Fig. 2*). By the end of the 21st century, the expected trend of increase in the mean annual temperature (TY) mean winter temperature (TW)is 0.51 °C per decade.

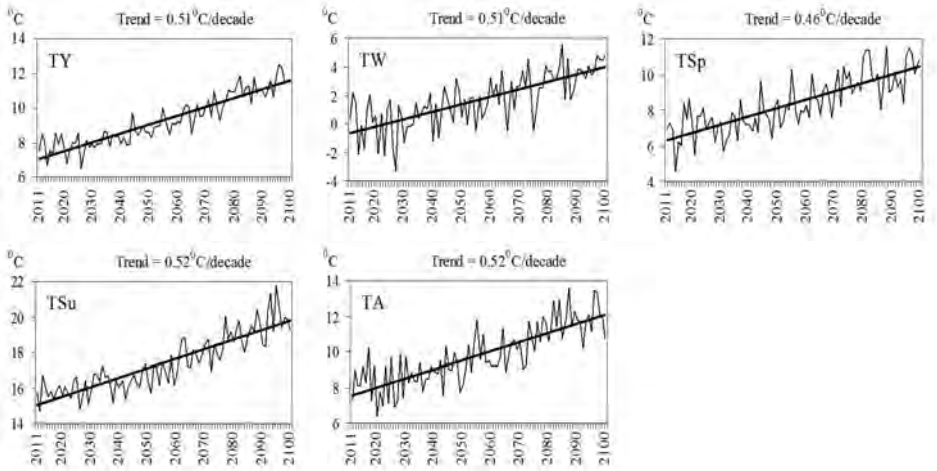

Fig. 2. Trend of the mean temperatures: annual (TY), winter (TW), spring (TSp), summer (TSu) and autumn (TA), at the significance level of $p<0.0001$, in Kolašin in the period 2011–2100 based on the A2 scenario of the EBU-POM model.

A trend project for the average annual minimum and maximum temperatures (TYn and TYx) in 2011–2100 is statistically very significant (risk of accuracy 0.001). The trend of increasing TYx (0.72 °C per decade) is more pronounced than TYn (0.52 °C per decade) (*Fig. 3*).

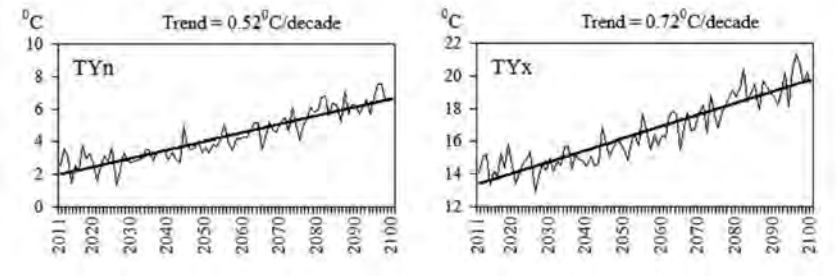

Fig. 3. Trend of the projected average annual minimum (TYn) and maximum (TYx) temperatures at the significance level of $p<0.0001$, in Kolašin in the period 2011–2100 based on the A2 scenario of the EBU-POM model.

3.2. Results of the ALADIN model for RCP4.5 and RCP8.5 scenarios

Recently, RCMs have been using RCP scenarios. Following current trends, the results of the ALADIN model are given below for the same temperature parameters, which were examined by the EBU-POM model in the previous section. A moderate variant (RCP4.5) was also considered, not only an extreme (RCP8.5) as in the previous model (A2). According to the RCP4.5 scenario, all temperature parameters show a warmer future. Therefore, even in a moderate scenario, the temperature in Kolašin is expected to increase by the end of the 21st century. In the period 2071–2100, the projected mean spring temperature (TSp) will be 2.4 °C higher than in the base period and the mean autumn (TA) will be higher by 1.9 °C (*Table 5*, left). For the same period (2071–2100), projections indicate that both maximum and minimum temperatures will rise the fastest in spring – TSpn by 2.6 °C and TSpx by 2.3 °C compared to the base period (1981–2010).

Table 5. Projections of the mean annual and seasonal temperatures (^{0}C) by 2100 in Kolašin, relative to the 1981–2010 base period, based on the RCP4.5 and RCP8.5 scenarios of the CNRM-ALADIN53 model

T (^{0}C)	**Base period**	**Scenario RCP4.5**			**Scenario RCP8.5**		
Avg.T	1981–2010	2011–2040	2041–2070	2071–2100	2011–2040	2041–2070	2071–2100
TY	9.3	+0.7	+1.4	+2.2	+0.8	+2.1	+3.6
TW	0.8	+0.8	+1.2	+2.0	+0.9	+2.0	+3.2
TSp	8.0	+0.9	+1.2	+2.4	+1.0	+2.2	+3.7
TSu	18.0	+0.9	+1.9	+2.2	+0.9	+2.1	+4.2
TA	10.4	+0.3	+1.2	+1.9	+0.5	+2.0	+3.2
Avg.Tn	1981–2010	2011–2040	2041–2070	2071–2100	2011–2040	2041–2070	2071–2100
TYn	4.6	+0.7	+1.4	+2.2	+0.8	+2.1	+3.7
TWn	–3.0	+0.8	+1.2	+1.9	+0.7	+1.8	+2.9
TSpn	3.4	+0.9	+1.2	+2.6	+0.8	+2.4	+3.9
TSun	12.4	+0.9	+1.9	+2.3	+1.0	+2.3	+4.4
TAn	5.7	+0.2	+1.2	+1.9	+0.7	+2.0	+3.3
Avg.Tn	1981–2010	2011–2040	2041–2070	2071–2100	2011–2040	2041–2070	2071–2100
TYx	13.9	+0.7	+1.4	+2.1	+0.9	+2.0	+3.5
TWx	4.6	+0.9	+1.3	+2.1	+1.0	+2.1	+3.4
TSpx	12.5	+0.8	+1.1	+2.3	+1.1	+2.1	+3.6
TSux	23.6	+0.9	+1.8	+2.2	+0.9	+1.9	+3.9
TAx	15.0	+0.3	+1.2	+1.9	+0.4	+1.9	+3.1

T- Avg.T - average temperature; Avg.Tn(Tx) - average max (min) temperature

The more extreme variant (RCP8.5) is expected to have a more intense temperature rise in Kolašin. In 2071–2100, according to the estimates of the RCP8.5 scenario, the summer temperature will grow the most rapidly: TSu will be higher by 4.2°C, TSun by 4.4 °C, and Tsux by 3.9 °C compared to the base period (*Table 5*, right). Thus, estimates indicate that the minimum temperature will grow more intensively than the maximum temperature. The only exception is the mean winter maximum temperature (TWx), which will under this scenario than that of increase (+3.4 °C) have a higher the mean winter minimum (TWn) temperature (+2.9 °C) in 2071–2100.

Comparing the results of A2 and RCP8.5 scenarios for the period 2071–2100, the projections of the EBU-POM model give a higher increase in the mean maximum temperatures (TYx, TWx, TSpx, TSux, and TAx) compared to the ALADIN model. When it comes to the mean and average minimum temperature for the mentioned period (2071–2100), the EBU-POM model gives a slight increase only in spring and summer compared to the ALADIN RCP8.5 scenario. At annual level, as well as in winter and autumn, the situation is reversed.

Specific day projections also indicate a warmer future, even under the RCP4.5 scenario. The moderate scenario (RCP4.5) estimates that in 2011–2040, the average number of summer days (SUs) will increase by 9.8 days compared to the base period (1981–2010). In 2041–2070, the number of SUs will be increased by about 20, and in the period 2071–2100 by 26.7 days. The number of tropical days and nights (TD and TR) is also expected to increase, followed by days with a maximum temperature above 35 °C and 40 °C (35+ and 40+). The expectation of a warmer future is also indicated by the decrease in the number of ice and frost days (ID and FD). According to the RCP4.5 scenario, for the period 2071–2100, the average annual FD number will be 23.4 days lower than in the base period (*Table 6*).

Table 6. Projections of the annual days with temperatures above fixed thresholds by 2100 in Kolašin, relative to the 1981–2010 baseline period, based on the RCP4.5 and RCP8.5 scenarios of the CNRM-ALADIN53 model

Number of	Base period	Scenario RCP4.5			Scenario RCP8.5		
days	1981–2010	2011–2040	2041–2070	2071–2100	2011–2040	2041–2070	2071–2100
SU	36.7	+9.8	+20.0	+26.7	+10.8	+20.6	+45.4
TD	4.2	+4.2	+9.1	+11.2	+2.1	+9.7	+23.2
TR	0.1	+0.4	+1.2	+1.3	0.0	+2.1	+10.2
ID	15.9	–1.3	–4.7	–8.2	–3.0	–7.1	–9.8
FD	93.3	–11.1	–14.2	–23.4	–7.0	–22.0	–33.1
35+	0.0	+1.0	+1.6	+1.5	+0.4	+2.6	+6.0
40+	0.0	0.0	0.0	+0.1	0.0	0.0	+0.9

ALADIN's more extreme RCP8.5 scenario predicts more intense changes to the days mentioned. According to this scenario, in the last 30–year period of the 21st century (2071–2100), the number of SUs is expected to be 45.4 days more than in the base period. In the period 2071–2100, RCP4.5 predicts 1–2 days with a temperature of 35+ per year, and RCP8.5 predicts about 6 such days. It has already been mentioned that for the period 2071–2100, according to the A2 scenario, the average annual number of days with a temperature of 35+ is expected to be twofold of the number calculated by the RCP8.5 projections. In most other specific days, more intensive changes are expected under the A2 scenario than under RCP8.5.

In 2011–2100, the average annual temperature increase is expected to be 0.25 °C per decade according to the RCP4.5 scenario, or 0.48 °C per decade according to RCP8.5. At the seasonal level, according to the RCP4.5 scenario, a more intense trend of increasing mean temperatures is expected in spring and autumn (TSp and TA) than in winter and summer (TW and TSu). For the period 2011–2100, the expected trend is 0.28 °C increase for TSp and 0.29 °C for TA per decade, while the projected TW and TSu are 0.20 °C and 0.24°C per decade, respectively (*Fig. 4*). According to the more extreme variant (RCP8.5), by the end of the 21st century, a more intense upward trend in TSu and TA (0.54 °C and 0.50 °C per decade) is expected than in TW and TSp (0.37 °C and 0.47 °C per decade). The projections of both scenarios (RCP4.5 and RCP8.5), according to the Mann-Kendall test, indicate that we should expect a significant trend of temperature increase for the observed period (2011–2100), both on annual and seasonal levels. Even the RCP4.5 scenario projects a 99.9% ($p<0.001$) positive momentum level by the end of the 21st century.

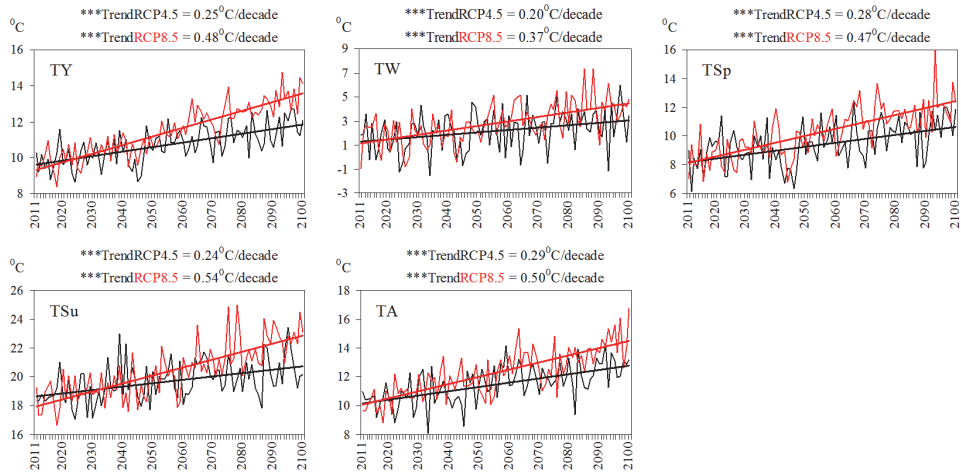

Fig. 4. Trend of average temperatures:: annual (TY), winter (TW), spring (TSp), summer (TSu), and autumn (TA), at the significance level of $p<0.0001$, in Kolašin in the period 2011–2100 based on the RCP4.5 and RCP8.5 scenario of CNRM-ALADIN53 model.

Also, projections of both scenarios indicate that a significant upward trend in mean annual maximum and minimum temperatures should be expected by 2100. According to the milder variant (RCP4.5), the mean annual minimum (TYn) and maximum (TYx) temperatures increase at a trend rate of 0.25 °C per decade (*Fig. 5*). A more extreme scenario (RCP8.5) predicts a slightly more intense increase in TYn than TYx (0.48 °C and 0.45 °C per decade, respectively). In this case too, the A2 scenario predicts a more intense upward trend in TYn and TYx relative to RCP8.5, which was not to be expected given that RCP8.5 is a slightly more extreme variant than A2 SRES scenario.

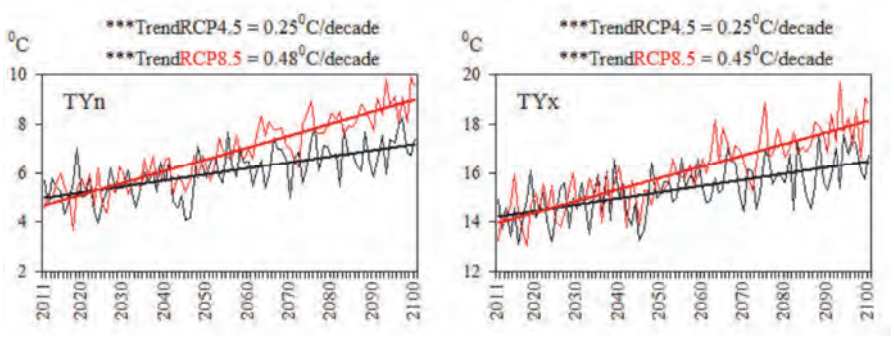

Fig. 5. Trend of projected average annual minimum (TYn) and maximum (TYx) temperatures in Kolašin, period 2011–2100, (Significance: ***p<0.001), RCP4.5 and RCP8.5 scenario CNRM-ALADIN53 model

The recorded absolute maximum temperature in Kolašin during the instrumentation period (1949–2019) is 37.1 °C and it was measured on August 23, 2012. According to A2 projections of the EBU-POM model scenario, the maximum temperature up to 43.8°C is possible by the end of the 21st century. The measured absolute minimum is –29.8 °C (registered January 13, 1985) and can be reduced to –32.1 °C by A2 scenario estimates. RCP scenarios give minor changes in temperature. According to RCP8.5, the projected absolute maximum temperature is 41.8°C and the absolute minimum is –19.1 °C (*Table 7*).

Table 7. Absolutely lowest and highest temperature in Kolašin registered and projected

	Registered	Projections to 2100		
T (°C)	**(1949–2019)**	**A2**	**RCP4.5**	**RCP8.5**
Abs. Tx	37.1	43.8	40.4	41.8
Abs. Tn	–29.8	–32.1	–16.5	–19.1

4. Discussion

Surveys for Montenegro, a spatially and population-small country belonging to the Mediterranean, show that in the second half of the 20th and the beginning of the 21st century, there was a significant trend of temperature increase (*Burić et al*., 2018; 2019). The results of the temperature projection in Kolašin (northern part of Montenegro) presented in this paper indicate a warmer future.

The results for neighboring Serbia show that the period 2071–2100 will be warmer by 2 and 4°C for the A1B and A2 scenarios with respect to 1971–2000, respectively. It is likely that the number of TD will increase, while the total number of FD will decrease in the future. A shorter duration of the frost period and a longer duration of dry and vegetation periods over the Serbian region is expected (*Kržič et al.*, 2011).

Not only in Serbia, but throughout the Western Balkans, temperatures are expected to increase during the 21st century. *Djurdjevic et al.* (2019) point out that at the end of the 21st century (2071–2100), the projected average annual temperature in the Western Balkans will be higher than 2 to 5.5 °C in relation to the 1971–2000 base period, depending on the selected scenario and part of the region. According to the NMMB model projections for the RCP8.5 scenario, the average increase in mean annual temperature over the period 2071–2100 is approximately 5.5 °C in most of the Western Balkans. Concerning precipitation, the results obtained by the aforementioned authors show that annual precipitation will have a negative tendency by the end of the 21st century in most of the Western Balkans, and in some areas the expected decrease may be up to –40% compared to the 1971 reference period –2000.

The uncertainty of climate models, both global (GCM) and RCM, has been considered in many papers (*Michaels et al*., 2002; *Laprise et al*., 2008; *Holtanová et al.*, 2010, 2014; *Kirtman et al.*, 2013; *Solman*, 2016; *Sanderson et al*., 2017; *Belda et al.*, 2017; *Ongoma et al*., 2018). *Holtanová et al*. (2019) point out that projections and interpretations of past and future climate change will be increasingly complicated, as there are significant differences in the results of both GCM and RCM between the two scenarios. When it comes to modeling, perhaps the best is *Box's* (1979) interpretation i.e., there is no exact model, but they are all useful.

In other words, modeling the climate future based on its current state is the only tool that indicates what can happen if we do not take care of the environment. That is why projections should be taken seriously. Modeling is improving day by day, different models and scenarios give different results. That is why our aim was to present the results of the latest climate simulations for the Western Balkans in this paper, using the example of temperature projections for the grid field to which Kolasin belongs (referring to RCP scenarios).

5. Conclusion

Montenegro is part of the Mediterranean and Southeastern Europe, that is, the Western Balkans, regions and subregions that are among the most vulnerable to climate change. This paper aimed to determine the magnitude and significance of the potential temperature change in Kolašin (north of Montenegro) according to projections of two models (EBU-POM and ALADIN), respectively, of three scenarios (A2, RCP4.5 and RCP8.5). All three scenarios give a significant increase in temperature by the end of the 21st century. Compared to the base period (1981–2010), projections indicate that the average annual temperature in 2071–2100 will be higher than +2.2 (RCP4.5) to + 3.6 °C (A2 and RCP8.5).

RCP8.5 is a slightly more extreme variant compared to the A2 SRES scenario. However, with the many temperature parameters considered for Kolašin, the A2 scenario predicts more intense changes than RCP8.5, which was not expected. For example, in 2071–2100, according to the A2 scenario, the annual average of SU and TD numbers will be +66.9 and +50.3 days higher than the base period, while RCP8.5 projects +45.4 and +23.2 days.This suggests that RCP scenarios are more reliable than SRES, which is logical because they have twice the resolution (better) than A2 (RCP = 12.5 km, A2 = 25 km).

In any case, the results of the study of several temperature parameters presented in this paper show that the Kolašin climate tends to become warmer with more frequent higher both maximum and minimum temperatures. These results can help decision makers take some mitigation and adaptation measures to potential climate change in the future, and generally environmental intervention. Montenegro is a small country and small economy, which has no impact on the global climate. But the slogan " work locally, think global " should be kept in mind. Therefore it is necessary to reduce the use of fossil fuels and switch to clean energy sources. As a Mediterranean country, Montenegro has significant potential for the use of solar energy.

Acknowledgements: The authors thank Professor *Djurdjevi*c and IHMSM, or CCCA Data Center for the necessary data for this study.

References

Adloff, F., Somot, S., Sevault, F., Jordà, G., Aznar, R., Déqué, M., Herrmann, M., Marcos, M., Dubois, C., Padorno, E., Alvarez-Fanjul, E. and *Gomis, D.*, 2015: Mediterranean Sea response to climate change in an ensemble of twenty first century scenarios. *Clim. Dyn. 45*, 2775–2802. https://doi.org/10.1007/s00382-015-2507-3

AllEnvi, (ed.), 2016: The Mediterranean region under climate change. Paris: IRD Editions, https://horizon.documentation.ird.fr/exl-doc/pleins_textes/divers16-11/010068463.pdf

Bucchignani, E., Mercogliano, P., Panitz, H.J., and *Montesarchio, M.*, 2018: Climate change projections for the Middle East-North Africa domain with COSMO-CLM at different spatial resolutions. *Adv. Clim. Change Res. 9,* 66–80. https://doi.org/10.1016/j.accre.2018.01.004

Burić, D., Ducić, V., and *Mihajlović, J.*, 2013: The climate of Montenegro: Modificators and types – part one. *Bull. Serbian Geograph. Soc. 93*(4), 83–102. https://doi.org/10.2298/GSGD1304083B

Burić, D., Ducić, V. and Mihajlović, J., 2014: The climate of Montenegro: Modificators and types – part two. *Bull. Serbian Geograph. Soc. 94*(1), 73–90. https://doi.org/10.2298/GSGD1401073B

Burić, D.B, Dragojlović, J.M, Milenković, M.Đ, Popović, Lj.Z., and *Doderović, M.M.*, 2018: Influence of variability of the East Atlantic Oscillation on the air temperature in Montenegro. *Thermal Sci. 22*(1 Part B), 759–766.https://doi.org/10.2298/TSCI170710211B

Burić, D., Dragojlović, J., Penjišević-Sočanac, I., Luković, J., and *Doderović, M.*, 2019: Relationship Between Atmospheric Circulation and Temperature Extremes in Montenegro in the Period 1951–2010. In: (eds. *Leal Filho W., Trbic G., Filipovic D.*) Climate Change Adaptation in Eastern Europe. Climate Change Management. 29–42. Springer. https://doi.org/10.1007/978-3-030-03383-5_3

B*elda, M., Holtanová, E., Kalvová, J.*, and *Halenka, T.*, 2017: Global warming-induced changes in climate zones based on CMIP5 projections. *Clim. Res. 71*, 17–31. https://doi.org/10.3354/cr01418

Box, G.E.P., 1979: Robustness in the strategy of scientific model building. In (Ed. *Robert L. Launer* and *G.N. Wilkinson*). Robustness in Statistics, Army Research Office in Research Triangle Park, North Carolina: Elsevier, 201–236. https://doi.org/10.1016/B978-0-12-438150-6.50018-2

Chimani, B., Heinrich, G., Hofstätter, M., Kerschbaumer, M., Kienberger, S., Leuprecht, A., Lexer, A., Peßenteiner, S., Poetsch, M.S., Salzmann, M., Spiekermann, R., Switanek, M., and *Truhetz, H.*, 2016: ÖKS15 – Klimaszenarien für Österreich. Daten, Methoden und Klimaanalyse. *Projektendbericht, CCCA*, Wien. https://hdl.handle.net/20.500.11756/06edd0c9

Djurdjevic, V. and *Rajkovic, B.*, 2010: Development of the EBU-POM coupled regional climate model and results from climate change experiments. In (Eds: *T.D. Mihajlovic* and Lalic B) Advances in Environmental Modeling and Measurements, Nova Publishers. http://haos.ff.bg.ac.rs/climatedb-srb/model.html

Djurdjevic, V., Trbić, G., Krzic, A. and *Bozanic, D.*, 2019: Projected changes in multi-day extreme precipitation over the Western Balkan region. In (eds. *Leal Filho W, Trbic G, Filipovic D.*) Climate change adaptation in Eastern Europe. Climate Change Management. 15–28. Springer, Cham. https://doi.org/10.1007/978-3-030-03383-5_2

Farda, A., Déué, M., Somot, S., Horányi., A, Spiridonov., V. and *Tóth, H.*, 2010: Model ALADIN as regional climate model for Central and Eastern Europe. *Studia Geophysica et Geodaetica, 54*, 313–332. https://doi.org/10.1007/s11200-010-0017-7

Formayer, H., Wind, M., and *König B.*, 2019: ClimaProof - Ensemble of Bias-Corrected Climate Change Scenarios. Methodical Background V2.0. Project ClimaProof - Deliverable 1.2.2. https://github.com/boku-met/climaproof-docs/find/master

Giorgi, F., 2006: Climate change hot-spots. *Geophys. Res. Lett. 33*(8), L08707. https://doi.org/10.1029/ 2006gl025734

Hochman, A., Harpaz, T., Saaroni, H., and *Alpert, P.*, 2018a: Synoptic classification in 21st century CMIP5 predictions over the Eastern Mediterranean with focus on cyclones. *Int. J. Climatol. 38*, 1476-1483. https://doi.org/10.1002/joc.5260

Hochman, A., Harpaz, T., Saaroni, H., and *Alpert, P.*, 2018b: The seasons' length in 21st century CMIP5 projections over the eastern Mediterranean. *Int. J. Climatol. 38*, 2627–2639. https://doi.org/10.1002/joc.5448

Holtanová, E., Kalvová, J., Mikšovský, J., Pišoft, P. and *Motl, M.*, 2010: Analysis of uncertainties in regional climate model outputs over the Czech Republic. *Studia Geoph. Geod. 54*, 513–528. https://doi.org/10.1007/s11200-010-0030-x

Holtanová, E., Kalvová, J., Pišoft, P., and *Mikšovský, J.*, 2014. Uncertainty in regional climate model outputs over the Czech Republic: the role of nested and driving models. *Int. J. Climat. 34*, 27–35. https://doi.org/10.1002/joc.3663

Holtanová, E., Mendlik, T., Koláček, J., Horová, I., and *Mikšovský, J.*, 2019: Similarities within a multi-model ensemble: functional data analysis framework. *Geosci. Model Dev. 12*, 735–747. https://doi.org/10.5194/gmd-12-735-2019

IPCC, 2014: Climate Change 2014: Synthesis Report. Contribution of Working Groups I, II and III to the Fifth Assessment Report of the Intergovernmental Panel on Climate Change (Core Writing Team, RK Pachauri and LA Meyer (eds.)). IPCC, Geneva, Switzerland, 151 pp.

Jacob, D., Petersen, J., Eggert, B., Alias, A., Christensen, O.B., Bouwer, L.M., Braun, A., Colette, A., Déqué, M., Georgievski, G., Georgopoulou, E., Gobiet, A., Menut, L., Nikulin, G., Haensler, A., Hempelmann, N., Jones, C., Keuler, K., Kovats, S., Kröner, N., Kotlarski, S., Kriegsmann, A., Martin, E., van Meijgaard, E., Moseley, C., Pfeifer, S., Preuschmann, S., Radermacher, C., Radtke, K., Rechid, D., Rounsevell, M., Samuelsson, P., Somot, S., Soussana, J.F., Teichmann, C., Valentini, C., Vautard, R., Weber, B., and *Yiou, P*., 2014: EURO-CORDEX: new high-resolution climate change projections for European impact research. *Reg. Environ. Change 14*, 563–578.https://doi.org/10.1007/s10113-013-0499-2

Kržič, A., Tošić, I., Djurdjević, V., Veljović, K., and *Rajković, B.*, 2011: Changes in climate indices for Serbia according to the SRES-A1B and SRES-A2 scenarios. *Clim. Res. 49*, 73–86. https://doi.org/10.3354/cr01008

Kirtman, B., S.B. Power, J.A. Adedoyin, G.J. Boer, R. Bojariu, I. Camilloni, F.J. Doblas-Reyes, A.M. Fiore, M. Kimoto, G.A. Meehl, M. Prather, A. Sarr, C. Schär, R. Sutton, G.J. van Oldenborgh, G.J., Vecchi, G. and *Wang, H.J*., 2013: Near-term Climate Change: Projections and Predictability. In: Climate Change 2013: The Physical Science Basis. Contribution of Working Group I to the Fifth Assessment Report of the Intergovernmental Panel on Climate Change. Cambridge University Press, Cambridge, United Kingdom and New York, NY, USA. 953-1028. https://www.ipcc.ch/site/assets/uploads/2018/02/WG1AR5_Chapter11_FINAL.pdf

Laprise, R., de Elía, R., Caya, D., Biner, S., Lucas-Picher, P., Diaconescu, E., Leduc, M., Alexandru, A., and *Separovic, L*., 2008: Challenging some tenets of Regional Climate Modelling, Meteorol. *Atmos. Phys. 100*, 3–22. https://doi.org/10.1007/s00703-008-0292-9

Lelieveld, J., Proestos, Y., Hadjinicolaou, P., Tanarhte, M., Tyrlis, E. and *Zittis, G.*, 2016: Strongly increasing heat extremes in the Middle East and North Africa (MENA) in the 21st century. *Climatic Change 137*, 245–260. https://doi.org/10.1007/s10584-016-1665-6

Mostafa, A.N., Wheida, A., El Nazer, M., Adel, M., El Leithy, L., Siour, G., Coman, A., Borbon, A., Magdy, A.W., Omar, M., Saad-Hussein, A. and *Alfaro, S.C.*, 2019: Past (1950–2017) and future (-2100) temperature and precipitation trends in Egypt. *Weather Climate Extr. 26* (In pres). https://doi.org/10.1016/j.wace.2019.100225

Moss, R.H., Edmonds, J.A., Hibbard, K.A., Manning, M.R., Rose, S.K., van Vuuren, D.P., Carter, T.R., Emori, S., Kainuma, M., Kram, T., Meehl, G.A., Mitchell, F.F.B., Nakicenovic, N., Riahi, K., Smith, S.J., Stouffer, R.J., Thomson, A.M., Weyant, J.P., and *Wilbanks, T.J*., 2010: The next generation of scenarios for climate change research and assessment. *Nature 463*, 747–756. https://doi.org/10.1038/nature08823

Michaels, P.J., Knappenberger, P.C., Frauenfeld, O.W., and *Davis, R.E*., 2002: Revised 21st century temperature projections. *Climat. Res. 23*, 1–9. https://www.int-res.com/articles/cr2003/23/c023p001.pdf

Nabat, P., Somot, S., Mallet, M., Sevault, F., Chiacchio, M., and *Wild, M*., 2015: Direct and semi-direct aerosol radiative effect on the Mediterranean climate variability using a coupled Regional Climate System Model. *Climate Dynamics 44*, 1127–1155. https://doi.org/10.1007/s00382-014-2205-6

Nakicenovic, N., Alcamo, J., Davis, G., de Vries, B., Fenhann, J., Gaffin, S., Gregory, K., Griibler, A., Jung, T.Y., Kram, T., La Rovere, E.L., Michaelis, L., Mori, S., Morita, T., Pepper, W., Pitcher, H., Price, L., Riahi, K., Roehrl, A., Rogner, H.H., Sankovski, A., Schlesinger, M., Shukla, P., Smith, S., Swart, R., van Rooijen, S., Victor, N., and *Dadi, Z*., 2000: Special Report on Emissions Scenarios (SRES): A Special Report of Working Group III of the Intergovernmental Panel on Climate Change, Cambridge University Press, Cambridge, U.K., 599 pp., ISBN 0-521-80493-0. Available at:http://pure.iiasa.ac.at/id/eprint/6101/1/emissions_scenarios.pdf

Nykjaer, L., 2009: Mediterranean Sea surface warming 1985-2006. *Climate Res. 39*, 11–17. https://doi.org/10.3354/cr00794

Ongoma, V., Chen, H., and *Gao, C*., 2018: Projected changes in mean rainfall and temperature over East Africa based on CMIP5 models. Int. J. Climatol. 38, 1375–1392. https://doi.org/10.1002/joc.5252

Roeckner, E., Bäl, G., Bonaventura, L., Brokopf, R., Esch, M., Giorgetta, M., Hagemann, S., Kirchner, I., Kornblueh, L., Manzini, E., Rhodin, A., Schlese, U., Schulzweida, U., and *Tompkins, A.*, 2003: The atmospheric general circulation model ECHAM 5. Part I: Model description. *Max Planck Institute for Meteorology, Report No. 349*, 140 pp. http://www.mpimet.mpg.de/fileadmin/publikationen/Reports/max_scirep_349.pdf

Sanderson, B.M., Wehner. M., and *Knutti, R.*, 2017: Skill and independence weighting for multi-model assessments. *Geosci. Model Dev. 10*, 2379–2395. https://doi.org/10.5194/gmd-10-2379-2017

Solman, S.A., 2016: Systematic temperature and precipitation biases in the CLARIS-LPB ensemble simulations over South America and possible implications for climate projections. *Climate Res. 68*, 117–136. https://doi.org/10.3354/cr01362

Sevault, F., Somot, S., Alias, A., Dubois, C., Lebeaupin-Brossier, C., Nabat, P., Adloff, F., Déqué, M., and *Decharme, B.*, 2014: A fully coupled Mediterranean regional climate system model: design and evaluation of the ocean component for the 1980–2012 period. *Tellus A: Dynam. Meteorol. Oceanogr. 66*, 23967.https://doi.org/10.3402/tellusa.v66.23967

Spiridonov, V. and *Valcheva, R.*, 2019: A new index for climate change evaluation – An example with the ALADIN and RegCM regional models for the Balkans and the Apennines. *Időjárás 123*, 551–576. https://doi.org/10.28974/idojaras.2019.4.9

Tramblay, Y., Ruelland, D., Somot, S., Bouaicha, R., and *Servat, E.*, 2013: High-resolution Med-CORDEX regional climate model simulations for hydrological impact studies: a first evaluation of the ALADIN-Climate model in Morocco. *Hydrol. Earth Syst. Sci. 17*, 3721–3739. https://doi.org/10.5194/hess-17-3721-2013

van Oldenborgh, G.J., Drijfhout, S., van Ulden, A., Haarsma, R., Sterl, A., Severijns, C., Hazeleger, W., and *Dijkstra, H.*, 2009: Western Europe is warming much faster than expected. *Clim. Past. 5*, 1–12. https://doi.org/10.5194/cp-5-1-2009

Vicente-Serrano, S.M., Lopez-Moreno, J.I., Beguería, S., Lorenzo-Lacruz, J., Sanchez-Lorenzo, A., García-Ruiz, J.M., Azorin-Molina, C., Morán-Tejeda, E., Revuelto, J., Trigo, R., Coelho, F. and *Espejo, F.*, 2014: Evidence of increasing drought severity caused by temperature rise in southern Europe. *Environ. Res. Lett., 9(4)*, 044001. https://doi.org/10.1088/1748-9326/9/4/044001

DOI:10.28974/idojaras.2020.4.2

IDŐJÁRÁS

Quarterly Journal of the Hungarian Meteorological Service
Vol. 124, No. 4, October – December, 2020, pp. 447–462

Frost risk indicator analysis in Sopron wine region (1961–2016)

Tamás Füzi * and **Márta Ladányi**

Szent István University
Department of Biometrics and Agricultural Informatics
Villányi street 29-43, 1118 Budapest, Hungary

**Corresponding author E-mail: fuzi.tamas@kertk.szie.hu*

(Manuscript received in final form January 28, 2020)

Abstract— A characteristic symptom of climate change is the modified distribution of frost events that has fundamental effect on agricultural production. To learn these changes in Sopron region, Hungary, we investigated daily minimum and maximum temperature data of the period 1961–2016 provided by the Hungarian Meteorological Service. The time interval 1961–2016 was split into two (1961–1990 and 1991–2016) in order to compare nearly two climate cycles statistically. We analyzed the 56-year trends of the last frosty day of spring and the first frosty day of autumn as well as the length of the longest yearly frost-free period. As for the winter period (October 16 – February 28), the frequencies of four different strengths of frosty days were examined. We analyzed how often an uninterrupted frost-free period (T_{min}>0 °C) longer than 12 days developed between two frosty periods in spring and in autumn, exactly when it occurred (Julian day), and how many days it lasted for. Finally, we investigated the trends of the yearly numbers of spring frosty days and their variances.

Amongst others, we show that the length of the longest uninterrupted frost-free periods has increased significantly over the past 56 years, with 70% of years in the recent climate cycle (1991–2016) having frost-free periods of more than 200 days. As an average change per 10 years, the last spring frost period ended four days earlier, while the onset of autumn frost shifted 2 days towards the end of the year. The number of days with minimum temperatures below -15 °C, -10 °C, -5 °C, and below 0 °C decreased significantly during the dormant period. These changes mean a prolongation of the growing season, partly a reduction of the winter regeneration period, and the potential higher overwintering success of the pests. The number of spring frost days also decreased significantly, while their variability has grown markedly.

Key-words: frost risk, grapevine, climate change, indicator analysis, spring refrost

1. Introduction

Extreme weather conditions caused by the change of the climate system can show up in different ways. Extreme events can be different in every region around the Earth as well as in Hungary. That is why it is expedient to analyze the changes in the climate system and the regional effects of global warming. The statistical examination of risk factors due to extreme weather conditions is crucial in order to prepare, adapt, and mitigate the vulnerability of certain regions (*Unterberger et al.*, 2018).

The most vulnerable sector to the potential consequences of changes is agriculture, while agriculture is responsible for producing food-ingredients. According to *Felkai* and *Varga* (2010), the most important risk factor in agriculture – due to its unpredictability – is climate change, because its causes and effects are not yet fully learned.

In Hungary, regarding agriculture, frost is one of the greatest risk factors caused by weather (*Kemény et al*., 2011).

According to a study by Agricultural Economics Research Institute, the most serious damage in 2016 was caused by spring frost and hailstorm. 33% of all the registered damaged areas was caused by spring frost. In most reports of spring frost, the size of damaged areas was almost four times the size of that of the previous year, exceeding 43 thousand hectares (*Keményné et al.*, 2017). Therefore, managing and mitigating frost events presents a great challenge to farmers, particularly, if it happens during the spring.

We investigate the frequency and permanency of low temperature values which can cause frost risk. Inspecting these events has a special importance with regards to the bud burst and blooming phenophases, because in the case of grapevine, late spring frost can cause yield loss in the following year as well (*Meier et al*., 2018).

The research of grapevine growing possibilities has utmost importance. According to Central Statistical Office data, in the year of 2016 from all the cultivated land in the country, grapevine was grown on more than 75 thousand hectares, and it contributed nearly 480 thousand tonnes of crop to the annual yield of agriculture.[1] With these production conditions, Hungary falls into the category of moderate wine producing countries in the world with more than 3 million hectoliters of wine. For the abovementioned reasons, safe cultivation of this crop has great importance to the national economy.[2]

For a reference station, we chose Sopron. This region is a perfect example for traditional viticulture and wine production. In terms of the average yield of grapevine, this historical wine region is one of the best in the country.

[1] http://www.ksh.hu/docs/hun/xstadat/xstadat_eves/i_omn024b.html (donwloaded March 31, 2019)
[2] http://www.ksh.hu/docs/hun/xstadat/xstadat_eves/i_omn005.html (donwloaded March 31, 2019)

2. Literature review

By climate change, we mean the upward tendency of global mean annual temperature, together with the extreme weather conditions which are becoming more common in certain regions.

In viticulture, temperature is the most important aspect among environmental factors. Viticulture is mainly defined by the annual mean temperature. Low risk open field viticulture can be carried out only within 9–21 °C annual mean temperature isotherms (*Zanathy*, 2008). The best regions lie within 10–16 °C isotherms (*Oláh*, 1979).

While in the Mediterranean region, grapevine can be grown safely due to the well-known balancing effects, the continental atmospheric conditions prevalent in the Carpathian Basin can cause such stress factors that lead to negative economic consequences both in quality and quantity (*Szenteleki et al*., 2011). One of these stress factors can be the frequency of extremely cold days (*Dunkel* and *Kozma*, 1981).

According to Hungarian Act CLXVIII of 2011 2§32, winter frost is defined as "temperature as low as -15 °C, measured during winter season at an altitude of 2 meters above ground level at the place of risk-taking". According to Section 2 Point 32a, winter frost damage is defined as "necrosis of the crop in a plantation followed by a decline in yields".

During the winter season, temperatures below -15 °C can cause serious damage to a wide variety of grapevine species. Late spring frost – even temperature as low as -1 °C – can cause a significant decline in yields (*Szenteleki et al.*, 2012, *Fila et al.*, 2014*; Bois et al*., 2015).

In spring, a cooling between 0 °C and -3 °C can seriously damage recently burst buds or intensively growing sprouts with inflorescences on them (*Hajdu* and *Saskői Bné*, 2009).

According to the second National Climate Change Strategy, the fact that due to mild winters, the resistance of perennials to the cold dwindles, causes another problem. In the case of an approximately 1–2.5 °C rise in temperature, bud burst happens 1-3 days earlier and the defoliation 1–2 days later per decade. As a result of a change in the climate system, certain phenophases of grapevine happen earlier, and the periods between phenological phases become shorter (*Jones* and *Davis*, 2000, *Leolini et al*., 2018). The earlier appearance of phenological phases, for example the early flowering periods, poses greater risk with the return of the late spring frosts. Late spring frosts – mainly "carried" frosts – can cause serious deformities in plants, thus leading to economic damage (*Vitasse* and *Rebetez*, 2018, *Leolini et al*., 2018).

For farmers, direct damage of frosts is the loss of revenue and consequent financing difficulties. Indirectly and in the short or long run, the following factors can cause serious problems: the increasing danger of alternation, the backlog of investments and developments required for maintaining competitiveness, and the loss of market as a consequence of commodity supply shortage (*Apáti*, 2013).

In Hungary, in year 2016, 62.6%, i.e., 3084.9 million HUF of the mitigating allowances were disbursed for frost damages. The majority of damage was inflicted among the plantations and field plants (*Keményné et al*., 2017).

In our study, we deal with quantifying frosty days and analyze the changes of extreme temperature values.

3. Methodology

We conducted our research with a focus on the Sopron wine region, between 1961 and 2016 with a time period of 56 years. For a reference station, we appointed Sopron with the adjacent wine region in a view of the fact that the city and its agglomeration have had a tradition in viticulture and winery for centuries.

The temperature data which we used for our study was provided by the monitoring station of the Hungarian Meteorological Service in Sopron.

We compared our results against two climatic cycles: the reference period between 1961–1990 and the more recent period from 1991 to 2016.

With respect to the 56-year-long period, we defined the Julian day (JD) of the last frosty day in spring and the first frosty day in autumn, and we analyzed the lengths of the longest annual frost-free periods. We calculated the slope of linear trends with their significance levels for the whole period (1961–2016), the reference period (1961–1990) and the more recent period (1991–2016).

We analyzed how often a frost-free period ($T_{min} > 0$ °C) longer than 12 days developed between two frosty periods in spring and in autumn, exactly when (JD) and how many days it lasted for.

With respect to the 56-year-long period, for the dormancy period (October 16 – February 28), we defined the frequency of occurrence of four types of frost with different intensities, when the minimum daily temperature was lower than -15 °C, -10 °C, -5 °C, and 0 °C, respectively.

Furthermore, we analyzed the continuous length of frosty days, that is, how long do frosts with certain intensity happen in spring and in autumn year after year.

Finally, we analyzed the number of frosty days during spring in the last 56 years, together with their moving variances with a 9-year window.

For the comparison of the changes that happened during the reference period (1961–1990) and the more recent period (1991–2016), we calculated linear trends and applied a two-sample ratio test (Z-test) and a Student's t-test. In the latter case we proved the normality by d'Agostino test ($p > 0.05$). We checked the assumption of homogeneity of variances by F-test; in case it was violated, Student's t-test was corrected by Welch's degrees of freedom.

4. Results

4.1. The beginning, the end, and the length of the longest frost-free period

In the last two climate cycles (1961–2016), in the area of Sopron, the longest uninterrupted frost-free period (Tmin < 0 °C) was longer than 150 days in every year (*Table 1*).

Between 1961 and 2016, a 150–174-day-long frost-free period happened in 8 years, while during the more recent period, the number of such years was zero. The number of years with frost-free periods longer than 200 days was 13 in the reference period, while in the more recent period (1991–2016) it was 18. This means that more than two-thirds of the 26-year period contained frost-free periods longer than 200 days (*Table 1*).

Table 1. Frequency of the longest frost-free periods in the two climate cycles studied (1961–1990 and 1991–2016) in Sopron

Indicator	1961–1990	1991–2016
150–174-day-long uninterrupted frost-free period	8	0
175–199-day-long uninterrupted frost-free period	10	9
Contained frost-free periods longer than 200 days	12	18

The length of frost-free periods has significantly increased in the past 56 years (slope of linear trend=m=0.62; $p < 0.01$). However, in the period between 1961 and 1990, the increase was not significant (m=0.81; p=0.14), while the change between 1991 and 2016 was significant (m=1.16; $p < 0.02$).

The linear, 56-year trend of the Julian day of the last frosty day in spring is significant (m= -0.40; $p < 0.01$), that is, these days are coming earlier (*Fig. 1*). The linear trend of the first frosty days in autumn is not significant (m=0.21; p=0.07), although the date of the onset of frosts shifted towards the end of the year.

Fig. 1 illustrates the Julian days of the last frosty days in spring (blue) and the first frosty days in autumn (red) between 1961 and 2016. According to the slope of the linear trends, the onset of autumn frost shifted forwards by 2 days (although the change is not significant), while the period of frost in spring ended an average of 4 days earlier per decade. The results of the comparison of the two time periods (1961–1990 and 1991–2016) done by a two-sample Student's t-test regarding the last frosty day in spring (JD), the first frosty day in autumn (JD), and the days that passed between the two events are shown in *Table 2.*

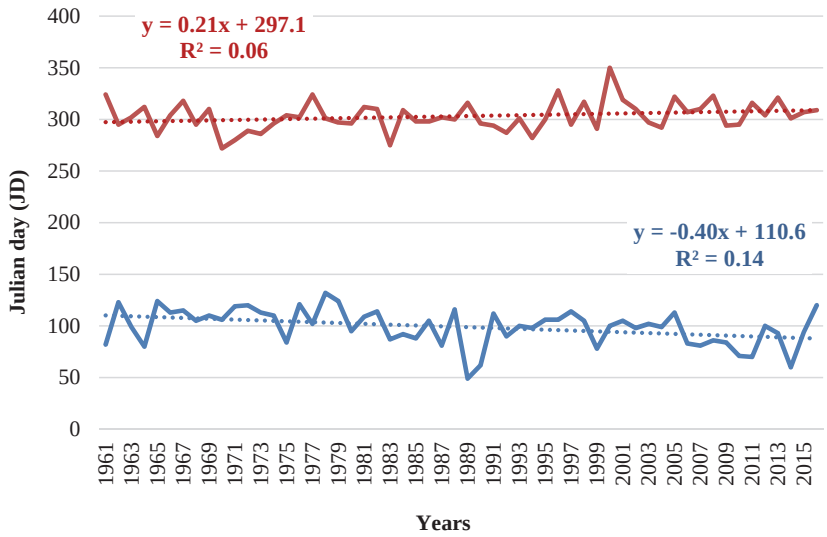

Fig. 1. Julian days of the last days of frost days in spring (blue) and the first days of frost days in autumn (red) between 1961 and 2016 in Sopron.

Table 2. The average of the last spring frost, the first autumn frost days, and the longest frost-free period (JD), and the comparison of these indicators with a two-sample Student's t-test between 1961-1990 and 1991–2016 in Sopron

Indicator	Average		t (df=54)	p
	1961–1990	1991–2016		
Julian day (JD) of the last frost in spring	103	95	1.66	0.10
Julian day (JD) of the first frost in autumn	300	307	-1.71	0.09
The length of the longest uninterrupted frost-free period (day)	197	211	-2.27	**0.03**

McCabe et al. (2015) got the same result by examining the temperature data collected from more than 500 stations throughout the United States. According to this data, in the past decades (1920–2012), the last frosty day in spring occurred earlier, while the first frosty day in autumn occurred later.

Although neither the Julian day (JD) of the last frost in spring, nor the Julian day (JD) of the first frost in autumn differ significantly ($p>0.05$) according to the two-sample Student's t-test, the length of the longest uninterrupted frost-free period within a year is significantly longer ($p<0.05$) by approximately two weeks in the more recent period (1991–2016) compared to the period 1961–1990.

In the following, we introduce three indicators regarding the *returning* frost in spring and three indicators in autumn.

Spring indicators:

- the starting point of a frost-free period (JD) longer than 12 days preceding a period of frost (frost-free (spring)>12-start);
- the length of a frost-free period (day) longer than 12 days preceding a period of frost (frost-free (spring)>12-lenght);
- the frequency and length of a period of frost (day) following a frost-free period longer than 12 days.

Autumn indicators:

- the starting point of a frost-free period (JD) longer than 12 days following a period of frost (frost-free (autumn)>12-start);
- the length of a frost-free period (day) longer than 12 days following a period of frost (frost-free (autumn)>12-lenght);
- the frequency and length of a period of frost (day) preceding a frost-free period longer than 12 days.

In the first 30 years of the examined period (*Fig. 2a*), the first frost-free period longer than 12 days happened after the 105th Julian day on average, (which was followed by another frosty period), while in the 26 years of the more recent period (*Fig. 2b*), the first frost-free period happened right after the 82nd Julian day on average. The difference is significant ($p<0.05$, *Table 3*). The lengths of frost-free periods (day) longer than 12 days following a period of frost did not change significantly ($p=0.19$).

Table 3. The average of the start and length of the frost-free period longer than 12 days prior to the spring frost period; the average of the start and length of the frost-free period longer than 12 days after the autumn frost period; and the comparison of these indicators with a two-sample Student's t-test for the 1961-1990 and 1991–2016 periods

Indicator	Average		t (df=54)	p
	1961–1990	1991–2016		
Frost-free (spring)>12_start (JD)	106	83	2.45	**0.02**
Frost-free (spring)>12_length (day)	23	19	1.35	0.19
Frost-free (autumn)>12_start (JD)	331	328	0.39	0.70
Frost-free (autumn)>12_length (day)	16	24	2.84	**0.01**

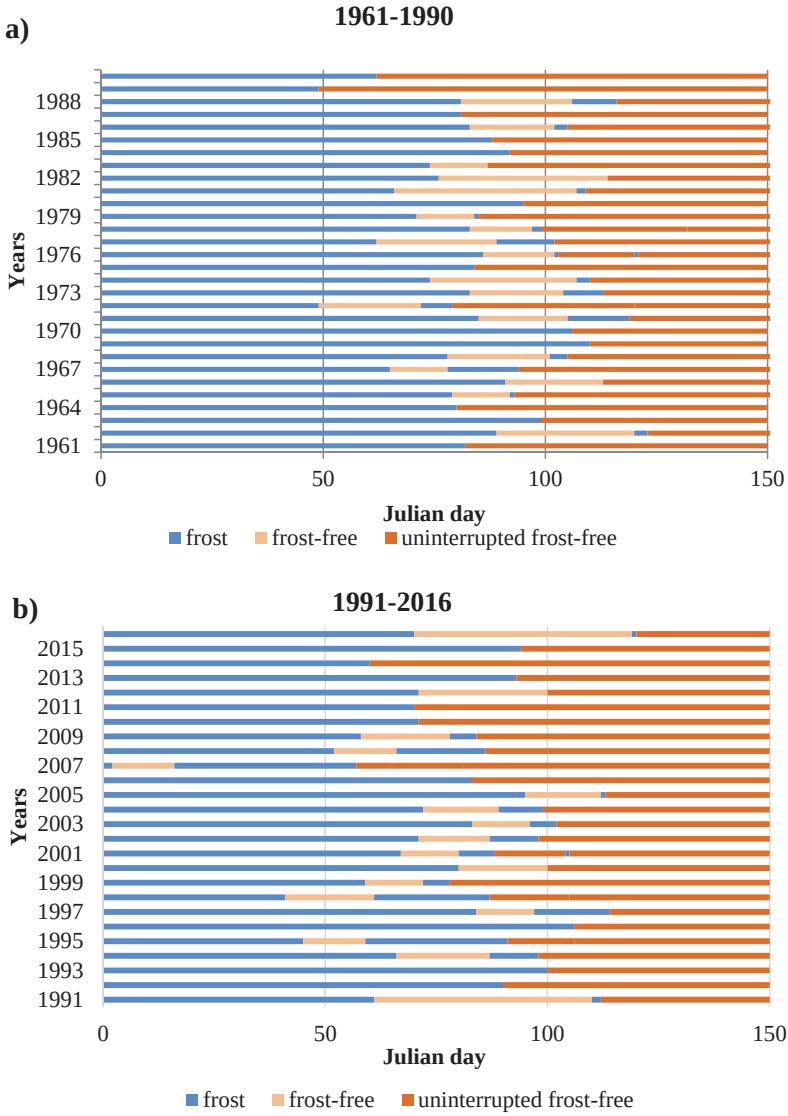

Fig. 2. Frost-free periods longer than 12 days preceding frost in spring period in Sopron: a) between 1961–1990 and b) 1991–2016.

In the spring time of the reference period, returning frost occurred six times after a second frost-free period longer than 12 days. The lengths of these frosty periods were 1, 1, 1, 2, 7, and 16 days, respectively. In the more recent period,

the number of such periods were 4 and the length of these periods were 8, 26, 32, and 41 days, respectively. Although the frequency of these periods does not differ significantly ($z=0.5$; $p=0.65$), their lengths in the recent period exceeded one week every time, so they pose a more serious risk.

In case of plantations, a persistently low temperature below zero after a frost-free period longer than 12 days can cause frost damage, which may lead to a decline in crop quantity, crop quality and increased production costs due to prolonged use of anti-frost methods (*Dami et al*, 2015). According to *Warmund et al.* (2008), a disruption of plant growth caused by spring frost is not only detrimental to the plant growth and reproduction, but it can also lead to a huge economic loss.

Note that in *Figs. 2* and *3*, preceding the periods of refrost, we only indicated the frost-free periods longer than 12 days. In the case of shorter frost-free periods, we depicted them as the uninterrupted frosty days.

As for the autumn period, the starting point of a frost-free period (JD) longer than 12 days following a period of frost did not change significantly ($p=0.70$), however, the lengths of such frost-free periods changed significantly compared to the reference period (1961–1990, *Table 3*, $p<0.05$).

The periods of frost in the more recent period (*Fig. 3b*) have shifted towards the end of the year and, compared to the reference period between 1961 and 1990 (*Fig. 3a*), the frost-free periods disrupt the continuity of the periods of frost typically in the last two months (after Julian Day 300) of the year.

Although the extent of frost damage is significantly more frequent in spring than in autumn, it is important to analyze the days of frost in autumn, because the frost resistance of crops depends on the number and intensity of frosty days occurring during the long endodormancy phenophase (*Lakatos et al*., 2017).

By quantifying the changes that happened during the past two climate cycles, we detected that, while in the reference period the beginning of the frost-free periods longer than 12 days is on the 331st day of the year on average, in the more recent period it is on the 328th day of the year (*Table 3*). The change is not significant ($p>0.05$). The average length of a frost-free period longer than 12 days in the reference period (16 days) became longer (24 days) in the more recent period, and the difference is significant ($p<0.05$, *Table 3*).

In autumn, considering the periods of frost between two frost-free periods longer than 12 days, we detected no significant differences between the two climatic cycles regarding their lengths and frequencies.

The frequency of frost-free periods longer than 12 days prior in spring (1961–1990: 18; 1991–2016: 17) do not differ significantly in the two climate cycles ($z=0.42$; $p=0.68$).

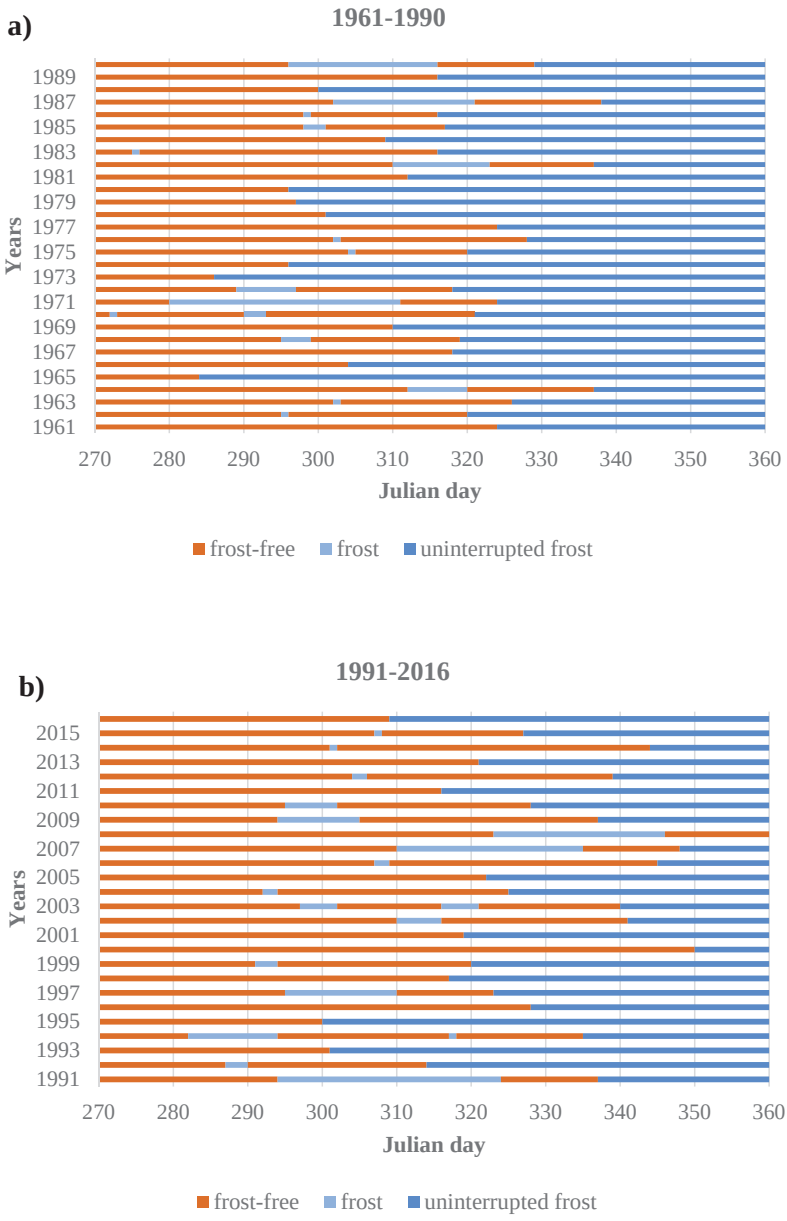

Fig. 3. Frost-free periods longer than 12 days following frost in autumn period in Sopron (between 1961–1990 and 1991–2016).

4.2. Winter frosts with different intensities

During the analyzed 56 years, with regards to the frequency of frosty days, a significant difference was detected in the winter season (between October 16 and February 28): the decrease of the number of frosty days with a minimum temperature below -15 °C is significant ($p<0.05$) in the past 56 years, the number of such days decreased by 0.5 day per decade (*Fig. 4; Table 4*). The number of days with a minimum temperature below -10 °C decreased more dramatically, the number of such days decreased by 1.5 days per decade, the change is significant ($p<0.05$; *Fig. 4; Table 4*). The number of days with a minimum temperature below -5 °C decreased significantly ($p<0.05$), by 3 days per decade, while the number of frosty days with a minimum temperature below 0 °C decreased significantly ($p<0.01$), by 4.5 days per decade (*Fig. 4; Table 4*).

These changes can partly lead to longer growing seasons, the decrease of length of the dormancy period and the decrease of mortality rates of pests. The significantly increasing temperature in winter can set out new conditions for Hungarian farmers (*Horváth et al*., 2017).

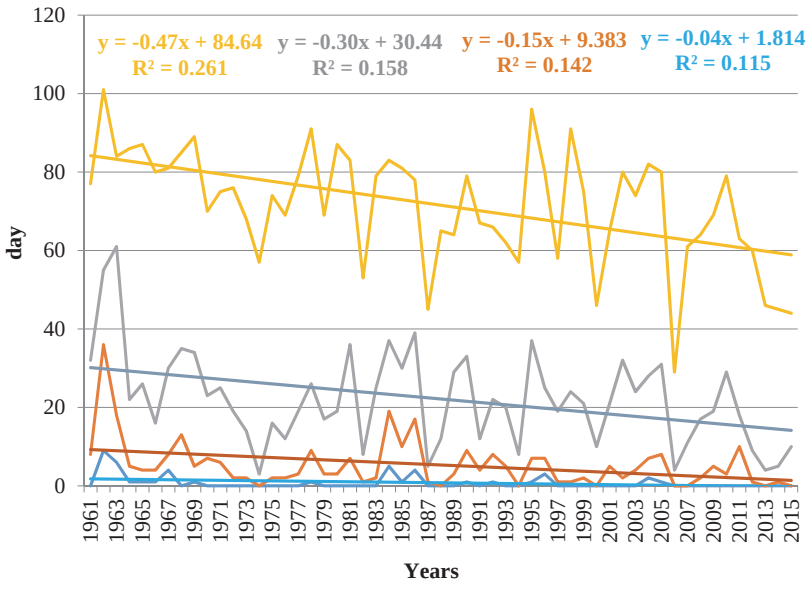

Fig. 4. Frequency of frosts with different intensities (day) (1961–2016).

Table 4. The average of the frequency of frost of different intensities in winter (between October 16 and February 28) (1961–2016) and the comparison of these indicators with a two-sample Student's t-test for the 1961–1990 and 1991–2016 periods.

Indicator	Average		t(df=54)	p
	1961–1990	1991–2016		
daily minimum temperature below -15 °C (day)	1.3	0.3	2.07	**0.04**
daily minimum temperature below -10 °C (day)	7.5	3.3	2.59	**<0.01**
daily minimum temperature below -5 °C (day)	26.2	19.0	2.27	**0.03**
daily minimum temperature below 0 °C (day)	79.1	66.3	3.39	**<0.01**

4.3. Spring frosts

The frequency of frosty days in spring decreased significantly in the period between 1961 and 2016 ($p<0.01$; *Table 1*, *Figs. 5* and *6*). The moving averages of the variance of the numbers of frosty days in spring with a 9-day window shows a significant increase in the analyzed 56-year-long time period ($p<0.01$; *Table 5*) with a scale of 1.5 days per decade (*Fig. 6*). This tendency can be seen in the case of both (reference and more recent) climate cycles with significant trend in the reference period ($p<0.05$) while with not significant trend in the recent time interval, although the increase is not significant ($p>0.05$; *Table 5*). These results mean increasing uncertainty of annual frequency of frosts and, as a consequence, the difficulties of plant protection.

This means that, according to the changes that happened during the two climate cycles, the number of frosty days decreased (blue) by nearly 4 days per decade in the spring period. This change means a 7-day (red) per decade decrease in the reference period and a 5-day (green) per decade decrease in the more recent period. These changes can be seen in *Fig. 5*.

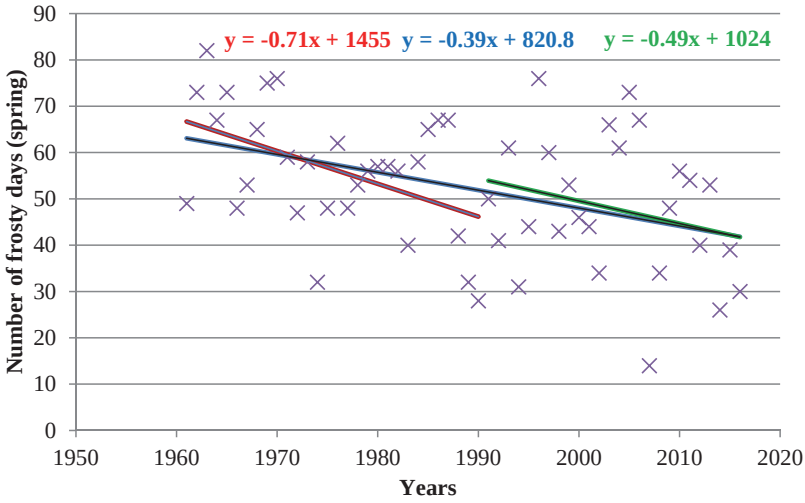

Fig. 5. The number of frosty days in the spring period under the three examined time zones (1961–2016, 1961–1990, 1991–2016) in Sopron.

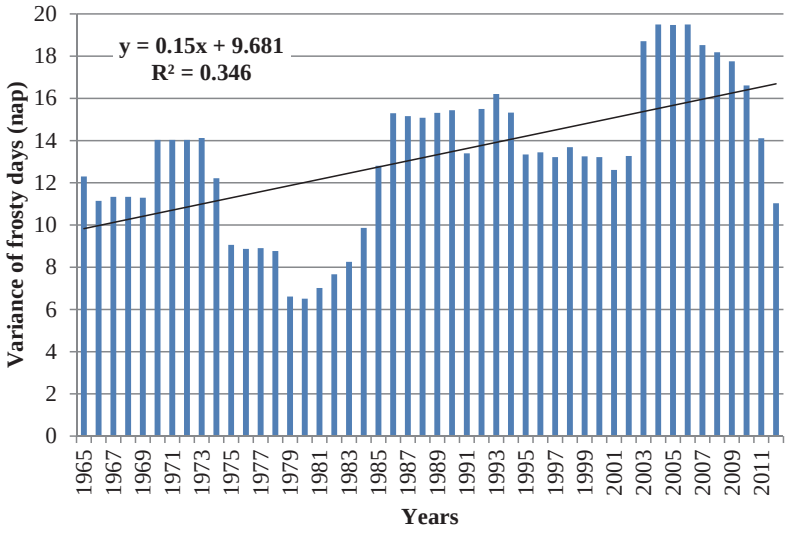

Fig. 6. The moving averages of the variances of the numbers of frosty days in spring with a 9-day window (1961–2016) in Sopron.

Table 5. The moving averages and the variances of the numbers of frosty days in spring with a 9-day window (1961–2016, 1961–1990, 1991–2016) in Sopron, together with their linear trends

Indicator	1961–2016 moving average of variance	slope	1961–1990 moving average of variance	slope	1991–2016 moving average of variance	slope
Numbers of frosty days (spring)	52	0.18**	56	0.21*	48	0.06 ns

ns: not significant; *p<0.05, **p<0.01

5. Conclusions

In our study, first the lengths of uninterrupted frost-free periods were discussed, and it was found that in two-thirds of the past 26 years, they have increased to more than 200 days per year. The change during the two analyzed climate cycles is significant. This increase is in relation to the shift of the last frosty day to earlier in spring and the shift of the first frosty day to later in autumn. Although we have not seen any significant changes in the alteration of these two indicators, the difference is still unfavorable, taking other signs of climate change into consideration; i.e., the so-called "false spring" at the end of the winter, which can cause the early development of plants followed by a frost, thus leading to problems in development and loss of crops (*Ma et al*., 2019).

In this context, *Unterberger et al*. (2018) draws attention to the vulnerability of crops, according to which an early blooming followed by a cold period (spring frost) can disrupt the growing season in the early spring.

We also considered the frost-free periods both in spring and autumn. Considering the examined climate cycles, we could see a significant change during the spring. According to our results, it can be concluded that in the past few decades, frost formed often after gradually longer frost-free periods, thus causing disruption in the plant development.

There is also a significant difference in the appearance of frost-free periods longer than 12 days preceding a refrost between the two climate cycles, that is, in the more recent climate cycle, a long frost-free period often appeared even in March. However, there is no significant difference in the frequencies of periods of frost longer than 12 days, so the frequency of such periods in the more recent period is similar to that of the reference period.

As for the number of frosty days with different intensities, it can be generally stated that over the past 56 years, the number of days with temperatures below

-15 °C, -10 °C, -5 °C, and 0 °C has decreased. In the winter period, the change is significant in every case.

At the same time, it can be concluded that the number of frosty days in spring shows a decreasing tendency. That change, with regards to the two climate cycles, is significant. However, this declining rate does not exclude the possibility of major hazard events (i.e., late spring frosts). Our expectations coincide with the conclusion of *Mosedale et al.* (2015) that, according to the HadCM3 climate model, the risk of late spring frosts will increase before bud burst.

Our results are supported by the results of the National Climate Change Strategy of Hungary, according to which, the number of frosty days will decrease significantly in the future due to the warming tendency: from an average of 96 days in the reference period (1961–1990), by 18–19 days until 2021–2050, by 32–55 days until 2071–2100. The decrease of the frequency of frosty days will likely affect every region of Hungary.[3]

A northward shift of the zone limit can be expected in viticulture and in the wine industry, meanwhile negative climatic effects (frost, water stress, sunburn, infections), decrease of grapevine lifetime, and decline in quantity and quality of wine may occur. In order to prevent the above-mentioned problems, the role of forecasts in meteorology with plant protection warning becomes more important in the future. Modifications in the variety structure may also become necessary in the future (*Szenteleki et al*., 2012).

Aknowledgement: This work was supported by the Human Resources Development Operational Program under grant number EFOP-3.4.3-16-2016-00012.

References

Apáti, F., 2013: A tavaszi fagykárok elleni védekezés lehetőségei a gyümölcstermesztésben, Gyümölcsösök védelme. *Agrofórum Extra 24: 48*. 56–60. Paper: 1, 5. (In Hungarian) https://www.farmit.hu/sites/default/files/documents/agroforum/ApatiF_2013jan_gyumi.pdf

Bois B., Moriondo M., and *Jones, G.V.*, 2014: Thermal risk assessment for viticulture using monthly temperature data. Xth International Terroir Congress, Tokaj, Eger, Hungary, 227-232.

Dami, I.E., Li, S., Bowen, P.A., Bogdanoff, C.P., Shellie, K.C., and *Willwerth, J.*, 2015: Foliar Applied Abscisic Acid Increases 'Chardonnay' Grapevine BudFreezing Tolerance during Autumn Cold Acclimation. *Hort Technol. 25*, 293–305. https://doi.org/10.21273/HORTTECH.25.3.293

Dunkel, Z. and *Kozma, F*., 1981: A szőlő téli kritikus hőmérsékleti értékeinek területi eloszlása és gyakorisága Magyarországon. *Légkör 26* (2), 13–15. (In Hungarian)

Felkai, B.O. and *Varga, T. (szerk.)*, 2010,: Az Egyedi- és Összkockázatú Agrárbiztosítások Hazai és Nemzetközi Gyakorlata. *Agrárgazdasági Információk 2010. 5*.

Fila, G., Gardiman, M., Belvini, P., Meggio, F. and *Pitacco, A.*, 2014: A comparison of different modelling solutions for studying grapevine phenology under present and future climate scenarios. *Agric.Forest Meteorol. 195–196*, 192–205.

[3] http://www.kormany.hu/download/f/6a/f0000/N%C3%89S_2_strat%C3%A9gia_2017_02_27.pdf

Hajdu, E. and *Saskői B.-né*, 2009: Abiotikus stresszhatások a szőlő életterében Agroinform Kiadó, Budapest.

Horváth, D., Fazekas I., and *Keszthelyi, S.*, 2017: Phthorimaea operculella (Zeller, 1873), first record of an invasive pest in Hungary (Lepidoptera, Gelechiidae). *Acta Phytopathologica et Entomologica Hungarica, 52*, 117–122. https://doi.org/10.1556/038.52.2017.006

Jones, G.V. and *Davis R.E.*, 2000: Climate influences on grapevine phenology, grape composition, and wine production and quality for Bordeaux, France. *Am. J. Enol. Vitic. 51*, 249–261.

Kemény, G., Varga, T., Fogarasi, J., Kovács, G., and *Tóth, O.*, 2011: A hazai mezőgazdasági biztosítási rendszer problémái és továbbfejlesztésének lehetőségei. Agrárgazdasági Könyvek. Agrárgazdasági Kutató Intézet, Budapest. http://repo.aki.gov.hu/296/1/ak_2010_07.pdf (In Hungarian)

Keményné, Horváth Z., Péter, K., Zubor-Nemes, A., Kiss, A., Lőrincz, K., and *Kóti, A.*, 2017: Az agrár-kockázatkezelési rendszer működésének értékelése 2016. (in Hungarian) http://repo.aki.gov.hu/2734/1/2017_06_AI_Kockazat%20web_pass.pdf

Lakatos, L., Molják, S., and *Nagy, R.*, 2017: Analyzes of autumnal, winter and spring frost damage at the wine regions of Hungary. Aerulsi Apa. Componenteale Mediului, 69–76. https://doi.org/10.24193/AWC2017_09

Leolini, L., Moriondo, M., Fila, G., Costafreda-Aumedes, S., Ferrise, R. and *Bindi, M.*, 2018: Late spring frost impacts on future grapevine distribution in Europe. *Field Crops Res. 222*, 197–208.

Ma, Q., Huang, J.G., Hänninen, H., and *Berninger, F.*, 2019: Divergent trends in the risk of spring frost damage to trees in Europe with recent warming. *Glob. Change Boil. 25*, 351–360. https://doi.org/10.1111/gcb.14479

McCabe, G.J., Betancourt, J.L., and *Feng, S.*, 2015: Variability in the start, end, and length of frost-free periods a cross the conterminous United States during the past century. *Int. J. Climatol. 35*, 4673–4680. https://doi.org/10.1002/joc.4315

Meier, M., Fuhrer, J., and *Holzkämper, A.*, 2018: Changing risk of spring frost damage in grapevines due to climate change? A case study in the Swiss Rhone Valley. *Int. J. Biometeorol. 62*, 991–1002. https://doi.org/10.1007/s00484-018-1501-y

Mosedale, J.R., Wilson, R.J., and *Maclean, I.M.*, 2015: Climate change and crop exposure to adverse weather: changes to frost risk and grapevine flowering conditions. *PloSone 10(10)*, e0141218. https://doi.org/10.1371/journal.pone.0141218

Ministry of National Development, 2017: The Second Climate Change Strategy of Hungary (NCCS-2) https://www.kormany.hu/download/f/6a/f0000/N%C3%89S_2_strat%C3%A9gia_2017_02_27.pdf

Oláh, L., 1979: Szőlészek zsebkönyve. Mezőgazdasági Kiadó, 38–42. (In Hungarian)

Szenteleki, K., Gaál, M., Ladányi, M., Mézes, Z., Szabó, Z., Zanathy, G., and *Bisztray, Gy.*, 2011: A klímaváltozás hatásai a Közép-magyarországi régió szőlő-, meggy- és cseresznyetermesztésére és a termésbiztonságra. Agrárinformatikai tanulmányok III. 3, 113–150. (In Hungrian)

Szenteleki, K., Gaál, M., Mézes, Z., Szabó, Z., Zanathy, G., Bisztray, Gy., and *Ladányi, M.*, 2012: Termésbiztonsági elemzések a Közép-magyaroroszági régióban a klímaváltozás tükrében. A szőlő-, a cseresznye-, és a meggytermelés helyzete és jövőképe. In: Fenntartható fejlődés, élhető régió, élhető települési táj 1. Budapesti Corvinus Egyetem, Budapest, 173–203. (In Hungarian)

Unterberger, C., Brunner, L., Nabernegg, S., Steininger, K.W., Steiner, A.K., Stabentheiner, E., and *Truhetz, H.*, 2018: Spring frost risk for regional apple production under a warmer climate. *PloSone, 13(7)*. https://doi.org/10.1371/journal.pone.0200201

Vitasse, Y. and *Rebetez, M.*, 2018: Unprecedented risk of spring frost damage in Switzerland and Germany in 2017. *Climatic Change, 149*, 233–246. https://doi.org/10.1007/s10584-018-2234-y

Warmund, M.R., Guinan, P., and *Fernandez, G.*, 2008: Temperatures and cold damage to small fruit crops a cross the eastern United States associated with the April 2007 freeze. *Hort Sci. 43*, 1643–1647. https://doi.org/10.21273/HORTSCI.43.6.1643

Zanathy, G., 2008: Gondolatok a klímaváltozás szőlőtermesztésre gyakorolt hatásáról, *Agro napló 12(2)* 92–94. (In Hungarian)

DOI:10.28974/idojaras.2020.4.3

IDŐJÁRÁS

Quarterly Journal of the Hungarian Meteorological Service
Vol. 124, No. 4, October – December, 2020, pp. 463–482

Application of vector autoregressive models to estimate pan evaporation values at the Salt Lake Basin, Iran

Ali Shahidi*, **Yousef Ramezani**, **Mohammad Nazeri-Tahroudi**, and **Saeedeh Mohammadi**

Department of Water Engineering
Faculty of Agriculture
University of Birjand, Birjand, Iran

**Corresponding author E-mail: ashahidi@birjand.ac.ir*

(Manuscript received in final form November 11, 2019)

Abstract— Thousands of billions of cubic meters of fresh water collected at great expense are evaporated annually from dams, and salts of evaporating water reduces water quality. In this study, the efficiency of the vector autoregressive model called VAR model has been examined on an annual scale using pan evaporation data in the salt lake basin, Iran, during the statistical period of 1996–2015. Since hydrologic modeling is concerned with the accuracy and efficiency of the model, therefore, we must try to evolve and improve the results of the models. In this study, VAR multivariable time series and nonlinear GARCH models have been used. The results of linear and nonlinear hybrid models in modeling the annual and monthly pan evaporation values of studied stations at the basin area of the salt lake indicated, that the pan evaporation values in the annual scale have the best fit with hybrid models. The results of the study of the accuracy of these models in modeling the pan evaporation values indicated, that the VAR-GARCH hybrid models have a high accuracy relative to the vector models and have been able to model the pan evaporation values with good accuracy and with the lowest error rate. Of the two models that have both annual nature (VAR and VAR-GARCH), the best model can be selected based on the estimation of the error values. In this study, we first examine the accuracy of the relatively new vector autoregressive model. The results of the estimation of error and efficiency of the model indicated the acceptable accuracy of this model in estimating the pan evaporation values in the annual scale. The 95% confidence interval confirmed the simulation results of the calibration step. Overall, the results showed that both VAR and VAR-GARCH models have high accuracy and correlation, and the model's performance criterion also confirms this. The percentage of improvement in the results from the model of the pan evaporation values in the annual scale using the VAR-GARCH model is about 4% relative to the VAR model. However, due to modeling the random section and reducing the uncertainty of the model, the results of modeling the pan evaporation values using the VAR-GARCH model are better than the VAR model. But due to the complexity of calculating the GARCH model, the VAR model can also be used.

Key-words: autoregressive conditional heteroscedasticity model, potential evapotranspiration, Salt Lake, single-variable model

1. Introduction

Since Iran has a dry and semi-arid climate, estimating and modeling hydrologic and meteorological parameters is important for planning and managing water resources. In the meantime, various prediction methods have tried to determine the relationship between independent and dependent variables, and many conceptual and statistical models have been used to predict climate variables. Time series models, as a mathematical-physical model, have a great ability to model linear and nonlinear phenomena. The time series model consists of two main parts, including random component and algebraic (deterministic) component of the model, where the algebraic component of the model is obtained using observational and random components using different stochastic methods. Therefore, the structure of time series models can be adapted to the structure of the hydrological series if the selection of the model and its calculations are correct (*Salas*, 1993). *Thomas* and *Fiering* (1962), *Yeyjevich* (1963), *Roesner* and *Yevjevich* (1966) used autoregressive models for modeling the annual and seasonal series of river flows. Since then, a lot of research has been done to develop and extend concepts of the time series models with modifying and correcting models. Many of the processes in the natural systems are nonlinear, although certain aspects of these systems may be closer to the linear process than others. However, the nature of non-linearity is not clear to us (*Tsonis*, 2001). Nonlinear models have been used more for statistical, economical, and mathematical researches. These include references such as *Priestley* (1988) and *Tong* (1990). Most of these models have been used to modeling and predicting the economic time series (*Franses* and *Van Dijk*, 2000). *Wang et al.* (2006) used the combination of the ARMA and GARCH[1] models to fit the variance and daily average of the Yellow River flow in China. The results showed that the ARMA-GARCH model offers very useful results in daily river flow modeling. *Caiado* (2007) examined the performance of time series one-parameter models in predicting the amount of water consumed in Spain in daily and weekly scales from 2001 to 2006. In this research, ARIMA and GARCH models were fitted on a series of observational data, and the performance of these models was evaluated and confirmed. In the meantime, combined models are used in order to improve the prediction results. *Ghorbani et al.* (2018) used the hybrid multilayer perceptron-firefly algorithm (MLP-FFA) model to predict the pan evaporation in the northern part of Iran. Results show that an optimal MLP-FFA model outperforms the MLP and SVM model for both tested stations. *Ashrafzadeh et al.* (2018) estimated the daily pan evaporation using neural networks and meta-heuristic approaches at two weather stations (Anzali and Astara) in the northern part of Iran. The results indicated that converting the simple multilayer perceptron with firefly algorithm makes it a powerful hybrid model for estimating pan evaporation.

[1] *Generalized Autoregressive Conditional Heteroscedasticity*

Regarding the increasing number of models simulating a various hydrological parameters, linear time series models need to be upgraded by combining these models with nonlinear models, but the accuracy of this combination must be measured. Also, considering the randomness of the time series models, their use in modeling parameters such as hydrological parameters, that themselves have a random nature, seems to be better. Since linear models have generally been found to be univariate in the survey, using multivariate models seems to be necessary due to correlation between hydrological variables. On the other hand, the VAR model is a random process used to create linear dependencies between multiple time series. The VAR model uses an integrated autoregressive model using several parameters. All variables in the VAR model are simultaneously entered into the model, where each variable explains an equation whose evolution is based on delay values of different model variables and an error value. VAR modeling requires a very high level of knowledge in order to found forces affecting a variable, as much as they do not have structural models with simultaneous equations. This model has high efficiency in econometrics, in estimating and predicting the economic parameters. But so far, no studies have been done in the water field. In this study, the efficiency of this model (VAR) is investigated using pan evaporation data in the Salt Lake Basin stations in Iran in the statistical period of 1996–2015 on an annual scale. Also, to study the efficiency of the VAR model, the nonlinear GARCH model has been used.

2. Materials and methods

2.1. Study areas and data

Iran with an area of over 1,648,000 square kilometers has been located in the northern hemisphere and on the Asian continent. The climate of Iran has almost four seasons in all its parts, and in general, one year can be divided into two cold and two hot seasons. Iran with an average annual rainfall of 62.1-344.8 mm has been located between the two meridians of 44° and 64° east and two orbits of 25° and 40° north. About 94.8 percent of the country's surface is in arid and semi-arid regions with low rainfall and high evapotranspiration.

In this study, pan evaporation data from stations in the Salt Lake Basin (Qom, Qazvin, Hamedan, Arak, Tehran, and Karaj stations) have been used in the annual period of 1996–2015. Since the objective model is multivariate, adjacent station data were also used. The specifications and the position of the stations are presented in *Table 1* and *Fig. 1*, respectively.

Table 1. Specifications of the stations in the statistical period 1996–2015 (mm per year)

Station	Min	Max	Mean	STD
Arak	1762.10	2268.70	1959.24	126.19
Hamedan	1415.30	1941.80	1668.19	144.79
Karaj	1601.30	2162.90	1932.77	175.22
Qazvin	1373.70	1805.50	1619.51	116.48
Qom	2453.60	2920.70	2650.87	133.30
Tehran	20.00	2690.40	2175.57	775.07

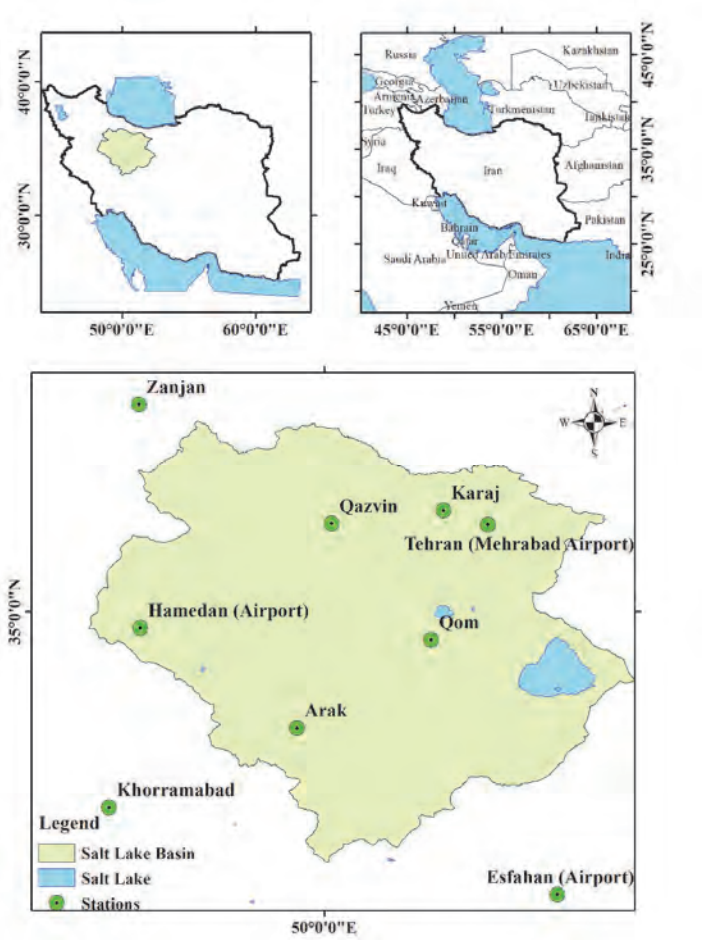

Fig. 1. Location of study areas in Iran.

2.2. Time series analysis

Time series modeling is performed on static random data. Therefore, certain components of the series should be removed and the series become static. The definitive components of a time series include trends and periods. In addition to statics, the series must also follow the normal distribution. To determine the trend in this study, the modified Mann-Kendall test was used (*Kendall*, 1938; *Mann*, 1945; *Khalili et al*, 2016; *Tahroudi et al*, 2019b; *Khozeymehnejad* and *Tahroudi*, 2019). After evaluation and deleting the trend (if any), the standardized and normal data will be prepared for use in the above models.

2.3. ARCH models

This model was first presented in economic studies by *Engle* (1982) and was the first to provide a systematic framework for modeling fluctuations. The main idea of the ARCH models is that (a) the modified average investment return is distinct but dependent and (b) the model is dependent and can be described by a simple quadratic function of the values before it. In summary, the ARCH model is assumed to be:

$$\varepsilon_t = \sigma_t z_t \quad and \quad \sigma_t^2 = a_0 + \sum_{i=1}^{m} b_i \varepsilon_{t-i}^2 , \tag{1}$$

where σ_t^2 is the conditional variance, ε_t is the error term or the remainder of the model with mean value of zero and variance of 1, $a_0 \geq 0, b_i \geq 0$ are the model parameters, *m* is equal to the order of the model, and z_t is also the time series of the desired parameter (*Engle*, 1982).

2.4. ARCH model structure

To better understand the model, the structure of the ARCH model (1) was considered.

$$a_t = \sigma_t \varepsilon_t , \ \sigma_t^2 = a_0 + a_1 a_{t-1}^2 , \tag{2}$$

where $a_1 \geq 0, a_0 \geq 0$. First of all, the conditional mean a_t must be zero, because:

$$E(a_t) = E[E(a_t \mid F_{t-1})] = E[\sigma_t E(\varepsilon_t)] . \tag{3}$$

Then, the conditional variance is obtained from the following equation:

$$Var(a_t) = E(a_t^2) = E[E(a_t^2 \mid F_{t-1})] = E[a_0 + a_1 a_{t-1}^2] = a_0 + a_1 E(a_{t-1}^2) . \tag{4}$$

Since, according to $E(a_t = 0)$ and $Var(a_t) = E(a_{t-1}) = E(a_{t-1}^2)$, a_t is a static and fixed trend, we will have:

$$Var(a_t) = a_0 + a_1 Var(a_t), \tag{5}$$

$$Var(a_t) = \frac{a_0}{(1-(a_0))}. \tag{6}$$

Since the variance of a_t should be positive, the range of a_1 should be between 0 and 1.

In some applications, values above (a_t) should also exist, and so, a_1 should provide some extra moments. For example, in studying the behavior of sequences, it is necessary to limit the fourth moment (a_t). Assuming that ε_t is normal, we will have the following equation (*Engle*, 1982):

$$E[E(a_t^4 \mid F_{t-1})] = 3[E(a_t^2 \mid F_{t-1})]^2 = 3E(a_0 + a_1 a_{t-1}^2)^2. \tag{7}$$

So:

$$E(a_t^4) = E[E(a_t^4 \mid F_{t-1})] = 3E(a_0 + a_1 a_{t-1}^2)^2 = 3E(a_0^2 + 2a_0 a_1^2 a_{t-1}^2 + a_1^2 a_{t-1}^4). \tag{8}$$

If a_t is considered as the fourth constant and $m_4 = E(a_t^4)$, then:

$$m_4 = 3E(a_0^2 + 2a_0 a_1 Var(a_t) + a_1^2 m_4) = 3a_0^2(1 + 2\frac{a_1}{1-a_1}) + 3a_1^2 m_4. \tag{9}$$

Eventually:

$$m_4 = \frac{3a_0^2(1+a_1)}{(1-a_1)(1-3a_1^2)}. \tag{10}$$

2.5. GARCH model

Although the ARCH model is simple, it often requires a lot of parameters to obtain the proper modeling process. For this reason, we have to look for alternative models (*Moffat et al.*, 2017). *Bollerslev* (1992) proposed the developed ARCH model as follows:

$$\alpha_t = \sigma_t e_t$$
$$\sigma_t^2 = \alpha_0 + \sum_{i=1}^{q} \alpha_i \alpha_{t-i}^2 + \sum_{j=1}^{p} \beta_j \sigma_{t-j}^2 , \quad (11)$$

where, e_t is equal to a random series with mean value of zero and variance of one. In fact, the EGARCH model is a natural logarithmic model of the GARCH method, which was presented by *Nelson* (1991).

2.6. Vector autoregressive models

VAR is one of the most successful and flexible models for analyzing multivariate series. This model is, in fact, a model extended from the uniform autoregressive model of multi-variable time series. The VAR model was introduced to describe the dynamic behavior of the economic and financial series and their prediction. This model often provides superior predictions for those who use similar and accurate time series models. VAR model predictions are quite flexible, since they can bet on the future path of potential variables. In addition to describing and forecasting data, the VAR model is also used for structural inferences and analysis policies. In structural analysis, specific hypotheses are imposed on the structure of the data under investigation, and the effects of unexpected shocks or innovations are summed up with the variables specified on the model variables. These effects are usually summarized with impact reaction and predicted error variance analysis functions. This model focuses on the analysis of constant covariance multivariate. VAR models in economics have been introduced by *Sims* (1980). The technical review of VAR models can be found in the *Lütkepohl* (1999) study, and updated VAR techniques are described in researches conducted by *Watson* (1994), *Lütkepohl* (1999), and *Waggoner* and *Zha* (1999). The use of VAR models for financial information has been given in the studies carried out by *Hamilton* (1994), *Campbell et al.* (1997), *Cuthbertson* and *Nitzsche* (1996), *Mills* (1999), and *Tsay* (2001).

If $Y_t = (y_{1t}, y_{2t}, ..., y_{nt})^{/}$ represents the vector ($n \times 1$) of the time series variables, then the VAR (p) model with a p-year base delay is as follows:

$$Y_t = c + \Pi_1 Y_{t-2} + ... + \Pi_p Y_{t-p} + \varepsilon_t , \quad t = 1, ..., T , \quad (12)$$

where Πi is equal to the coefficient ($n \times n$) of the matrix and ε_t is equal to the matrix ($n \times 1$) of the white noise values with mean value of zero (non-dependent or independent) with constant covariance matrix Σ. For example, the equation of the two-variable VAR model is as follows:

$$\begin{pmatrix} y_{1t} \\ y_{2t} \end{pmatrix} = \begin{pmatrix} c_1 \\ c_2 \end{pmatrix} + \begin{pmatrix} \pi_{11}^1 & \pi_{12}^1 \\ \pi_{21}^1 & \pi_{22}^1 \end{pmatrix} \begin{pmatrix} y_{1t-1} \\ y_{2t-1} \end{pmatrix} + \begin{pmatrix} \pi_{11}^2 & \pi_{12}^2 \\ \pi_{21}^2 & \pi_{22}^2 \end{pmatrix} \begin{pmatrix} y_{1t-2} \\ y_{2t-2} \end{pmatrix} + \begin{pmatrix} \varepsilon_{1t} \\ \varepsilon_{2t} \end{pmatrix} \tag{13}$$

or

$$\begin{aligned} y_{1t} &= c_1 + \pi_{11}^1 y_{1t-1} + \pi_{12}^1 y_{2t-1} + \pi_{11}^2 y_{1t-2} + \pi_{12}^2 y_{2t-2} + \varepsilon_{1t} \\ y_{2t} &= c_2 + \pi_{21}^1 y_{1t-1} + \pi_{22}^1 y_{2t-1} + \pi_{21}^2 y_{1t-1} + \pi_{22}^2 y_{2t-1} + \varepsilon_{2t} \end{aligned}, \tag{14}$$

where $\text{cov}(\varepsilon_{1t}, \varepsilon_{2t}) = \sigma_{12}$ for $t = s$, otherwise it is zero. Note that each equation has a similar regression of the remainder of y_{1t} and y_{2t}. Hence, the VAR (p) model is just an indirect regression model with remaining variables and definitive terms as common regressions. From a user's perspective, the VAR (p) model is written as:

$$\Pi(L)Y = c + \varepsilon_t , \tag{15}$$

where $\Pi(L) = I_n - \Pi_1 L - ... - \Pi_1 L^p$. Now if the value of the determinant value of $(I_n - \Pi_1 z - ... - \Pi_p z^p)$ is zero, then the VAR (p) will be static.

If the eigenvalues of a composite matrix have a modulus of less than one, it is outside the complex unit loop (with a modulus greater than one), or equivalent, if the eigenvalues of the composite matrix have a modulus less than one. It is assumed that the process in the past has been initiated from infinite value, then it is a stable process of VAR (p) with constant mean variance and covariance. If Y_t in Eq.(13) is constant covariance, then the mean is given by:

$$F = \begin{pmatrix} \Pi_1 & \Pi_2 & .... & \Pi_n \\ I_n & 0 & .... & 0 \\ 0 & . & 0 & : \\ 0 & 0 & I_n & 0 \end{pmatrix} \tag{16}$$

$$\mu = (I_n - \Pi_1 - ... - \Pi_p)^{-1} c . \tag{17}$$

After the adjusted mean of the VAR (p) model:

$$Y_t - \mu = \Pi_1 (Y_{t-1} - \mu) + \Pi_2 (Y_{t-2} - \mu) + ... + \Pi_p (Y_{t-p} - \mu) + \varepsilon_t . \tag{18}$$

The basic VAR (p) model may be very limited to show the main characteristics of the data. Specifically, other conditions of determinism such as a linear time trend or seasonal variables may be used to display data correctly. Additionally, random variables may also be required. The general form of the VAR (p) model with definitive terms and external variables is as follows:

$$Y_t = \Pi_1 Y_{t-1} + \Pi_2 Y_{t-2} + ... + \Pi_p Y_{t-p} + \Phi D_t + G X_t + \varepsilon_t , \quad (19)$$

where D_t is the matrix (l × 1) of the definite components, X_t is equal to the matrix (m × 1) of the external variables, and Φ and G are also matrix of the model parameters.

2.7. Model performance

In order to evaluate the performance of the model, two Nash-Sutcliff and root mean square error criteria were used. Lower RMSE and higher Nash-Sutcliff coefficients represent the higher accuracy of the model.

$$RMSE = \sqrt{\frac{\sum_{i=1}^{n} (\widehat{Q}_i - Q_i)^2}{n}} . \quad (20)$$

$$NSE = 1 - \frac{\sum_{i=1}^{n} (\widehat{Q}_i - Q_i)^2}{\sum_{i=1}^{n} (Q_i - \overline{Q_i})^2} . \quad (21)$$

In the above relations, Q_i, $\widehat{Q}_i$, and $\overline{Q_i}$ are the observational computational, and mean values of the observational values respectively, and n is the number of data (*Akbarpour et al*., 2020; *Tahroudi et al*., 2019a).

3. Results and discussion

At first, preliminary results of time series including trend, randomness of data, and data normal survey have been presented. Then the results of the vector multivariate annual model of time series have been presented in the modeling of annual pan evaporation rates. After reviewing, correcting, and completing the data, the trend of data changes was studied for modeling and initial data analysis. By eliminating the trend of time series, data changes are considered to be constant over time, and this increases the modeling accuracy in ARMA family models. The results of the trend of pan evaporation changes and slope of trend line are presented in the two annual and monthly scales are in *Tables 2* and *3*.

Table 2. Results of the slope of trend line in the statistical period of 1996-2015 in annual and monthly scales

Station	Jan	Feb	Mar	Apr	May	Jun	Jul	Aug	Sep	Oct	Nov	Dec	Annual
Arak	0.00	0.00	-0.49	-0.27	-0.36	-0.08	1.03	0.01	-0.32	-1.42	-2.45	0.00	-9.69
Hamedan	0.00	0.00	0.00	3.62	1.53	1.57	2.65	1.54	1.71	-0.28	-0.27	0.00	11.09
Karaj	0.00	0.00	0.00	2.00	4.70	5.03	6.65	3.05	3.02	1.75	1.16	0.00	12.89
Qazvin	0.00	0.00	0.00	0.44	-0.35	-0.62	2.90	0.32	-0.37	-0.49	-0.99	0.00	0.9
Qom	0.00	0.00	8.61	1.07	-1.43	-1.26	0.28	-1.73	-2.58	-1.69	-1.45	0.17	-6.40
Tehran	0.00	0.00	3.50	4.60	0.67	2.20	0.00	-3.20	-4.03	-2.76	-2.39	-0.62	-6.09

Table 3. Results of the Z statistics of modified Mann-Kendall test in the statistical period of 1995–2015 annual and monthly scales

Station	Jan	Feb	Mar	Apr	May	Jun	Jul	Aug	Sep	Oct	Nov	Dec	Annual
Arak	1.39	-0.63	-0.33	-0.23	-0.16	-0.03	0.62	0.00	-0.36	-0.75	-1.20	-0.07	-1.22
Hamedan	-0.68	-0.69	1.80	1.65	1.07	1.14	1.98	1.91	1.52	-0.1	-0.36	-1.21	1.27
Karaj	0.50	0.00	-1.51	0.63	1.40	1.26	3.15	2.04	1.52	0.75	0.65	0.65	1.10
Qazvin	1.04	-0.87	-0.79	0.36	-0.29	-0.36	1.59	0.23	-0.23	-0.36	-0.29	-1.19	0.03
Qom	-0.16	2.66	3.10	0.29	-0.94	-1.40	0.10	-0.98	-2.24	-1.14	-1.14	0.23	-1.40
Tehran	-1.08	0.33	1.95	1.54	0.11	0.77	0.06	-0.75	-1.33	-1.04	-1.56	-0.93	-0.40

The variation trend of annual pan evaporation rates at the stations showed that the variation of this parameter in the studied area is a combination of increasing and decreasing trends. The results of the annual variation of the stations showed that the north and northwest areas of the studied basin had a decreasing trend, and the border areas have experienced a significant incremental trend in the annual pan evaporation values during the statistical period. These results indicate an increase in the pan evaporation during the statistical period in these areas, which can be attributed to the increase in temperature and climate change, as well as global warming. On the other hand, *Tabari* and *Talaee* (2011), *Saboohi et al.* (2012), *Kousari et al.* (2013), *Zamani et al*. (2018), and *Khalili et al.* (2016) showed that there is an increasing trend in

temperature in Iran, especially in the cold months of the year, therefore, temperature variations can be considered as one of the reasons for the decrease or increase of evaporation in the study area. In the meanwhile, the boundary and southern stations of the study area have experienced a decreasing trend in the annual pan evaporation rates in the studied statistical period that the trend of changes in the values of this parameter on the southern border is reduced and significant. In general, the results of the study of the changes in the values of the parameter in the studied period showed that the southern half of the study area experienced decreasing trend, while the northern part of the study area experienced incremental trend. Regarding the slope of the trend line, the maximum incremental changes in annual pan evaporation rates is related to the Karaj station, and the highest decreasing changes in the parameter values are at the annual scale is associated with the Arak station. It should be noted that the stations where the process of evaporation changes from the mattress in them had decreasing or significant increase. Using the 3-year moving average, the trend of annual and monthly changes of these data changed from significant to non-significant. Regarding the length of the statistical period, the significance level of 1% was considered as the base level. The randomness of the data was also evaluated using the Wald-Wolfowitz test. The results showed that the pan evaporation rates at the stations at the significance level of 1% and 5% were randomized. After reviewing the existing data, normalization methods were used to normalize the data, and the results are presented in *Table 4*. Also, to test the normality of the time series of the data, the skewness coefficient test was used. The results of the investigation of the normality of the data under investigation after fitting them with normal distribution functions showed, that based on the skewness test, the normalized data are in the confidence range of normality. After reviewing the normalization functions and ensuring that the data are normal, normal data were standardized and fitted by multivariable vector models in the annual scale.

Table 4. Results of normalization methods in normalizing the data

Station	Initial skewness coefficient	Secondary skewness coefficient	Distribution coefficient	Normalized distribution
Arak	0.69	0.08		Gamma
Hamedan	0.13	0.00	0.19	Box-Cox
Karaj	-0.36	-0.25	2.00	Box-Cox
Qazvin	-0.33	-0.19	2.00	Box-Cox
Qom	0.34	0.04		Gamma
Tehran	-1.62	0.12		Gamma

4. Results of modeling the pan evaporation values using VAR model

After the preliminary review of the data in this study, we examined the number of permitted delays and valid data to predict and interfere with the effective parameters in the data combination. For example, the results of examining the effective parameters and the number of permitted delays are presented in *Table 5*. 95% confidence intervals were used in the calculations in order to approve the permitted number of delays and the number of effective parameters.

Table 5. Results of investigation of correlation and number of delay of Arak station with other stations

Station	Lags	Coefficient	Standard error	z	P>|z|	95% confidence intervals		Results
Arak	L1.	0.279	0.189	1.470	0.140	-0.092	0.651	Reject
	L2.	0.495	0.179	0.770	0.806	0.145	0.845	Accept
Hamedan	L1.	0.006	0.180	0.030	0.973	-0.347	0.359	Accept
	L2.	0.341	0.137	2.480	0.013	0.072	0.611	Reject
Karaj	L1.	-0.261	0.178	-1.470	0.141	-0.610	0.087	Reject
	L2.	-0.068	0.182	-0.370	0.370	-0.425	0.289	Accept
Qazvin	L1.	-0.543	0.240	-2.260	0.024	-1.014	-0.072	Reject
	L2.	0.124	0.265	0.470	0.369	-0.369	0.644	Accept
Qom	L1.	0.605	0.186	3.250	0.001	0.240	0.969	Reject
	L2.	-0.183	0.223	0.120	0.512	-0.620	0.245	Accept
Tehran	L1.	0.085	0.042	0.101	0.545	0.002	0.186	Accept
	L2.	0.037	0.039	0.940	0.346	-0.040	0.114	Reject
Total		-217.212	707.080	-0.310	0.759	-1603.063	1168.640	Accept

According to the results of the study of the contribution of pan evaporation data in modeling and predicting the mentioned values, it can be seen that in the prediction of pan evaporation values of Arak station (*Table 5*), Arak, Karaj, Qazvin and Qom stations contribute with the second delay and Tehran station with the first delay. In the modeling and prediction of pan evaporation values of the Hamadan station, the pan evaporation values of Arak, Hamedan, and Tehran stations contributed with the first delay, and pan evaporation values of Karaj, Qazvin, and Qom stations contribute with the second delay in modeling and predicting pan evaporation. Similarly, stations of Arak, Hamedan, Karaj, and Qazvin contribute with the first delay and Qom and Tehran stations with the second delay in predicting pan evaporation rates of the Karaj Station. The results of the study on the participation of pan evaporation values in predicting and modeling this parameter at Tehran station showed, that both delays contributed in the stations of Arak,

Hamadan, Karaj, Qazvin, and Qom. However, the pan evaporation values of Tehran station will not contribute to the modeling and prediction of this parameter.

According to the mentioned conditions, modeling of pan evaporation values at the stations was studied using vector autoregressive models. The modeling of the values was done with the VAR model based on the 1000-value Monte Carlo simulation. The results of the modeling of the pan evaporation values in the annual scale using the VAR model are presented in *Figs. 2* and *3*. The results of the study on the accuracy of the model in time series simulation of pan evaporation in the simulation stage are also presented in *Table 6*.

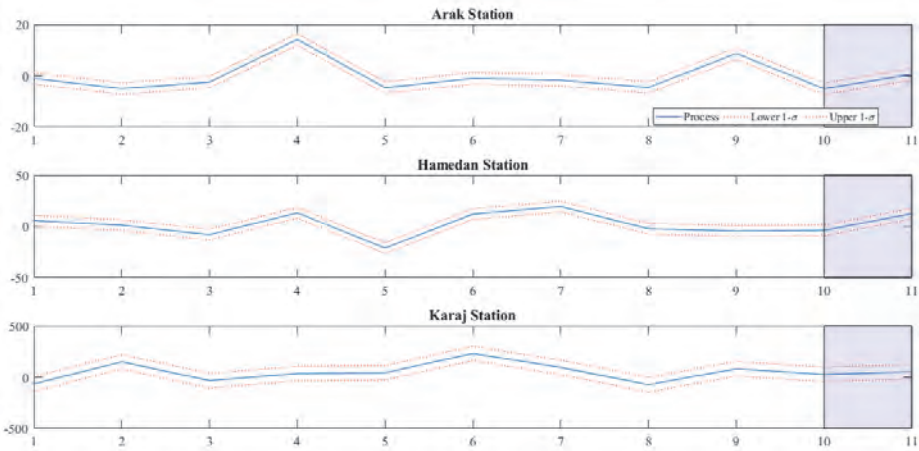

Fig. 2. Verification of simulated values by using vector autoregressive model at Arak, Hamedan, and Karaj stations.

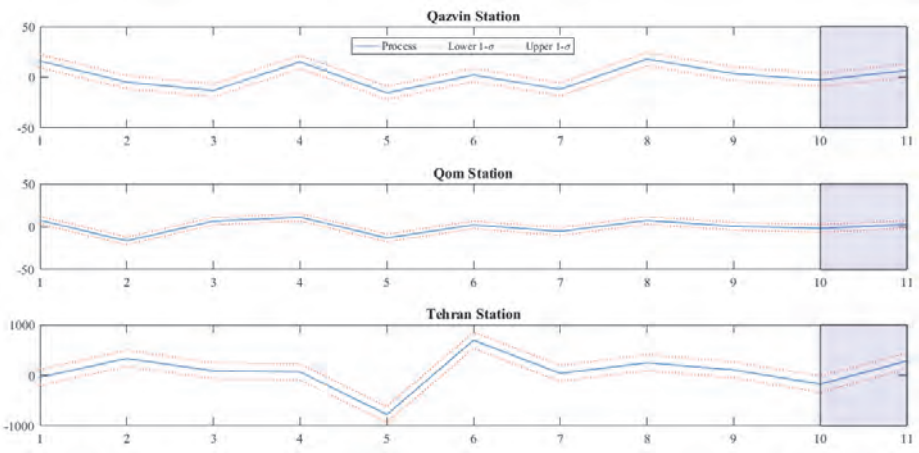

Fig. 3. Verification of simulated values by using vector autoregressive model at Qazvin, Qom, and Tehran stations.

Table 6. Results of the accuracy and efficiency of the VAR model in simulating the annual pan evaporation values

Station	Arak	Hamedan	Karaj	Qazvin	Qom	Tehran
Correlation coefficient	0.61	0.99	0.98	0.98	0.90	0.99
Nash- Sutcliffe coefficient	0.25	0.99	0.97	0.97	0.85	0.99
RMSE	11.37	6.62	14.48	13.45	25.50	21.34

The results of the study of accuracy of the model using the correlation coefficient extracted from the simulated and observed values of pan evaporation time series showed, that the accuracy of the model between the existing stations is between 61% and 99%. On average, the accuracy of the VAR model in simulating pan evaporation values of the existing stations is about 91%. The maximum accuracy of modeling and prediction of pan evaporation values is associated with the Hamedan and Tehran stations, and the minimum accuracy related to the pan evaporation time series of the Arak station in the annual scale. The results of the study of the error rate of the VAR model in simulating pan evaporation values of the studied stations in the Salt Lake Basin were estimated in annual scale using the root mean square error (RMSE). The results showed that the error values in the existing stations varied from 6.62 to 25.55 mm per year. The highest error is related to Qom station, and the lowest error rate is related to Hamedan station. The average error rate of the VAR model in simulating pan evaporation values in the verification stage at an annual scale is 15.46 mm/year. The results of the evaluation of the error values due to pan evaporation time series modeling of the stations in the annual scale showed, that all simulated cases are in the 95% confidence intervals and acceptable. Considering the range of time series variations, the accuracy of the models and their error rate are accepted and confirmed. The efficiency of the VAR model in simulating pan evaporation in the Salt Lake Basin was investigated using the Nash-Sutcliffe test (N-S). The average model efficiency for stations in the Salt Lake Basin is about 84%. Except for Arak station, other stations have efficiency more than 90%.

After verifying the accuracy and efficiency of the VAR model in estimating the pan evaporation values in the salt lake basin, the remaining series values of the VAR model resulting from the modeling of the parameters in the annual scale using the nonlinear GARCH model were investigated and fitted. After combining the vector autoregressive model with the GARCH model, the hybrid model of VAR-GARCH was formed. The results of the study and comparison of the two VAR and VAR-GARCH models in modeling and estimating the pan evaporation values in the annual scale in the catchment area of the Salt Lake in the statistical period are presented in *Table 7*.

Table 7. Comparison of the error rate and efficiency of the two studied models

Station	Percentage of getting better the error of hybrid model	Percentage of getting better the performance of hybrid model	RMSE of hybrid model (mm/year)	N-S of hybrid model (%)	Correlation coefficient of hybrid model
Arak	3.38	-1.40	10.98	95	0.99
Hamedan	3.97	1.32	6.35	99	0.99
Karaj	7.78	3.20	13.35	92	0.94
Qazvin	1.40	2.08	13.26	99	0.99
Qom	5.98	0.80	23.97	92	0.96
Tehran	3.28	0.40	20.64	98	0.97

After verifying the accuracy of the VAR-GARCH model in simulating pan evaporation values on an annual scale, this parameter was simulated using pan evaporation values of adjacent stations and predicted for 5 years (2015–2020). The results of the prediction of pan evaporation values are presented in *Figs. 4* and *5* using the VAR-GARCH model.

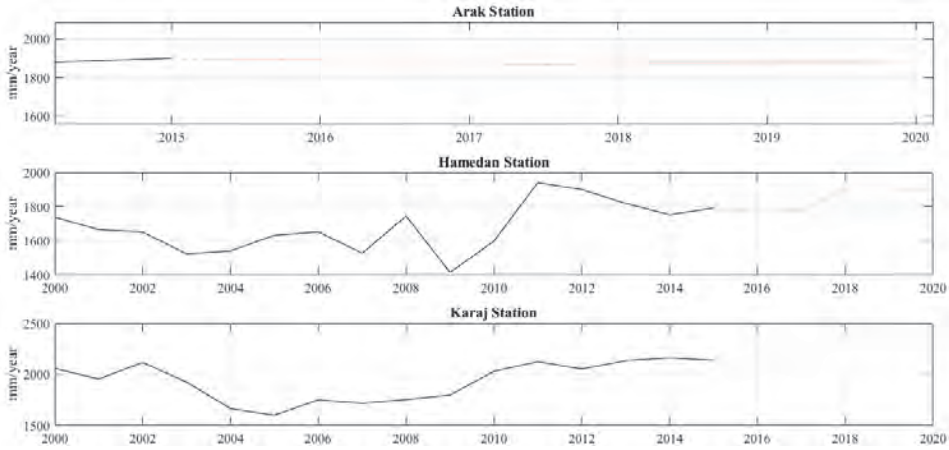

Fig. 4. Prediction of pan evaporation values in the period of 1996-2020 at Arak, Hamadan, and Karaj stations using the VAR-GARCH model.

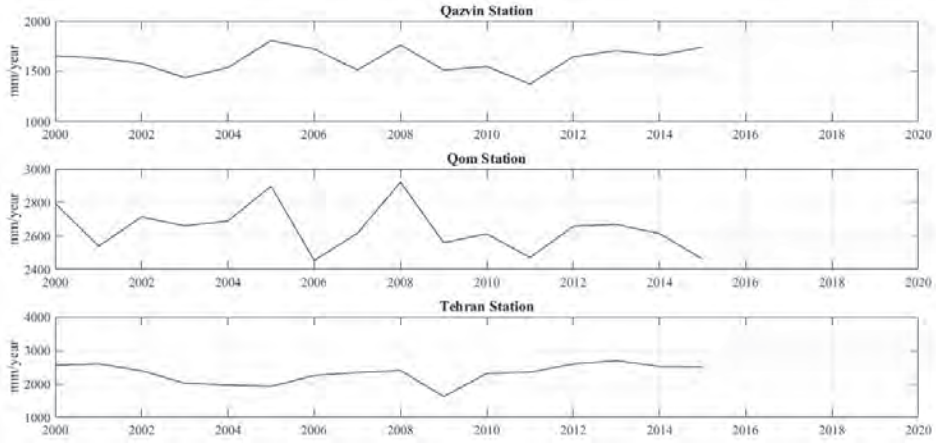

Fig. 5. Prediction of pan evaporation values in the period of 1996-2020 at Qazvin, Qom, and Tehran stations using the VAR-GARCH model.

The results of modeling pan evaporation values using multivariate vector time-series models showed, that these models have high ability to model these values under the influence of pan evaporation of other stations. As it can be seen from the results, the VAR and VAR-GARCH models have been able to simulate and predict pan evaporation values. It is clear, that at all stations the correlation between observational and computational data and the performance of the model at all stations are high. The results of the modeling of the monthly pan evaporation values under the influence of annual pan evaporation values of other adjacent stations showed that multivariable vector hybrid models at the Tehran station located in the northeast of the basin have lower accuracy and lower efficiency.

The results of the vector-hybrid models showed that using these models improved the error of modeling of the pan evaporation values of the Arak, Hamedan, Karaj, Qazvin, Qom, and Tehran stations on average by 4, 4, 8, 1, 6, and 3% respectively. The results of the accuracy of the studied models showed that vector-hybrid models provide better results than vector time series models. Also, due to the large effect of the pan evaporation parameter of the adjacent stations and the interference of this parameter, pan evaporation values of each station were modeled well. For this reason, by interfering with the parameters associated with the data used in modeling, the accuracy of modeling and analysis can be greatly increased. The results obtained by *Camacho et al.* (1985) showed the superiority of multivariate models compared to single-variable models. Also, the results showed that among two hybrid and multivariate models, hybrid models provide better fitness and less error than multivariate

models, although the accuracy of multivariate models is acceptable, which is consistent with the studies conducted by *Tesfaye et al*. (2006) in the modeling of seasonal flow discharge of the British Frieser River. On the other hand, by adding nonlinear models to linear time series models, the model's uncertainty can be partially eliminated. The results showed that the hybrid model was more accurate than the linear time series model, which is consistent with *Wang et al* (2005), *Caiado* (2007), and *Laux* (2011). Since the autoregressive model is an annual and single-variable model, using the VAR model as an alternative to the AR model is the best option. Because in addition to using multivariate mode, other effective parameters are introduced with appropriate delays.

5. Conclusion

Using monthly and annual pan evaporation time series data, the variation trend of the parameter was investigated in monthly and annual scales. The data of the evaporation gauge stations of the center provinces of Iran located in the catchment area of the Salt Lake during the period of 1996–2015 were analyzed using a modified Mann-Kendall test. The results of this study showed that the southern and eastern stations of the studied area have a decreasing trend and the northern and western stations have an increasing trend. On the annual scale, the highest incremental trend happened at the Karaj station based on the trend line slope, which was about 257 units during the 20-year-long statistical period. According to the results of the study, the Arak station has experienced the most evaporation reduction during the 20-year-long statistical period. These decreasing trends were around 200 units over the past 20 years. On a monthly scale, the results of the study of the pan evaporation data showed, that in all studied months, the trend of changes in the parameter values in the studied period in the north and northwest parts of the study area and the Karaj, Hamedan, and Qazvin stations have an unreasonable and significant increase, indicating a decrease in humidity, an increase in evaporation and temperature in the area. In general, the results indicate an increase in the pan evaporation rate in the north and northwest basin in all months, which indicates warming and increasing temperature in these areas. As the temperature increases and the humidity decreases, the pan evaporation rate increases.

The conditional nonconformity (variable time variance or oscillation) is usually ignored in the context of meteorological variable modeling. The present study shows that although the VAR approach is sufficient to model the conditional average of pan evaporation time series, the ARCH effect will still improve the results. Identification of ARCH effects and the inability of the VAR method to eliminate the effect of conditional variance are out of the scope of this study. However, the presence of the ARCH effect in the pan evaporation rates may be due, in part, to fluctuations in variance reported by *Wang et al*. (2005).

Other factors which may prove the effects of ARCH in hydrological periods are fluctuations in air temperature, effective factor for snow drops, and evapotranspiration and precipitation changes. Similar reports have been presented by *Modarres* and *Ouarada* (2013) on the reasons for this work. In these reports, conditional non-correlation may be due to climate factors that affect the hydrological series variance changes. The VAR-GARCH approach demonstrated the ability to model conditional variance. On the other hand, this approach improves the performance of multi-criteria error estimation. This result can be one of the important aspects of pan evaporation modeling in areas, where some of the evaporation stations are located within a region with climatic variation. As a result, this study shows that the VAR-GARCH model with a suitable change can increase the performance of time series and have a conditional nonconformity stability. Regarding the structure of conditional-covariance variance and correlation, *Modarres* and *Ouarada* (2013) stated that this is a physical feature of the watershed that may affect the existence of the variance of the time variable in the remainder. The results of linear and nonlinear hybrid vector models in modeling the annual and monthly pan evaporation rates at the site of evaporation stations studied at the catchment area of the Salt Lake showed, that pan evaporation values of the studied stations have the best fitness in annual scale with hybrid models. The results of the study of the accuracy of these models in modeling the pan evaporation values of the stations showed, that the VAR-GARCH hybrid models have a high accuracy relative to the vector models and have been able to model the pan evaporation rates with the lowest error rate. Of the two models that both have annual nature (VAR and VAR-GARCH), the best model can be selected based on the estimation of the error values. In this study, we first looked at the accuracy of the relatively new autoregressive vector model called VAR. The results of the estimation of error and the efficiency of the model indicated the acceptable accuracy of this model in estimating the pan evaporation values in the annual scale. The 95% confidence interval confirmed the simulation results of the calibration step. Generally, according to the range of data variations, as well as the computational errors and accuracy, we can see the appropriate performance of this model. The improvement percentage in the results of modeling pan evaporation rates in the annual scale using the VAR-GARCH model is about 4% relative to the VAR model. However, due to modeling the random section and reducing the uncertainty of the model, the results of modeling the pan evaporation rates using the VAR-GARCH model are better than the VAR model. However, considering the complexity of the GARCH model calculations, we can ignore the 4% improvement of the model. However, this model is presented for a salt lake watershed, and more research is needed in different climates for general conclusion, and generalizing it to all areas.

References

Akbarpour, A., Zeynali, M.J., and Tahroudi, M.N., 2020: Locating optimal position of pumping Wells in aquifer using meta-heuristic algorithms and finite element method. *Water Res. Manag 34*, 21–34. https://doi.org/10.1007/s11269-019-02386-6

Ashrafzadeh, A., Malik, A., Jothiprakash, V., Ghorbani, M.A., and *Biazar, S.M.*, 2018: Estimation of daily pan evaporation using neural networks and meta-heuristic approaches. *ISH J. Hydraulic Engin.*, 1–9. https://doi.org/10.1080/09715010.2018.1498754

Bollerslev, T., Chou, R.Y., and Kroner, K.F., 1992: ARCH modeling in finance. A selective review of the theory and empirical evidence. *J. Econometrics 52*, 5–59. https://doi.org/10.1016/0304-4076(92)90064-X

Caiado, J., 2007: Forecasting water consumption in Spain using univariate time series models. Munich Personal RePEc Archive, no: 6610.

Camacho, F., McLeod, A.I., and Hipel, K.W., 1985: Contemporaneous autoregressive - moving average (CARMA) modeling hydrology. *Water Res. Bull. 21*,709–720. https://doi.org/10.1111/j.1752-1688.1985.tb05384.x

Campbell, J.Y., Lo, A.W., and *MacKinlay, A.C.*, 1997: The econometrics of financial markets (Vol. 2.) Princeton, NJ: Princeton University press. 149–180. https://doi.org/10.1515/9781400830213

Cuthbertson, K. and *Nitzsche, D.*, 1996: Quantitative financial economics: stocks, bonds and foreign exchange. John Wiley & Sons.

Engle, R.F., 1982: Autoregressive conditional heteroscedasticity with estimates of the variance of United Kingdom inflation. Econometrica: *J. Econometric Soc. 50*, 987–1007. https://doi.org/10.2307/1912773

Franses, P.H. and V*an Dijk, D.*, 2000: Non-linear time series models in empirical finance. Cambridge University Press. https://doi.org/10.1017/CBO9780511754067

Ghorbani, M.A., Deo, R.C., Yaseen, Z.M., Kashani, M.H., & *Mohammadi, B.*, 2018: Pan evaporation prediction using a hybrid multilayer perceptron-firefly algorithm (MLP-FFA) model: case study in North Iran. *Theor. Appl. Climatol. 133*, 1119–1131. https://doi.org/10.1007/s00704-017-2244-0

Hamilton, J.D., 1994: Time series analysis (Vol. 2). Princeton, NJ: Princeton Univ. Press. 690–696.

Kendall, M.G., 1938: A new measure of rank correlation. *Biometrika 30*, 81–93. https://doi.org/10.1093/biomet/30.1-2.81

Khalili, K., Tahoudi, M.N., Mirabbasi, R., and Ahmadi, F., 2016: Investigation of spatial and temporal variability of precipitation in Iran over the last half century. *Stoch. Environ. Res. Risk Assess. 30*, 1205–1221. https://doi.org/10.1007/s00477-015-1095-4

Khozeymehnezhad, H. and *Tahroudi, M.N.*, 2019: Annual and seasonal distribution pattern of rainfall in Iran and neighboring regions. *Arabian J. Geoscie. 12*, 271. https://doi.org/10.1007/s12517-019-4442-9

Kousari, M.R., Ahani, H., and *Hendi-zadeh, R.*, 2013: Temporal and spatial trend detection of maximum air temperature in Iran during 1960–2005. *Glob. Planet. Change 111*, 97–110. https://doi.org/10.1016/j.gloplacha.2013.08.011

Laux, P., Vogl, S., Qiu, W., Knoche, H.R., and *Kunstmann, H.*, 2011: Copula-based statistical refinement of precipitation in RCM simulations over complex terrain. *Hydrol. Earth Syst. Sci. 15*, 2401–2419. https://doi.org/10.5194/hess-15-2401-2011

Lütkepohl, H., 1999: Vector autoregressions. A companion to theoretical econometrics, 678–699. https://doi.org/10.1002/9780470996249.ch33

Mann, H.B., 1945: Nonparametric tests against trend. *Econometrica 13*, 245–259. https://doi.org/10.2307/1907187

Mills, T.C., 1999: The Econometric Modeling of Financial Time Series, Second Edition. Cambridge University Press, Cambridge.

Modarres, R. and *Ouarda, T.B.*, 2013: Generalized autoregressive conditional heteroscedasticity modelling of hydrologic time series. *Hydrol. Proc. 27*, 3174–3191. https://doi.org/10.1002/hyp.9452

Moffat, I.U., Akpan, E.A., and *Abasiekwere, U.A.* 2017: A time series evaluation of the asymmetric nature of heteroscedasticity: an EGARCH approach. *Int. J. Stat. Appl. Math. 2 (6)*, 111–117.

Nelson, D.B., 1991: Conditional heteroskedasticity in asset returns: A new approach. *Econometrica: 59*, 347–370. https://doi.org/10.2307/2938260

Priestley, M.B., 1988: Non-linear and non-stationary time series analysis. Academic Press, London.

Roesner, L.A. and *Yevjevich, V.M.*, 1966: Mathematical models for time series of monthly precipitation and monthly runoff. *Hydrol. Papers 15*, 28–29.

Saboohi, R., Soltani, S., and *Khodagholi, M.*, 2012: Trend analysis of temperature parameters in Iran. *Theor. Appl. Climatol. 109*, 529–547. https://doi.org/10.1007/s00704-012-0590-5

Salas, J.D., 1993: Analysis and modeling of hydrologic time series. Handbook of hydrology 19. 1–72.

Sims, C.A. 1980: Macroeconomics and reality. *Econometrica 48*, 1–48. https://doi.org/10.2307/1912017

Tabari, H. and *Talaee, P.H.* 2011: Temporal variability of precipitation over Iran: 1966–2005. *J. Hydrol. 396*, 313–320. https://doi.org/10.1016/j.jhydrol.2010.11.034

Tahroudi, M.N., Khalili, K., Ahmadi, F., Mirabbasi, R., and Jhajharia, D., 2019a: Development and application of a new index for analyzing temperature concentration for Iran's climate. *Int. J. Environ. Sci. Technol. 16(6)*, 2693-2706. https://doi.org/10.1007/s13762-018-1739-2

Tahroudi, M.N., Ramezani, Y., and *Ahmadi, F.*, 2019b: Investigating the trend and time of precipitation and river flow rate changes in Lake Urmia basin, Iran. *Arabian J. Geosci. 12*, 219.

Tesfaye, Y.G., Meerschaert, M.M., and *Anderson, P.L.*, 2006: Identification of periodic autoregressive moving average models and their application to the modeling of river flows. *Water Resour. Res. 42*, W01419. https://doi.org/10.1029/2004WR003772

Thomas, H.A., and *Fiering, M.B.*, 1962: Mathematical synthesis of streamflow sequences for the analysis of river basins by simulation. In (Eds. *Mass et al.*) Design of Water Resource Systems, Harvard University Press, Cambridge 459–493. https://doi.org/10.4159/harvard.9780674421042.c15

Tong, H., 1990: Non-linear time series: a dynamical system approach. Oxford University Press.

Tsay, R.S., 2001: Analysis of financial time series (Vol. 543). John Wiley & Sons.

Tsonis, A.A., 2001: Probing the linearity and nonlinearity in the transitions of the atmospheric circulation. *Nonlinear Proc. Geophys. 8*, 341–345. https://doi.org/10.5194/npg-8-341-2001

Waggoner, D.F. and *Zha, T.*, 1999: Conditional forecasts in dynamic multivariate models. *Rev. Economics Stat. 81*, 639–651. https://doi.org/10.1162/003465399558508

Wang, W., Van Gelder, P.H.A.J.M., and *Vrijling, J.K.*, 2005: Testing and modeling autoregressive conditional heteroskedasticity of streamflow processes. *Nonlin. Process. Geophys. 12*, 55–66. https://doi.org/10.5194/npg-12-55-2005

Wang, W., Vrijling, J.K., Van Gelder, P.H., and *Ma, J.*, 2006: Testing for nonlinearity of streamflow processes at different timescales. *J. Hydrol. 322*, 247–268. https://doi.org/10.1016/j.jhydrol.2005.02.045

Watson, M.W., 1994: Vector autoregressions and cointegration. Handbook of econometrics, 4, 2843–2915. https://doi.org/10.1016/S1573-4412(05)80016-9

Yeyjevich, V., 1963: Fluctuations of wet and dry years. Part I: Research data assembly and mathematical models. *Hydrology Paper 1*.

Zamani, R., Mirabbasi, R., Nazeri, M., Meshram, S.G., and *Ahmadi, F.*, 2018: Spatio-temporal analysis of daily, seasonal and annual precipitation concentration in Jharkhand State, India. *Stoch. Environ. Res. Risk Ass. 32*, 1085–1097. https://doi.org/10.1007/s00477-017-1447-3

DOI:10.28974/idojaras.2020.4.4

IDŐJÁRÁS

Quarterly Journal of the Hungarian Meteorological Service
Vol. 124, No. 4, October – December, 2020, pp. 483–497

Foehn classification and climatology in Sofia for 1975–2014

Krasimir Stoev[1,2]* and **Guergana Guerova**[2]

[1]*National Institute of Meteorology and Hydrology,*
66 Tsarigradsko shose Blvd., BG-1784 Sofia, Bulgaria

[2]*Sofia University "St. Kliment Ohridski"*
Department of Meteorology and Geophysics
5 James Bourchier blvd., BG-1164 Sofia, Bulgaria

* *Corresponding author Email:krasimir.stoev@gmail.com*

(Manuscript received in final form January 22, 2020)

Abstract— Foehn is a warm, dry, and downslope wind blowing in the lee side of a mountain range. It is a well known example of a local atmospheric circulation. The foehn wind is also an extreme weather event, and its forecasting is an important task for the short-range weather forecaster. The foehn in Bulgaria is observed on the northern slopes of the mountains, as a result of warm air advection from the south and southwest. Its occurrence is highest north of the Vitosha and Balkan mountains. In this study, a synoptic classification of the meteorological conditions leading to foehn in the central meteorological station in Sofia for the period 1975–2014 is made. Foehn climatology is prepared, and in addition, an evaluation of the foehn as an extreme weather event by wind gust is presented. For the period 1975–2014, there were 298 days with foehn in Sofia, which resulted from 220 synoptic cases. A manual foehn classification was developed with four major types. Type I is associated with the Mediterranean cyclone with the highest frequency – 52% of the foehn days. Foehn climatology gives average annual number of 7.5 foehn days but with a large variance between decades. The lowest annual number of days (4.5) is registered for the 2005–2014 period, and it was associated with the lowest recorded wind gust (22 m/s).

Key-words: foehn; extreme weather event; foehn climatology; foehn classification

1. Introduction

Foehn is a warm, dry, and downslope wind blowing in the lee side of a mountain range. In Europe, foehn is observed in many Alpine stations in Switzerland, Austria, and Italy. Studying the Altdorf foehn, *Gutermann et al.* (2012) and *Richner* and *Hachler* (2013) conclude that: 1) there is no long-term trend in the foehn frequency for a period of over 150 years, 2) there is considerable year to year variability averaging of 60 foehn observations per year, with a maximum of 114 observations (1872) and a minimum of 27 observations (1955), and 3) the foehn frequency has a pronounced seasonal cycle. Numerical modeling of foehn flows remains a challenge, even for the 1 km horizontal resolution Numerical Weather Prediction model, currently operated by MeteoSwiss (*Willemse* and *Furger,* 2016).

The occurrence of the foehn is related to the development of cyclonic vortices in the presence of an advection of warm and moist air masses from south and southwest. The Mediterranean sea is a well known area where cyclones form, and their influence over the weather and the climate in Bulgaria are discussed by many authors, such as *Stanchev* (1954), *Pisarski* (1955a,b), *Blagoev* (1961), *Martinov* (1967), *Peiter* (1975), and *Radinovic* (1987). In these works, the cyclones are identified and classified on the basis of synoptic analysis. Results for monthly and annual distribution of the cyclones, generated over the Mediterranean during the period 1980–2001, show that the highest cyclones frequency occurs during winter, from December to March (*Bocheva et al.*, 2007). After 1990, the frequency of the cyclogenesis over the Mediterranean was found to be two months shorter than average occuring mainly over the central part of the sea *(Marinova et al.* 2005*).*

The first investigations of the Mediterranean cyclone trajectories were made more than 100 years ago, to explain the different climatological conditions in particular regions in Europe (*van Bebber,* 1891). Later on, the main paths of the Mediterranean cyclones and their seasonal variability are studied by many authors: *Pisarski* (1955a,b), *Popova et al.* (1975), *Martinov* (1983), and *Jansa et al.* (2001). In almost all studies, 3 main trajectories are mentioned: path I (northwest NW), through Croatia and Hungary; path II (east E), through the Adriatic Sea and the Balkan Peninsula toward the Black Sea; path III (southeast SE then E), through the southern parts of the Balkan Peninsula toward Asia Minor.

In Bulgaria, classical foehn occurs when a Mediterranean cyclone trajectory is NW of Bulgaria (*Pisarski* 1955a,b*)*. The cyclones on path I, have different frequency through the different years. When they are predominant, winters in Bulgaria are warm (*Weather types in Bulgaria, IMH*, 1960). Path I, through Croatia and Hungary, is not typical any more *(Marinova et al.*, 2005*)*. Almost all cyclones on path I are formed over the Gulf of Genoa. Then they pass over the Apennines, the Adriatic Sea, the Dinaric Mountains, and the Hungarian

lowland. In this case, the frontal system of the cyclone is situated northwest of Bulgaria, and the Balkan Peninsula is in the warm sector of the cyclone. These synoptic conditions are most pronounced during the transitional seasons and winter. Most frequently, the upper flow consists of tropical air transported from North Africa over Bulgaria. First, the south wind orographically rises because of the mountains. When the cyclone moves over Hungary, a foehn occurs north of the mountains, and it may lead to a significant increase of temperature. When the cyclone moves NE-E of Hungary, over Bulgaria a cold front passes. Cold air advection is caused by strong NW wind.

The formation of the foehn is connected to the modification of the air flow which is influenced by the orography. The foehn in Bulgaria is observed on the northern slopes of the mountains as a consequence of warm air coming from south (S) and southwest (SW). It occurs most frequently north of the Vitosha (Sofia plain) and the Balkan mountains. Most often wind gusts reach 15–20 m/s during the foehn in Bulgaria, but there are cases when it is observed as a violent gusty wind with speeds up to 25–30 m/s, causing considerable damage.

The foehn in Sofia usually occurs during the advection of warm and moist air masses from S or SSW. After passing over the Vitosha and Lulin mountains, the air descends to the lee side (Sofia plain), and adiabatically warms and dries. When such wind is present, a cloud wall forms south of the Cherni Vruh peak (2290 m asl.) of Vitosha Mountain. The studies of *Hristov* and *Tanev* (1970) for the period 1955–1964 show that there are annually 7–8 days on average with a foehn in Sofia. In 59% of the observations with foehn there is an increase in the temperature ranging from 5 to 10 ^{o}C in 64%, from 11 to15 ^{o}C in 34%, and from 16 to 20 ^{o}C only in 2% of cases. The authors of the studies report a maximum number of days with foehn in February and March, and a minimum from June to October. More than half of the cases are with wind gust below 20 m/s.

The aim of this study is to make foehn climatology and classification of the synoptic conditions that lead to its occurrence in Sofia plain during the period 1975–2014. To achieve this, a 40-year-long period is analyzed. In Section 2, the data and the method are described. In Section 3, the results are presented. In Section 3.1, classification of the foehn type is made. In Section 3.2, the climatology of the foehn in Sofia is presented. In Section 3.3, the foehn is assessed as a severe weather event. Conclusions are given in Section 4.

2. Method and data sets

To determine the days with foehn, observations from the central meteorological station of the National Institute of Meteorology and Hydrology (NIMH) in Sofia for a 40-year-long period is analyzed. Synoptic observations are made every 3 hours at 00, 03, 06, 09, 12, 15, 18, and 21 UTC. Observations are made according to the standards and recommendations of the World Meteorological

Organization (WMO), namely: 1) wind speed and direction are measured at 10 m height above ground, and 2) the other meteorological elements are measured in a meteorological station, situated at 2 m above ground. In this study, the following meteorological elements are analyzed: 1) wind speed and direction, 2) air temperature, including the maximum temperature, 3) relative humidity, and 4) atmospheric pressure at the station level (595 m).

Foehn is best observed during the morning and evening hours, when the rise of temperature and the fall of the relative humidity are following unusual patterns. Special attention is paid to the increasing speed of the wind, accompanied by the sharp and significant increase of the temperature and sharp and significant drop of the relative air humidity. *Hristov* and *Tanev* (1970) analyzed the period 1955–1964 and proposed a quantitative criteria for determination of the occurrence of foehn: 1) appearance of a wind from south (112–247°) and an increase of its speed at least with 5 m/s, 2) sharp and considerable increase of the temperature (5 °C or above), and 3) decrease of the relative air humidity with more than 20% for 3 hours, especially in the observations in the morning and evening. The quantitative foehn criteria proposed by *Hristov* and *Tanev* (1970) are used in this study and presented in *Fig. 1*.

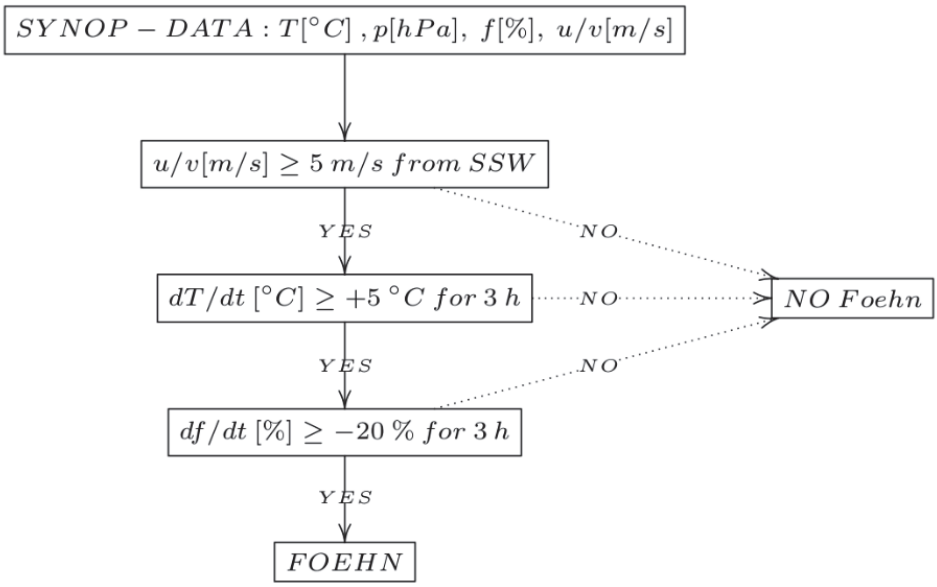

Fig. 1. Schematic presentation of the foehn selection criteria.

Synoptic conditions are analyzed for a 40-years period from 1975 to 2014. For the analysis, the reanalysis archive of the National Centres for Environmental Prediction (NCEP, www.wetterzentrale.de/topkarten/fsres.2eur.html) is used. Charts of surface pressure, geopotential height at 500 hPa (AT500), geopotential height and temperature at 850 hPa (AT850), and relative humidity at 700 hPa (AT700) are analyzed. Depending on the atmospheric circulation, a classification is made of the conditions that lead to the appearance of the foehn in the area of the central meteorological station in Sofia. Satellite images from the archive of Dundee University (http://www.sat.dundee.ac.uk/) are used in addition. Satellite data are from a polar orbiting satellite AVHRR in the Visible channel (VIS 0.58 – 0.68 μm) and infra-red channel (IR, 0.725 and 1.10 μm). For assessment of the foehn as a severe weather phenomenon, the criteria of the European system Meteoalarm is used (http://weather.bg/images/static/Meteoalarm_0.pdf).

3. Foehn classification and climatology for Sofia

3.1. Foehn classification for Sofia

Classification of synoptic conditions is made manually on the basis of the surface pressure charts from the NCEP reanalysis. For this purpose, the movement of the main synoptic centers and frontal systems is traced, and those causing foehn in the area of Sofia are selected.

3.1.1. Foehn type I

In *Fig. 2a*, the cyclone trajectories of type I foehn and the classes Ia, Ib, Ic, Id, and Ie are shown. Class Ia (54 cases) corresponds to the Mediterranean cyclone moving NW of Bulgaria. Foehn class Ib is observed in 13 cases. The cyclone forms over Italy moving through the NW regions of the Balkan Peninsula, west of path Ia (*Fig. 2a*). Foehn class Ic is observed in 15 cases. In this case the cyclone forms over the southern parts of Italy, moves in E-NE direction, and most often passes close to the west border of Bulgaria. Foehn class Id is observed in 26 cases. During class Id, the cyclone forms over North Italy and passes through the Hungarian plain. Foehn class Ie is observed in 6 cases. During class Ie foehn, the cyclone moves from Italy directly to the north.

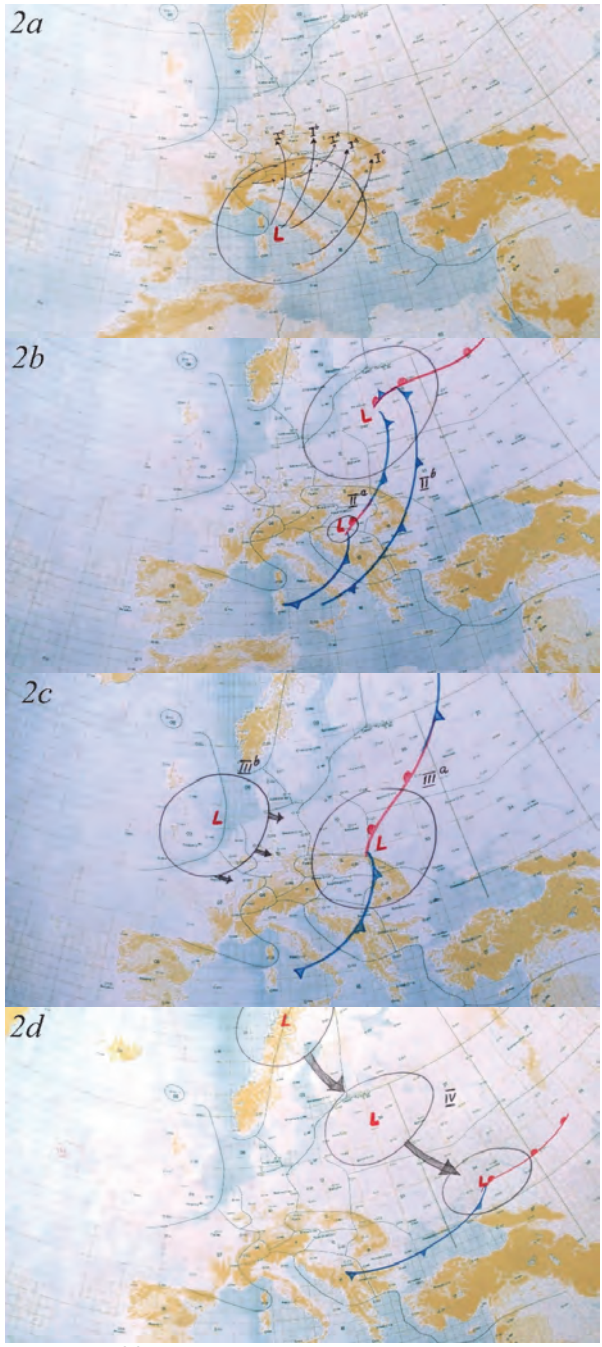

Fig. 2. Schematic chart of foehn: a) type I, b) type II, c) type III, and d) type IV.

In *Figs. 3a* and *3b* a typical foehn class Ia is presented, on February 11 and 12, 1983. At the 500 hPa chart on February 11, 1983, at 00 UTC *(fig. 3a)* it is

seen, that the Balkan Peninsula is situated in front of a sharp trough with an axe over West Europe and the Iberian Peninsula, and in the upper-levels, the cyclone is over France. The pressure gradient is large. At the 850 hPa chart, the transport of air masses is from S-SW, and it is seen that the entire Balkan Peninsula is in a warm air mass, with a temperature from 5 to 10 ^{o}C. From the surface chart it can be seen that the cyclone over the Central Mediterranean is deep with pressure in its centre reaching 995 hPa. At the 500 hPa chart at 12 UTC on February 11, the cyclone moves south of France and deepens. The air masses transportation over the Balkans intensifies, and the warm air advection continues. From the surface chart (not shown) it is seen, that the cyclone moves N-NE through Central Italy and deepens over the Adriatic Sea with pressure in its centre reaching 990 hPa. a Mediterranean cyclone is clearly seen from the satellite images (*Fig. 4*) , formed on February 11 over the Adriatic Sea. In Sofia, at 18 UTC, a S wind is registered with a wind gust of 18–22 m/s. During the evening, the temperature is 11.2 ^{o}C, the relative humidity 56%, and the pressure is 931.9 hPa. In *Fig. 3b* are presented the synoptic conditions at 00 UTC on February 12, 1983 are presented. On February 12, at 500 hPa, the Balkan Peninsula remains in the front part of the trough, and the cyclone in the upper-levels is centered over South France. There is a large pressure gradient and a strong SW warm air advection aloft. At 850 hPa, a large part of the Balkans is still in a warm air mass, but with the withdrawal of the surface vortex towards Ukraine, cold air is advecting from NW to the peninsula. At the surface, the Mediterranean cyclone passes through Hungary, next towards Ukraine, and it is gradually filling up. In Sofia, a strong foehn, with wind gust ranging from 19 to 25 m/s, is recorded during the night of 11 and the afternoon of February 12. In the morning of February 12, the temperature is 7.4 ^{o}C and the relative humidity is 54%.

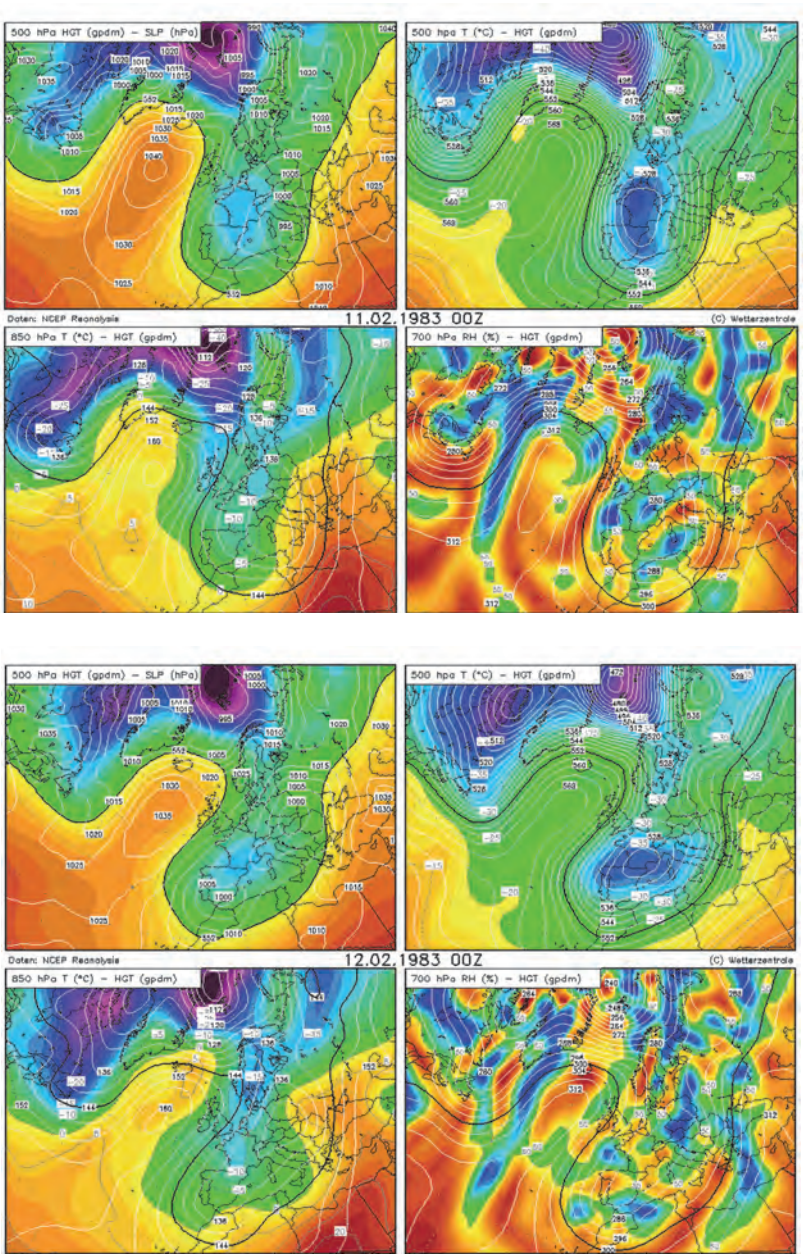

Fig. 3. Upper left panel – chart of surface pressure (with isolines) and geopotential height (in colors), upper right panel – chart 500 hPa (with isolines), lower left panel – chart 850 hPa, lower right panel – chart 700 hPa for the synoptic conditions on: a) February 11, 1983, at 00 UTC and b) February 12, 1983, at 00 UTC.

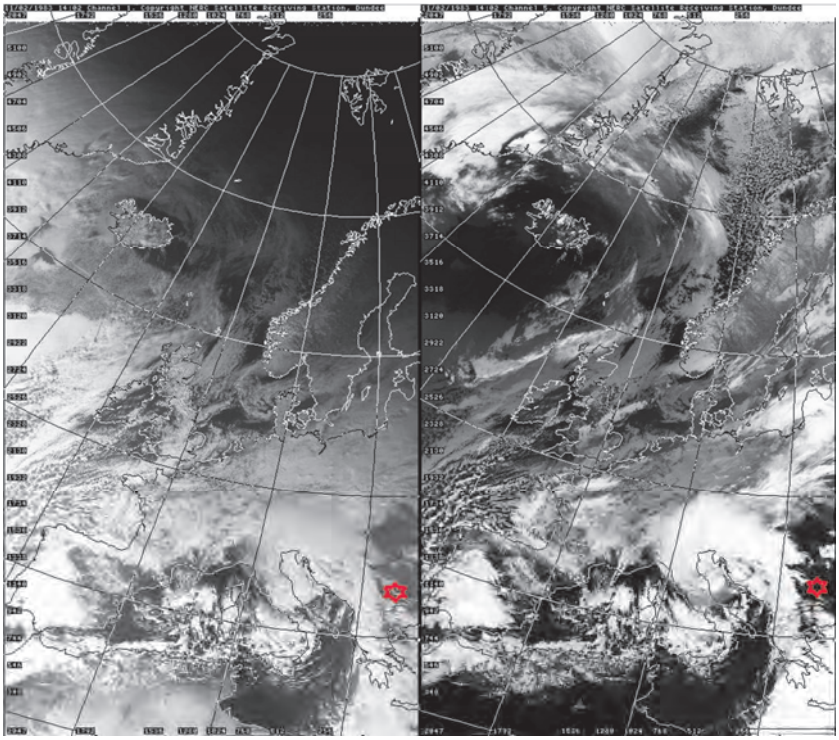

Fig.4. Satellite image in VIS (left panel) and IR (right panel) channels at 14 UTC on February 11, 1983.

3.1.2 Foehn type II, III and IV

Type II foehn is observed in 54 cases. In *Fig. 2b*, a schematic chart of foehn synoptic conditions of classes IIa and IIb are presented. These synoptic conditions are related to the evolution of a cyclone in the Baltic area. Class IIa is associated with cyclogenesis over Hungary during the cold front passage. Class IIb is ahead of the cold front passaging over the western part of the Balkan Peninsula. Foehn synoptic conditions of class IIb are observed in 19 cases.

Type III foehn is observed in 45 cases. In *Fig. 2c*, a schematic chart of foehn classes IIIa and IIIb are shown. Foehn class IIIa results from a cyclone in the North Sea, that moves over Central Europe. Class IIIb happens when the cyclone remains blocked over the British Isles and the North Sea. Foehn synoptic conditions of class IIIb are observed in 4 cases.

Type IV foehn is observed in 7 cases. In *Fig. 2d*, foehn type IV is shown. It is caused by a cyclone over the Scandinavian Peninsula, moving through the

Baltic area towards the southern part of European Russia. These are the so-called “diving” cyclones.

Using the quantitative criteria of *Hristov* and *Tanev* (1970), 298 days with foehn are identified for the period 1975–2014. They resulted from 220 synoptic cases of which: 1) 114 (52%) are type I, 2) 54 (25%) are type II, 3) 45 (20%) are type III, and 4) 7 (3%) are type IV. Type I is divided into 5 classes: 1) Ia with 54, 2) Ib with 13, 3) Ic with 15, 4) Id with 26, and 5) Ie with 6 cases. Type II has two classes: 1) IIa with 35 cases and 2) IIb with 19 cases. Foehn type III comprises two classes: 1) IIIa with 41 and 2) IIIb with 4 cases. Synoptic conditions of type IV are observed in 7 cases.

3.2. Foehn climatology in Sofia for the period 1975–2014

Fig. 5 depicts the number of days with foehn in Sofia per year. It is seen that the year with maximum days (18) with foehn is 1978. Only one day with foehn is registered in 2005 and 2012. *Table 1* presents the average annual number of days with foehn in Sofia, which is 8.9, 8.1, 8.3, and 4.5 for the periods 1975–1984, 1985–1994, 1995–2004, and 2005–2014, respectively. For the period 1955–1964, *Hristov* and *Tanev* (1970) report 7 foehn days. After 2004, there is a tendency for decreasing of the number of days with foehn per year. The study of *Marinova et al.* (2005) demonstrates that the path I of the Mediterranean cyclones over Hungary is not typical any more. This is probably the reason for the decreasing of the mean annual number of days with foehn in Sofia after 2004. In *Fig. 6*, the number of days with foehn per month is shown. It is clearly seen, that the month with the largest number of days is March (56), followed by April (46), February (43), December (32), and November (29). The least frequent is the foehn in June (4). During the 40-year-long period, the longest foehn lasted from February 24 to March 2, 1989 (total – 7 days). There are 3 cases with 4-day foehn, namely: 1) February 26 to March 1, 1990, 2) February 24 to 27, 1995, and 3) April 9 to 12, 1998. The number of cases with foehn persisting 72 hours are 10. Totally for the period 1975–2014, the most frequent foehn cases (47) lasted2 days. In *Fig. 7*, the distribution of foehn cases with 2 days duration is presented. 25% and 23% of the foehn cases with 2 days duration occurred in March and April. For the 40-year-long period, the most persistent foehn, 44 hours, is type IIIa, which occurred in April 9–12, 1978. The foehn events with highest wind gust are types I and II.

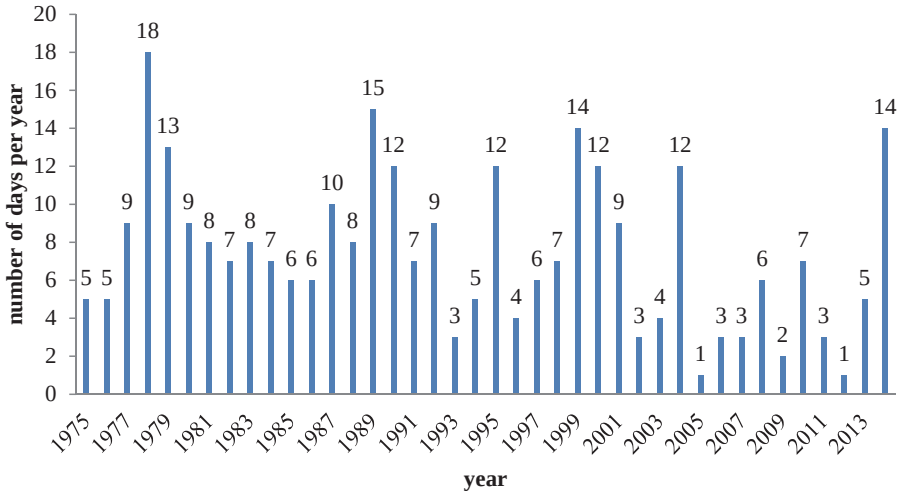

Fig. 5. Mean annual number of days with foehn in Sofia for the period 1975–2014.

Table 1. Number of foehn cases by type in Sofia during the period 1975–2014

Type	Ia	Ib	Ic	Id	Ie	IIa	IIb	IIIa	IIIb	IV
Number	50	12	11	24	6	33	15	40	4	6

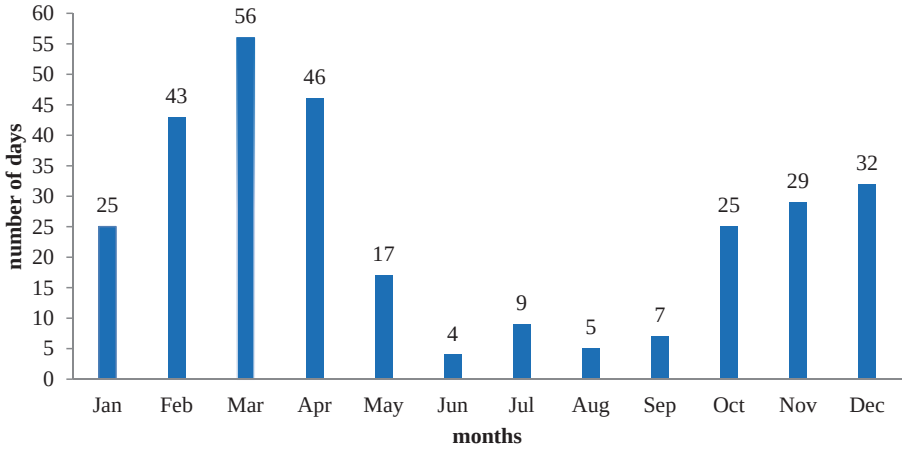

Fig. 6. Number of days with foehn in Sofia per month for the period 1975–2014.

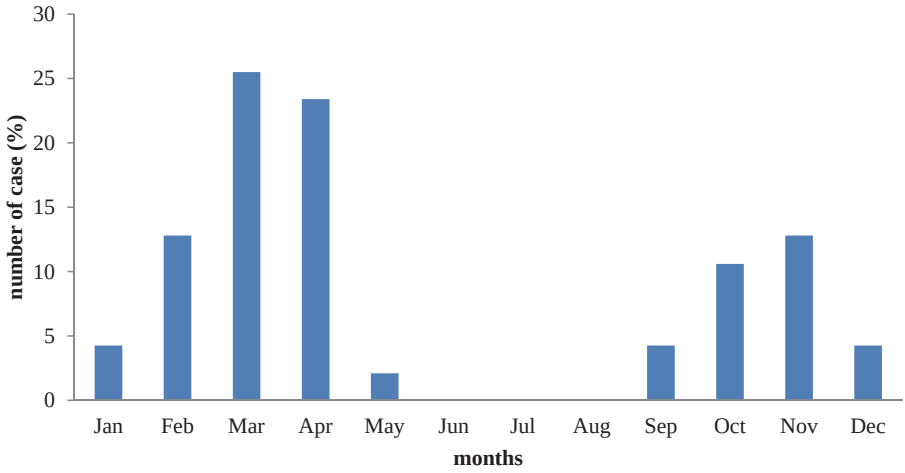

Fig. 7. Fractional monthly distribution of foehn cases with 2 days duration for the period 1975–2014.

3.3. The foehn as a severe weather event

As it can be seen from *Fig. 8*, in 26% of the foehn days, the wind gust is less than 14 m/s, i.e., the foehn is not classified as a severe weather event according to the criteria used in Bulgaria. In 52% of the days, the wind gust is from 14 to 19 m/s, and this corresponds to code "yellow" of the severe weather criteria of Meteoalarm in Bulgaria. In 21% of the days, the wind gust is 20–29 m/s corresponding to code “orange”, and in 1 % of the days the wind gust is over 30 m/s, i.e., the alarm code is “red”. For the 40-year-long period, the number of cases with stormy wind over 30 m/s are only 4, i.e., on average once per decade, the foehn is stormy in Sofia. The highest wind gust was registered in April 1975, with 32 m/s, and the weakest, with 5 m/s on March 23, 2006. *Table 2* presents the maximum wind gust per decade (1975–2014), and it is in the range 30–32 m/s up to 2004. For the last decade (2005–2014), the maximum wind gust is 22 m/s. For the period 1955–1964, investigated by *Hristov* and *Tanev* (1970), the maximum registered wind gust during foehn in Sofia is 35–37 m/s.

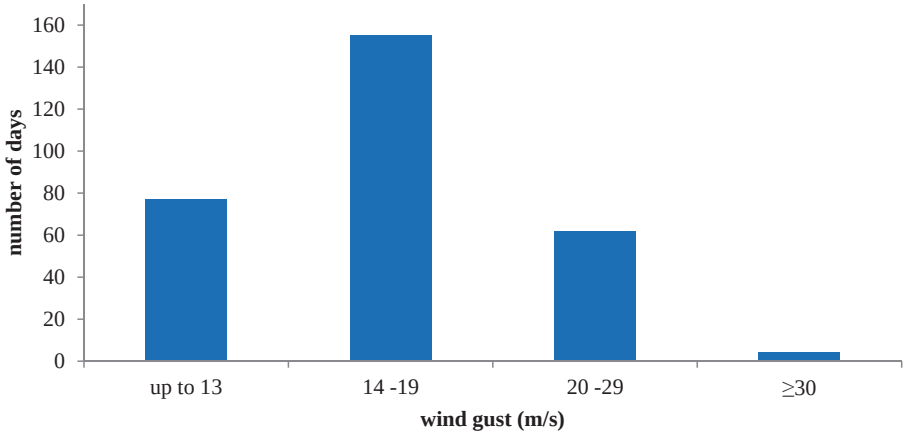

Fig. 8. Number of foehn days with wind speed: 1) up to 13 m/s, 2) %14-19 m/s, 3) 20-29 m/s , and 4) over 30 m/s for the 40-year-long period.

Table 2. Number of foehn days per decade per year, and maximum wind gust per decade

Period	Number of days	Average number of days per year	Maximum wind gust (m/s)
1975–1984	89	8.9	32
1985–1994	81	8.1	30
1995–2004	83	8.3	30
2005–2014	45	4.5	22

In addition, the mean sea level pressure (msl), registered at 12 UTC in Sofia for the foehn days, is used to make a quantitative evaluation of the pressure for the 4 classification types. *Fig. 9* presents the number of days with pressure in 5 hPa bins for each classification type. It is clearly seen, that for type IV the msl pressure peak is at 1020 hPa, which is linked to the position of the low pressure system over the Baltic region *(see Fig. 2d).* Classification type I has an msl pressure peak at 1005 hPa. This is expected result and is linked to the Mediterranean cyclone trajectory, which influences the circulation over the Balkan Peninsula (*Fig. 2a*). For types II and III, the peak is at 1010 hPa with a cyclone positioned mostly to the northwest of Bulgaria.

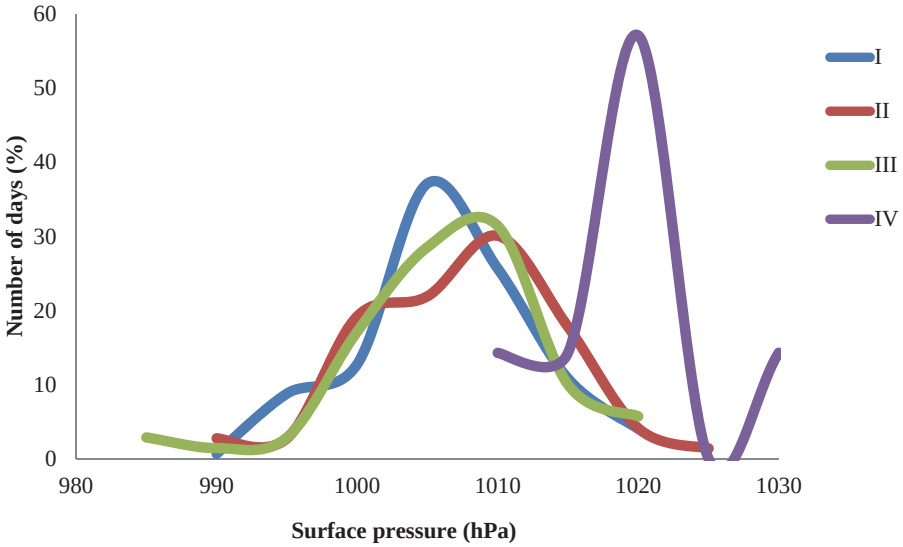

Fig. 9. Mean sea level pressure in Sofia for the classification types I (blue line), II (red line), III (green line), and IV (purple line). The number of days is given in percentage to take into account the different sample sizes of the classification types.

4. Conclusion

The work presents a classification of the synoptic conditions leading to a foehn in Sofia for the 40-year-long period 1975–2014. In this period, there were 298 days with foehn in Sofia, which resulted from 220 synoptic events from which: 1) 114 (52%) are type I, 2) 54 (25%) are type II, 3) 45 (20%) are type III, and 4) 7 (3%) are type IV. Type I is divided into 5 classes: 1) Ia with 54 cases, 2) Ib with 13, 3) Ic with 15, 4) Id with 26, and 5) Ie with 6 cases. Type II has two classes: 1) IIa with 35 cases and 2) IIb with 19 cases. Foehn type III comprises two classes: 1) IIIa with 41 and 2) IIIb with 4 cases. Synoptic conditions of type IV are observed in 7 cases. The average annual number of days with foehn in Sofia is 8.9, 8.1, 8.3, and 4.5 for 1975–1984, 1985–1994, 1995–2004, and 2005–2014, respectively. After 2004, a decrease of the average annual number of days with foehn is found and the lowest maximum wind gust is registered.

During the 40-year-long period, the longest foehn lasted from February 24 to March 2, 1989 (7 days in total). There are 3 foehn cases with duration of 4 days each. Cases with 72 hours duration are 10. For the period 1975–2014, the most frequent foehn is with 2 days duration (47 cases). The months with the largest number of foehn cases is March (56) followed by April (46), and February (43). In addition, a foehn climatology for Sofia is made and the foehn

is classified as a severe weather event by wind gust. In 52% of the foehn days, the wind gust is 14–19 m/s, corresponding to code “yellow” of the severe weather criteria of Meteoalarm in Bulgaria. In 21% of the days, the wind gust is 20–29 m/s (Meteoalarm code “orange”), and only in 1 % of the days (4 cases in total), the wind gust exceeds 30 m/s (Meteoalarm code “red”). The work will continue with evaluation of the foehn in the ERA5 reanalysis.

Acknowledgments: We are very grateful to Mrs. Mariana Popova from the National Institute of Meteorology and Hydrology for her contribution in editing the English version of the manuscript.

References

Blagoev, H., 1961: Patishta na Sredizemnomorskite Tsikloni,. *Hydrol. Meteorol. 1,* 43–51. (In Bulgarian)

van Bebber, W., 1891: Die zugstrassen der barometrischen minima nach den bahnenkarten der deutschen seewarte für den zeitraum 1875–1890. *Meteor. Zeitschr. 8,* 361–366. (In German)

Bocheva, L., Georgiev, Ch., and *Simeonov, P.,* 2007: Aclimatic study of severe storms over bulgaria produced by mediterranean cyclones in 1990-2001 period. *Atmos. Res. 83,* 284–293. https://doi.org/10.1016/j.atmosres.2005.10.018

Gutermann, T., Durr, B., Richner, H., and *Bader, S.,* 2012: Fohnklimatologie Altdorf: die lange reihe (1864–2008) und ihre weiterf¨uhrung, vergleich mit anderen stationen. (In German) https://www.research-collection.ethz.ch/bitstream/handle/20.500.11850/60511/eth-6318-01.pdf

Hristov, P. and Tanev, A., 1970: The climate of Sofia. Nauka i izkustvo. Sofia.

Jansa, A., Genoves, A., Picornell, M., Campins, J., Riosalido, R., and Carretero, O., 2001: Western Mediterranean cyclones and heavy rain. part 2. Stat. Approach Meteorol. Appl. 8, 43–56. https://doi.org/10.1017/S1350482701001049

Marinova, T., Bocheva, L., and *Sharov, V.,* 2005: On some climatic changes in the circulation over the mediterranean area. *Időjárás 109,* 55–67.

Martinov, M., 1967: Some peculiarities of cyclogenesis in the region of the Mediterranean sea and the Balkan Peninsula. *Hydrol. Meteorol. 6,* 7–21. (In Bulgarian)

Martinov, M., 1983: Synoptical and statistical processing of historical data for Mediterranean depression. *WMO, PSMP Report Series 3,* 121–144.

Peiter, E., 1975: Handbook for forecasters in the Mediterranean. Technical Report 344, Environmental Prediction Research Facility, Naval Postgraduate School, Monterey, California.

Pisarski, A., 1955a: Sredizemnomorskite Tskiloni i tyahnoto vilyanie na vremeto v Bulgaria, part I. *Hidrologia i Meteorologia. 5,* 33–50. (In Bulgarian)

Pisarski, A., 1955b: Sredizemnomorskite Tskiloni i tyahnoto vilyanie na vremeto v Bulgaria, part II. *Hidrologia i Meteorologia 6,* 3–15. (In Bulgarian)

Popova, T., Runcanu, T., Tanczer, T., and *Sharov, V.,* 1975: Sredizemnomorskie tsiklony v pole oblachnosti. Gidrometeoizdat. Leningrad. (In Russian)

Radinovic, D., 1987: Mediterranean cyclones and their influence on the weather and climate. *WMO, PSMP Report Series 24.* 131.

Richner, H. and *H¨achler, P.,* 2013: Understanding and forecasting alpine foehn. In: Mountain Weather Research and Forecasting, Springer.. 219–260. https://doi.org/10.1007/978-94-007-4098-3_4

Stanchev, K., 1954: Yuzhnite Tsikloni, dvizhenieto im prez Balkanskiya poluostrov i vliyanieto im nad vremeto v Bulgaria. *Hidrologia i Meteorologia 5,* 19–39. (In Bulgarian)

Willemse, S. and *Furger, M.,* 2016: From weather observations to atmospheric and climate sciences in Switzerland. vdf Hochschulverlag AG an der ETH Zürich. http://e-collection.library.ethz.ch/

DOI:10.28974/idojaras.2020.4.5

IDŐJÁRÁS

Quarterly Journal of the Hungarian Meteorological Service
Vol. 124, No. 4, October – December, 2020, pp. 499–519

Spatial and temporal patterns of precipitation in Montenegro

Golub Ćulafić[1], **Tatjana Popov**[2*], **Slobodan Gnjato**[2], **Davorin Bajić**[2], **Goran Trbić**[2], and **Luka Mitrović**[1]

[1]*Institute of Hydrometeorology and Seismology of Montenegro*
IV proleterske 19, 81000 Podgorica, Montenegro

[2]*University of Banja Luka*
Faculty of Natural Sciences and Mathematics
Mladena Stojanovića 2, 78000 Banja Luka
Republic of Srpska, Bosnia and Herzegovina

**Corresponding author E-mail: tatjana.popov@pmf.unibl.org*

(Manuscript received in final form January 7, 2020)

Abstract—The paper analyses, spatial and temporal patterns of precipitation over Montenegro. Data on mean monthly precipitation during the period 1961–2015 from 17 meteorological stations were used for the analysis. Four regions with different spatial precipitation regimes were identified by using the principal component analysis and the agglomerative hierarchical clustering method. A downward tendency in annual precipitation prevails over Montenegro. The most prominent reduction was present in the summer season. In contrast, precipitation increased during autumn. However, the majority of estimated trend values was low and statistically insignificant.

Key-words: precipitation, principal component analysis, agglomerative hierarchical clustering, trend analysis, climate change, Montenegro

1. Introduction

Over the past several decades, studies on climate regionalization have intensively used eigenvector analysis (*White et al.*, 1991). The principal component analysis (PCA), as an eigenvector-based regionalization, has been widely used in climatology and meteorology for investigation of spatial and temporal variability of different physical fields (*Demšaret et al.*, 2013). The PCA was particularly commonly used for regionalizations based on precipitation in numerous researches all over the world (*Almazroui et al.*, 2015; *Guirguis* and *Avissar*, 2008; *Lovino et al.*, 2014; etc.) and Europe (*Gocic* and *Trajkovic*, 2014; *Goossens*, 1985; *Journée et al.*, 2015; *Mills*, 1995; *Muñoz-Díaz* and *Rodrigo*, 2004; *Popov et al.*, 2019b; *Stathis* and *Myronidis*, 2009; *Türkeş et al.*, 2009; *Wigley et al.*, 1984). It is generally used to reduce temporal and spatial climatic data to manageable and physically interpretable abstractions (*White et al.*, 1991). It reduces the dimensionality of a data set consisting of a large number of interrelated variables (while retaining as much as possible of the variation present in the data set) by transforming it to a new set of variables, i.e., the principal components (PCs), which are uncorrelated, and which are ordered so that the first few PCs retain most of the variation present in all of the original variables (*Jolliffe*, 1986). The cluster analysis (CA) is also often applied as a helpful method to group areas with similar patterns of precipitation (*Bravo Cabrera et al.*, 2012; *Lyra et al.*, 2014; *Singh et al.*, 2017; *Tu et al.*, 2011; etc.).

Global studies on temporal variability of precipitation (annual and seasonal) found trends that were not spatially unified, but were low in magnitude (*Alexander et al.*, 2006). Similar changes were obtained for the European continent (*Chen et al.*, 2015) and its different parts (*Bartholy* and *Pongrácz*, 2010; *Napoli et al.*, 2019; etc.). However, over the Mediterranean region, a downward tendency in total precipitation prevailed (*Çiçek* and *Duman*, 2015; *Dayon et al.*, 2018; *Gajić-Čapka* and *Cindrić*, 2011; *Popov et al.*, 2019a).

Previous studies on precipitation in Montenegro mainly focused on recent trends in extreme precipitation over the entire country (*Burić et al.*, 2015) or over a certain part of its territory (*Ducić et al.*, 2012).

The aim of this study was to investigate the spatial and temporal patterns of changes in precipitation over Montenegro. The main goal was to identify regions with similar spatial precipitation regimes and to determine trends in annual and seasonal precipitation during the observed period of 1961−2015.

2. Study area

The study area covers the territory of Montenegro which is a Mediterranean country located in Southeast Europe. The investigated territory lies between the latitudes 41°52'–43°32' N and longitudes 18°26'–20°21' E. It covers a total surface area of 13,812 km^2.

Geographical position, atmospheric circulation (activity of centers such as the Mediterranean lows, the Icelandic Low, the Genoa Low, the Azores High, the Siberian High, etc.), morphological characteristics of the terrain, and the vicinity of the Adriatic Sea have a primary impact on the climate of Montenegro (*Burić et al.*, 2013).

Montenegro covers several different macro-morphological regions: the coastal region in the western and southeastern parts of the country, the mountainous region in the north, and the central region between them. The narrow Adriatic coastal region is characterized by a typical Mediterranean climate with long, warm, and dry summers (mean July temperature is about 25 °C), and short, mild, and rainy winters (mean January temperature is about 8 °C). The average annual temperature over the coastline is 15–16 °C, and the total annual precipitation is 1200–2000 mm (*Institute of Hydrometeorology and Seismology of Montenegro*, 2006). Areas with Mediterranean climate are characterized by high precipitation variability often enhanced by orography, strong seasonality in its monthly distribution, and large inter-annual variations (*Piras et al.*, 2016). In Montenegro, annual precipitation is the highest in the mountainous coastal hinterland (for instance, at the Orjen Mountain about 4500 mm annual precipitation occurs on average). These precipitation maxima at the mountain ridges are connected with orographic precipitation (*Lionello et al.*, 2012). Beside the high mountains (Orjen, Lovćen and Rumija Mountains), which rise steeply above the coastline, the central region of Montenegro encompasses the lowlands – Skadar Lake Basin, Zetsko-Bjelopavlići Plain, and Nikšić Karst Field. The lowlands are characterized by the sub-Mediterranean climate with very warm summers (the maximum temperatures rise up to above 40 °C) and winters colder than in the Mediterranean climate (minimum temperatures in winter can drop to -10 °C). Mean annual temperature and precipitation are in the range of 11–15 °C and 1600–2000 mm, respectively (*Institute of Hydrometeorology and Seismology of Montenegro*, 2006). At the high karst mountains in the north, the climate is mountainous with cold and snowy winters and moderately warm summers. The mean annual temperature ranges between 4 °C and 7 °C, whereas the total annual precipitation is in the range of 1500 –2200 mm (*Institute of Hydrometeorology and Seismology of Montenegro*, 2006). The lowest precipitation in Montenegro (about 800 mm) occurs in the far northern part of the territory, which is characterized by moderate-continental climate.

According to the Köppen climate classification, warm temperate and cold temperate climates are present over Montenegro – the coastline and the Zetsko–Bjelopavlićka Plain are characterized by the typical Mediterranean Csa climate; the karst fields and plains in the inland have typical features of Csb climate; the northern and northeastern parts of the country, with precipitation uniformely distribuited throughout the year, are characterized by the Cfb climate; whereas cold temperate Df climate is found at the higher mountain areas (above 1000 m) (*Burić et al.*, 2014).

3. Data and methods

Spatial and temporal patterns of precipitation in Montenegro have been analyzed using data on mean monthly precipitation during the period 1961–2015 from 17 meteorological stations located in all macro morphological regions of the country: Adriatic coastal region, central region covering mountains in the coastal hinterland and lowlands, and mountainous region in north (*Fig. 1*). Given such terrain configuration, meteorological stations used for the analysis cover a wide range of altitudes from the lowest-located station at the Adriatic coast (Budva 2 m) to the highest-located station at the Durmitor Mountain (Žabljak 1450 m). The Institute of Hydrometeorology and Seismology of Montenegro provided data on precipitation. Given that there were certain short breaks in observations at a few stations, missing data were extrapolated based on data from the nearest meteorological station with available measurements in that period.

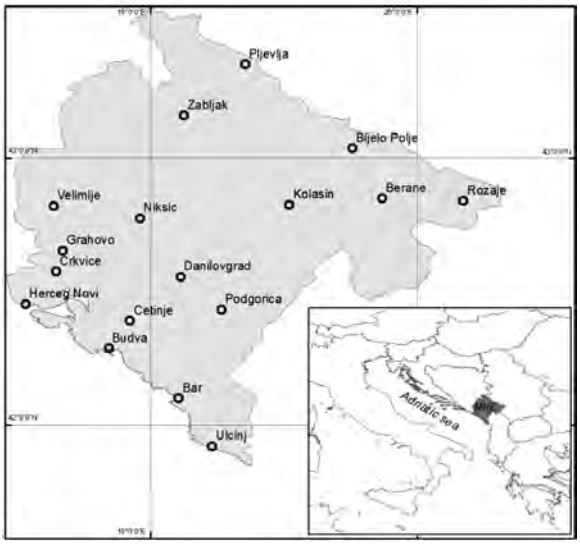

Fig. 1. Study area with locations of the meteorological stations used for the analysis.

Spatial patterns of precipitation in Montenegro were determined using principal component analysis, PCA with varimax orthogonal rotation (*Jolliffe*, 1998) and the CA (*Everitt et al.*, 2011). As input data for principal component analysis, PCA, seven variables based on mean precipitation were used: total annual precipitation, growing season (April−September) precipitation, seasonal precipitation (winter (December of the previous year and January and February of the current year), spring (March–May), summer (June–August), and autumn (September–November)), and the precipitation concentration index (*PCI*), representing intra-annual variability of precipitation. It was calculated following the formula given by *Oliver* (1980):

$$PCI = \sum_{i=1}^{12} p_i^2 / \left(\sum_{i=1}^{12} p_i\right)^2 \times 100 \,, \quad (1)$$

where p_i is the monthly precipitation in month i.

Given that variables were in different units, data normalization was performed prior to a further analysis as follows:

$$x = (x_I - \bar{x}) / \sigma \,, \quad (2)$$

where x_i is the value to normalize, $\bar{x}$ is the arithmetic mean of the distribution, and σ is the standard deviation of the distribution.

The inverse distance weighted (IDW) interpolation technique was used to map spatial distribution of precipitation patterns in ArcGIS.

The Bartlett's sphericity test was applied to verify that correlations among the precipitation variables are significant. The Kaiser−Meyer−Olkin (*KMO*) value, which measures sampling adequacy (*Kaiser*, 1974), was used to determine the quality of the input variables for the PCA. Eigenvalues and eigenvectors were computated using correlation matrix. Following *Gocic* and *Trajkovic* (2014), R-mode data matrix, with variables in columns and meteorological stations in rows, was applied. The first two principal components (PCs) (*North et al.*, 1982) were subjected to the varimax orthogonal rotation. The factor scores of rotated PCs were mapped to display their spatial distribution over the Montenegro territory. The results were then subjected to CA in order to identify areas with similar spatial regimes of precipitation. The agglomerative hierarchical clustering (AHC) method was applied to the rotated PCs scores – Euclidean distance was chosen as dissimilarity measure and Ward's method as an agglomeration method (*Everitt et al.*, 2011; *Ward*, 1963). Clusters were mapped using Iso Cluster in ArcGIS. Average values of precipitation variables for the identified clusters were obtained as the average precipitation at meteorological stations corresponding to each cluster.

Temporal patterns of precipitation variability in Montenegro were determined based on trend analysis. Trends in annual and seasonal precipitation

during the period 1961−2015 were estimated using the nonparametric Mann-Kendall test (*Mann*, 1945; *Kendall*, 1975) and Sen's estimator of slope (*Sen*, 1968). Further, the rainfall anomaly index (*RAI*) was discussed in order to identify years with extreme precipitation (both low or high). It was calculated as follows:

$$RAI = -3 \times \frac{P_i - \bar{P}}{\bar{E} - \bar{P}}, \tag{3}$$

where P_i is the annual precipitation for each year, $\bar{P}$ is the average annual precipitation for the period 1961−1990, and $\bar{E}$ is the average precipitation for the ten years in the observed period 1961−2015 with the lowest annual precipitation (*Van Rooy*, 1965).

4. Results

Mean annual precipitation, four mean seasonal precipitations, mean growing season precipitation, and the *PCI* were used to determinate spatial patterns of precipitation over Montenegro. The mean annual and seasonal precipitations in Montenegro are shown in *Fig. 2*. Total annual precipitation ranges between 797 mm in Pljevlja to 4575 mm in Crkvice. Summer season is substantially drier than the rest of the year over most of the territory of Montenegro, except at the northern stations Pljevlja and Rožaje, which are characterized by a moderate temperate climate with more evenly distributed precipitation throughout the year. The *PCI* values in the range of 10.9–15.0 (*Fig. 3*) also indicate seasonality in precipitation distribution in Montenegro.

Chi-square value of 497.95 (with $df = 21$ and $p < 0.0001$) of Bartlett's sphericity test and the *KMO*=0.579 verified that the selected variables were adequate for the PCA analysis. Scree plot of the variables factor loadings on the components is displayed in *Fig. 4*. The total variances of first two PCs were 87.29% and 11.62%, respectively, giving a cumulative variance of 98.90% (*Fig. 5*). Eigenvectors of the variables for the first two PCs are shown in *Table 1*. Annual, autumn, and winter precipitation influence first PC the most, whereas summer precipitation has strongest influence on the second PC (*Table 1*). Results of varimax rotation of these two PCs are shown in *Table 2*. Spatial distribution of the components scores coefficients is displayed in *Fig. 6*.

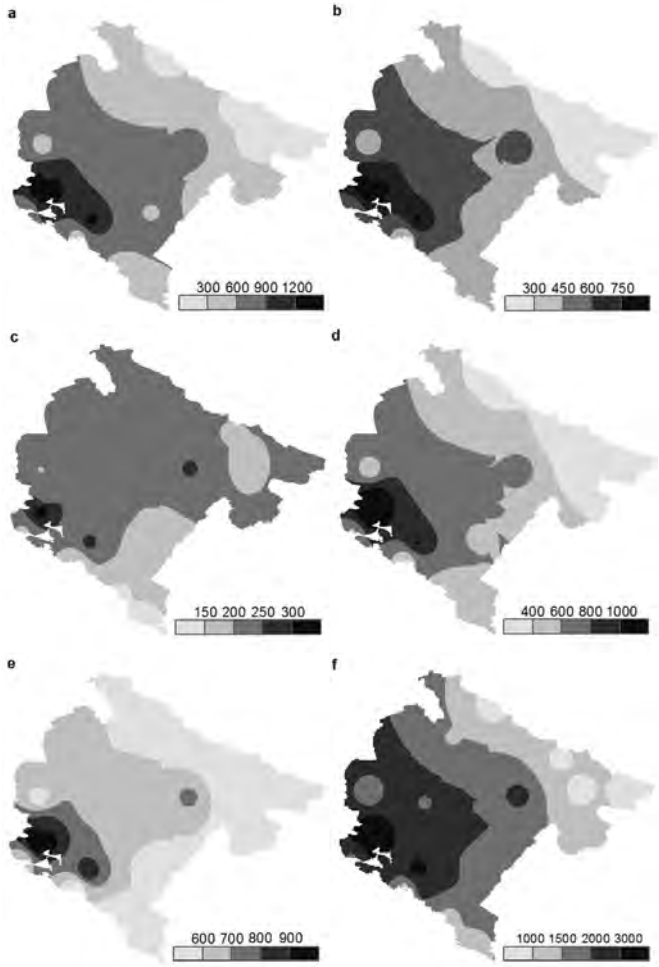

Fig. 2. Spatial distribution of precipitation in Montenegro for the period 1961–2015 (in mm) − winter (a), spring (b), summer (c), autumn (d), growing season (e), and year (f).

Fig. 3. Spatial distribution of *PCI* over Montenegro in the period 1961–2015.

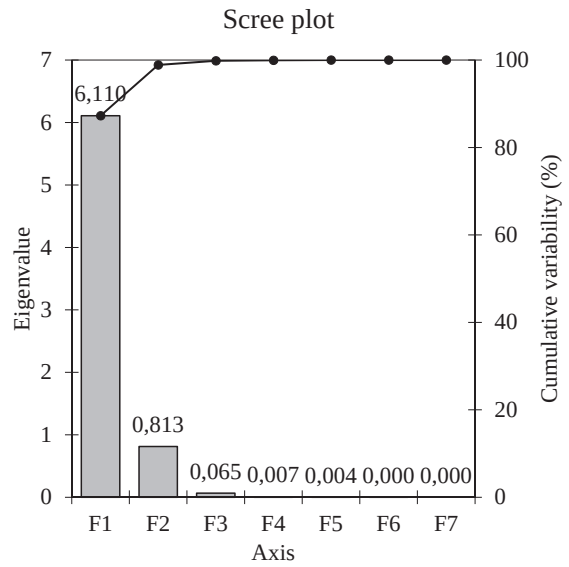

Fig. 4. Scree plot of the eigenvalues and cumulative variability.

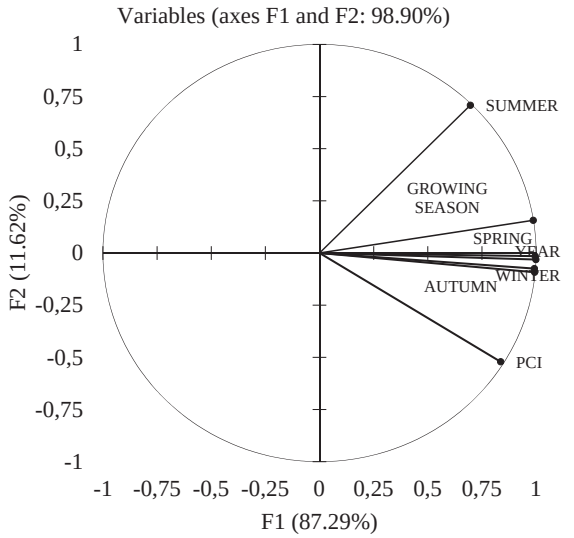

Fig. 5. Correlation of factor loadings of the F1 and F2 variables.

Table 1. Eigenvectors of the variables for the first two PCs

Variables	Year	Winter	Spring	Summer	Autumn	Growing season	PCI
PC1	0.404	0.401	0.402	0.282	0.402	0.399	0.338
PC2	-0.035	-0.083	-0.017	0.785	-0.102	0.174	-0.578

Table 2. Results of the varimax rotation of PCs

Variables	Factor loadings		Contribution of the variables (%)		Squared cosines	Component score coefficients	
	R-Loading 1	R-Loading 2	D1	D2		RPC1	RPC2
Year	0.853	0.519	16.070	11.261	0.728	0.158	0.057
Winter	0.871	0.479	16.764	9.582	0.759	0.186	0.012
Spring	0.842	0.531	15.637	11.763	0.708	0.147	0.073
Summer	0.196	0.973	0.849	39.581	0.947	-0.380	0.792
Autumn	0.882	0.465	17.168	9.029	0.778	0.198	-0.006
Growing season	0.741	0.670	12.105	18.768	0.548	0.030	0.250
PCI	0.985	0.020	21.407	0.016	0.970	0.465	-0.462

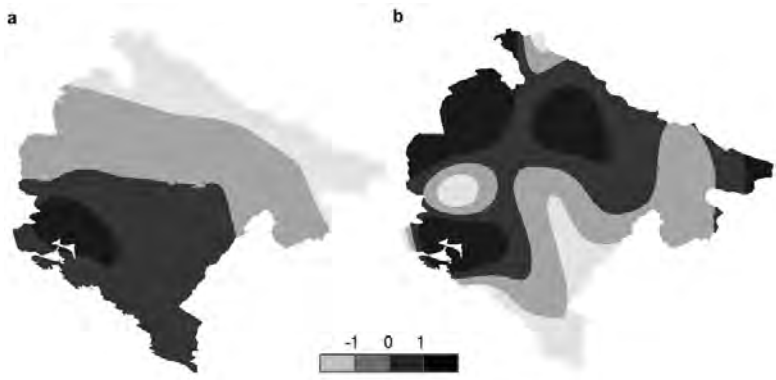

Fig. 6. Spatial distribution of the components scores coefficients – RPC1 (a) and RPC2 (b).

The results obtained by the varimax rotation of the two PCs were subjected to the AHC, which identified four distinct clusters with different spatial patterns of precipitation in Montenegro (*Fig. 7*):

– C1 cluster with 4 stations (Bar, Budva, Podgorica, and Ulcinj),
– C2 cluster with 5 stations (Berane, Bijelo Polje, Pljevlja, Rožaje, and Žabljak),
– C3 cluster with 7 stations (Cetinje, Danilovgrad, Grahovo, Herceg Novi, Kolašin, Nikšić, and Velimlje), and
– C4 cluster with 1 station (Crkvice).

Fig. 7. Spatial regionalization of Montenegro based on precipitation.

The obtained variance decomposition within the class was 26.68% (absolute value of 0.5669), and between the classes it was 73.32% (absolute value of 1.5581). Bar, Pljevlja, Nikšić, and Crkvice meteorological stations were identified as central objects of the C1, C2, C3, and C4 clusters, respectively.

C1 cluster includes the southeastern part of Montenegro; C2 cluster covers the northern and northeastern parts of the territory; the spatially largest C3 cluster encompass the central and western parts of the country; whereas C4 cluster includes only one station Crkvice, located at the southeastern slope of the Orjen Mountain, which is characterized by the highest precipitation in the Mediterranean region (*Ducić et al.*, 2012).

Mean annual and seasonal precipitation of the four identified clusters for the period 1961–2015 are shown in *Table 3*. The annual total precipitation of C1 cluster (1444.3 mm) and C2 cluster (1003.6 mm) are characterized by

precipitation below state average (1862.4 mm), whereas over the C3 cluster and particularly C4 cluster, precipitation is substantially above the state average (2321.9 mm and 4595.1 mm, respectively).

Table 3. Seasonal and annual precipitations and the PCI by clusters and state averages in the period 1961–2015

Cluster	Winter		Spring		Summer		Autumn		Growing season		Year		PCI
	mm	%	mm	%	mm	%	mm	%	mm	%	mm	%	
C1	491.1	33.9	343.0	23.7	148.2	10.2	466.5	32.2	476.6	33.0	1444.3	100.0	12.9
C2	251.7	25.1	236.4	23.6	217.0	21.6	298.5	29.7	468.2	46.8	1000.2	100.0	11.4
C3	815.0	35.1	530.4	22.8	224.2	9.7	752.3	32.4	699.6	30.3	2312.3	100.0	13.5
C4	1763.9	38.4	1060.1	23.1	325.8	7.1	1445.4	31.5	1179.9	25.8	4575.2	100.0	14.3
C	628.9	33.8	431.0	23.1	210.2	11.3	592.4	31.8	607.3	32.7	1855.3	100.0	12.8

C1 cluster is characterized by spring and autumn precipitation shares in the total annual precipitation above state averages and summer precipitation below average (winter amounts are about average). Seasonal precipitation in C2 cluster is above the state averages in the warmer part of the year (in spring and summer seasons), whereas in autumn and particularly in winter, it is substantially less than the average. In contrast, C3 cluster is characterized by seasonal precipitation far above the average during the winter and autumn seasons, whereas in the summer season only 9.7% of total annual precipitation occurs on average. In C4 cluster, substantially more/less than average precipitation occurs in the winter/summer season (spring precipitation is about average, and autumn is slightly below average). During the growing season, in C1 and C2 clusters occurs the 33.0% and 46.8% of total annual precipitation, respectively (state average is being 32.7%), whereas C3 and C4 clusters are characterized by lower than average precipitation shares in total annual precipitation during this part of the year (30.3% and 25.8%, respectively). *PCI* values in the range of 11.4–14.3% suggest that intra-annually, precipitation over Montenegro does not show uniform distribution. The *PCI* values higher than 11 in all four clusters denote seasonality in monthly precipitation distribution. The highest *PCI* values were determined for C4 and C3 clusters (14.3 and 13.5, respectively).

Trends in annual and seasonal precipitations of the identified clusters during the period 1961–2015 are shown in *Table 4* and *Fig. 8*. Total annual precipitation decreased over the entire territory of Montenegro, except in the north (C2 cluster) and in Cetinje. The estimated negative trend values ranged between -1.12 percent per decade averaged for C1 cluster and -1.34 percent per

decade for C4 cluster, whereas in C2 cluster, precipitation slightly increased by 0.43 percent per decade averaged for the cluster. The highest trend values were estimated at meteorological stations Velimlje (-4.71 percent per decade), Herceg Novi (-2.25 percent per decade), and Ulcinj (-1.69 percent per decade). Cumulative anomalies of the annual precipitation displayed in *Fig. 9* show that drying period over the entire territory of Montenegro (in all four clusters) started at the beginning of the 1980s.

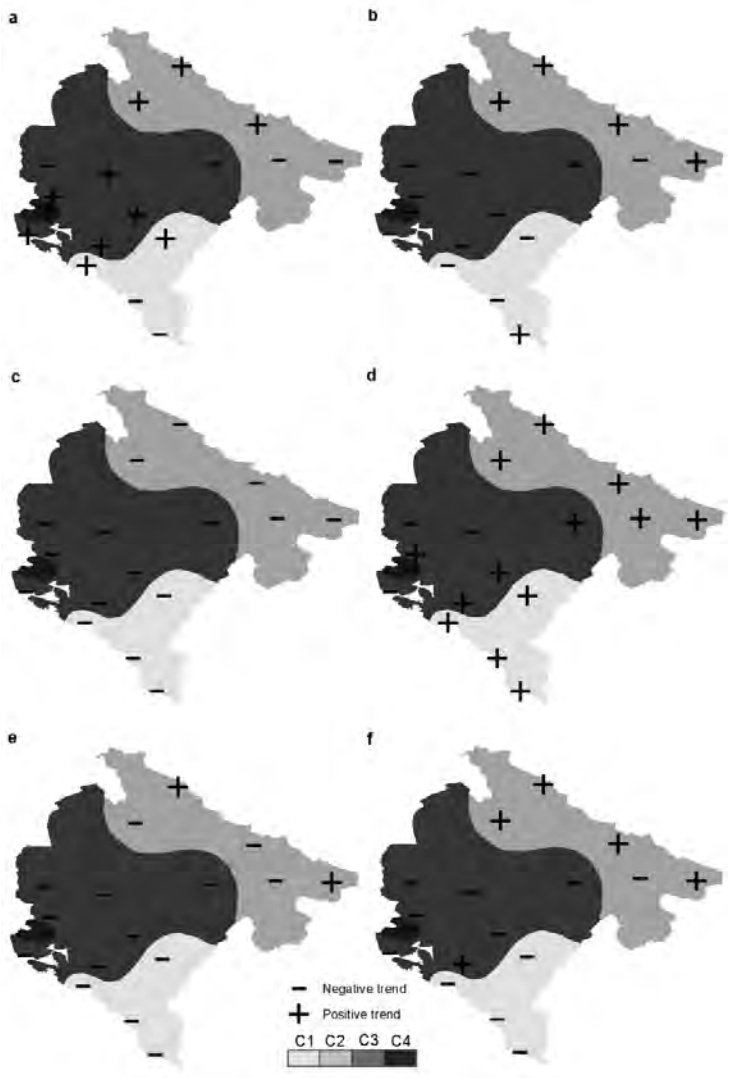

Fig. 8. Trends in seasonal and annual precipitation in the period 1961–2015 – winter (a), spring (b), summer (c), autumn (d), growing season (e), and year (f).

Table 4. Precipitation trends by clusters in the period 1961–2015 (in percent per decade)

M. s.	Winter	Spring	Summer	Autumn	Growing season	Year
C1 cluster	1.53	-0.55	-3.13	3.07	-0.67	-1.12
Bar	-0.33	-1.05	-2.26	3.88	-1.50	-1.16
Budva	3.55	-1.40	-2.74	0.94	-0.72	-0.82
Podgorica	0.97	-0.85	-4.09	3.75	-0.22	-0.08
Ulcinj	-0.54	0.59	-3.62	1.92	-0.33	-1.69
C2 cluster	1.68	0.37	-2.55	2.27	-0.72	0.43
Berane	-1.22	-0.23	-4.42	4.79	-1.53	-0.42
Bijelo Polje	1.26	1.25	-4.25	4.80	-1.35	0.40
Pljevlja	0.29	1.54	-1.15	0.77	0.18	0.02
Rožaje	-1.60	3.18	-1.69	3.52	0.82	0.58
Žabljak	4.58	0.45	**-5.53**	0.19	-2.42	0.60
C3 cluster	0.93	-2.25	-4.24	0.31	-1.36	-1.34
Cetinje	3.91	-2.01	-2.38	0.13	-1.76	0.00
Danilovgrad	1.39	-2.12	-1.68	1.82	-0.16	-0.22
Grahovo	1.38	-0.59	-4.51	1.34	-0.27	-0.28
Herceg Novi	0.27	-3.03	-2.88	-3.31	-1.83	-2.25
Kolašin	-1.99	-0.99	-4.26	2.38	-0.13	-1.33
Nikšić	2.11	-0.92	-5.74	-0.87	-2.39	-1.49
Velimlje	-5.63	-1.67	**-8.59**	-3.84	-3.81	-4.71
C4 cluster	3.08	-0.11	**-8.15**	-1.42	-1.70	-1.30
Crkvice	3.08	-0.11	**-8.15**	-1.42	-1.70	-1.30

Note: Bold values represent statistically significant trends ($p < 0.05$)

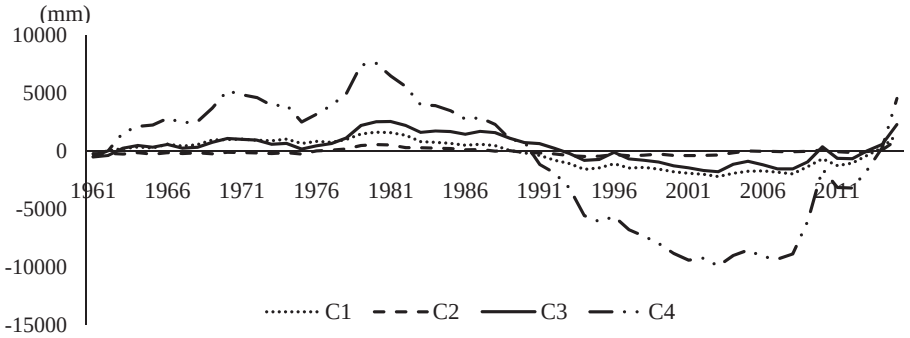

Fig. 9. Cumulative anomalies of the annual precipitation by clusters in the period 1961–2015.

Seasonal precipitation did not display unified trends (both positive and negative tendencies were present) (*Table 4* and *Fig. 8*). Trend analysis showed that negative trends ranging between -1.15 percent per decade at Pljevlja (C2 cluster) and -8.15 percent per decade and -8.59 percent per decade at Crkvice (C4 cluster) and Velimlje (C3 cluster), respectively, were present in the summer season over the entire territory. However, a statistically significant trend was found only at Žabljak, Velimlje, and Crkvice. In the spring season, over the Montenegro territory also a weak downward tendency prevailed (-0.11– -3.03 percent per decade), except in C2 cluster, where a low positive trend was recorded (0.45–3.18 percent per decade). In autumn, the upward trends ranging between 0.13 percent per decade at Cetinje and 4.79–4.80 percent per decade at Berane and Bijelo Polje were found over most of the country (all insignificant). Downward trends were registered only in C4 cluster (Crkvice -1.42 percent per decade), and at two stations in C3 cluster (Herceg Novi -3.31 percent per decade and Velimlje -3.84 percent per decade). In the winter season, precipitation displayed less coherent changes – precipitation reduction was registered at 6 stations (-0.33– -5.63 percent per decade), whereas precipitation increased at 11 stations (0.27– 4.58 percent per decade), but both trends are still insignificant.

The analysis of *RAI* showed that since the 1990s, as climate change intensifies, precipitation variability in Montenegro has also been increasing. Many years with extreme precipitation (both extremely wet and extremely dry years) occurred during this period. During the observed period 1961–2015, there was 3–7 extremely wet years, 2–8 very wet years, 4−5 extremely dry years, and 4−7 very dry years (*Table 5* and *Fig. 10*) – majority of them has been recorded since 1990. Extremely wet years were 2013, 2010, 2009, and 1979 over the entire territory (except in the north), 2014 in C1 and C4 clusters, 2004 in C2 and C3 clusters, 1996 in C3 cluster, 1963 in C3 and C4 clusters, 1976 in C2 cluster, and 1970 in C4 cluster. Extremely dry was 2011 over the entire territory, and 1994 and 1983 in all clusters except in C2 cluster, 1992 and 1989 in C1 cluster, 1990, 1982, and 1961 in C2 cluster, 2015 in C3 cluster, and 1991 and 1975 in C4 cluster.

Table 5. Years based on the RAI in the period 1961–2015

RAI Category	C1 cluster	C2 cluster	C3 cluster	C4 cluster
Extremely dry [≤ -3.00]	5	4	4	5
Very dry [-2.99– -2.00]	4	7	7	4
Moderately dry [-1.99– -1.00]	10	7	8	12
Slightly dry [-0.99– -0.50]	8	5	6	7
Near normal [-0.49–0.49]	7	11	10	9
Slightly wet [0.50–0.99]	4	4	2	3
Moderately wet [1.00–1.99]	7	6	8	6
Very wet [2.00–2.99]	5	8	3	2
Extremely wet [≥ 3.00]	5	3	7	7

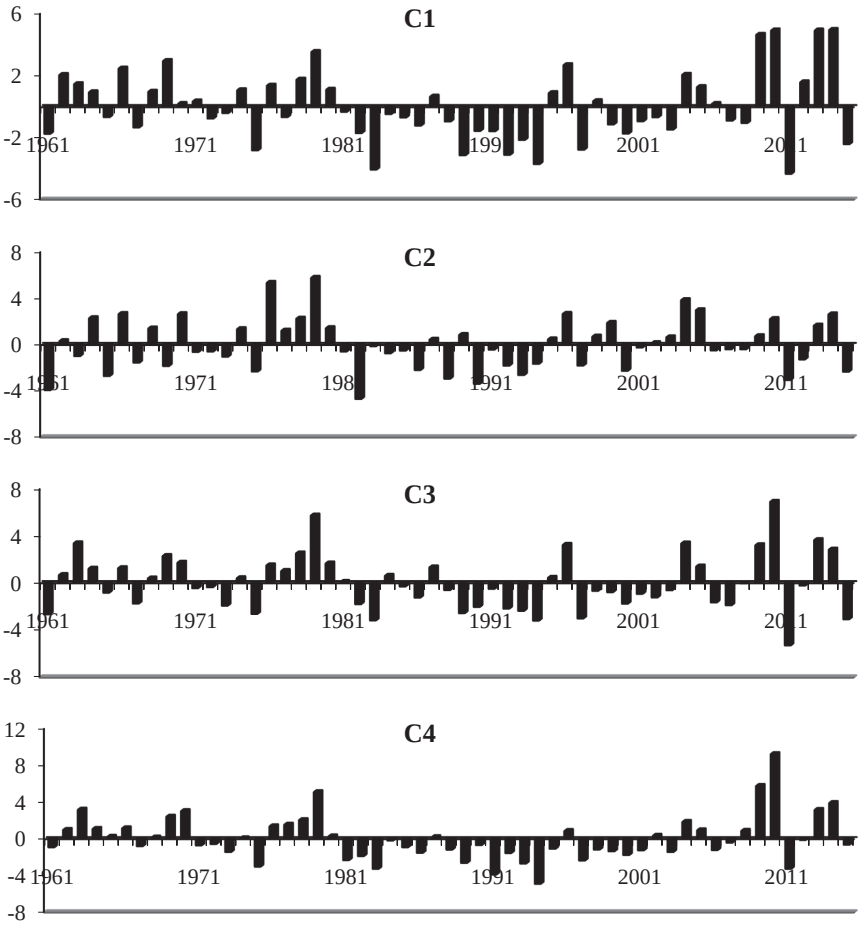

Fig. 10. Annual RAI by clusters in the period 1961–2015.

5. Discussion

In this study, spatial regionalization of Montenegro, i.e., four distinct clusters with different spatial patterns of precipitation was performed applying the PCA and CA on seven variables based on mean precipitation. *Gocic* and *Trajkovic* (2014) and *Popov et al.* (2019b) used the same precipitation-based variables for spatial regionalization of Serbia and Bosnia and Herzegovina, respectively,

based on the PCA and clustering techniques. *Goossens* (1985) applied the PCA to annual precipitation data from the stations in the European part of the Mediterranean region in order to identify homogeneous regions. Based on comparison of several approaches, *Journée et al.* (2015) concluded that the PCA extracts best main spatial and temporal characteristics of the annual precipitation in Belgium. The PCA was also used for investigation of spatiotemporal patterns of precipitation in Spain (*Mills*, 1995; *Muñoz-Díaz* and *Rodrigo*, 2004), Greece (*Stathis* and *Myronidis*, 2009), Turkey (*Türkeş et al.*, 2009), etc.

Results of trend analysis obtained in the survey (prevailing negative trends in annual and seasonal precipitations, except in the autumn season) are in concordance with the results of similar researches on changes in precipitation over Montenegro and other areas of the Mediterranean region.

Previous studies conducted for the whole Mediterranean region showed a marked negative trend in the annual precipitation during the period 1901–2009 over majority of Mediterranean regions, particularly prominently in the eastern part of the basin (Montenegro was one of the regions with the highest estimated trend values) (*Caloiero et al.*, 2018). Most areas were also characterized by a downward trend in the summer precipitation (*Deitch et al.*, 2017). During this period, reduction in annual and summer precipitations has predominated over the Iberian Peninsula (*Río et al.*, 2011; *Rodrigo* and *Trigo*, 2007), Italy (*D'Oria et al.*, 2017), France (*Dayon et al.*, 2018), Greece (*Markonis et al.*, 2017), Croatia (*Gajić-Čapka* and *Cindrić*, 2011), Turkey (*Çiçek* and *Duman*, 2015), Israel (*Yosef et al.*, 2019), etc. Over the eastern part of the Mediterranean region, trends in precipitation indices consistent with drier conditions were also found, i.e., positive trends in the maximum number of consecutive dry days and negative trends in the annual number of days with precipitation higher than 10 mm (*Kostopoulou* and *Jones*, 2005). Change towards drier conditions with increasing drought frequency occurred after about 1970 (*Hoerling et al.*, 2012). Increased frequency and intensity of droughts in the Mediterranean region is not just a consequence of natural variability; evidences for anthropogenically forced drying were also determined (*Cook et al.*, 2016), among which key forcings were anthropogenic greenhouse gasses and aerosols, and the sea surface temperatures (*Hoerling et al.*, 2012). Despite a decrease in the total precipitation, studies found an upward tendency in the extreme precipitation over many Mediterranean areas (*Abbasnia* and *Toros*, 2019; *Nastos* and *Zerefos*, 2008; *Ribes et al.*, 2019; *Yosef et al.*, 2019; etc.).

Similar changes in precipitation were observed in the Mediterranean part of Southeast Europe where Montenegro is located. A downward trend in annual and summer precipitations have been present throughout Croatia (*Gajić-Čapka* and *Cindrić*, 2011), Slovenia (*Tošić et al.*, 2016), and over the sub-Mediterranean part of Bosnia and Herzegovina (where, similarly to Montenegro, a drying period started in the early 1980s) (*Popov et al.*, 2019a). Furthermore, despite a reduction in the total precipitation amounts, an upward tendency in the

precipitation intensity was also found over many areas in Southeast Europe (*Kostopoulou* and *Jones*, 2005). Previous research conducted in Montenegro also determined a dominant decreasing trend in the total annual precipitation (as well as in the annual number of days with precipitation) all over the country; however, despite a general decline in the total precipitation, precipitation intensity slightly increased (*Burić et al.*, 2015). Due to stated changes in precipitation (negative trends in total precipitation and increasing tendency of precipitation intensity), both extreme floods and droughts have become more frequent (*Ćulafić et al.*, 2017). The decreasing rainfall and a prominent increase in temperature already reflected on the river flows. For instance, the Lim River displayed a decreasing trend in flow during the period 1948–2014 (*Ćulafić et al.*, 2017).

Projections show that by the end of the 21st century, the eastern part of the Mediterranean region will be strongly affected by climate change, i.e., by decreases in precipitation and increases in the intensity and frequency of droughts and warm spells occurrence (*Lelieveld et al.*, 2012). Over the Mediterranean region in the 21st century, as temperature continues to increase (particularly rapidly in summer), precipitation will decrease (*Cardoso Pereira et al.*, 2019; *Giorgi et al.*, 2019; *Lionello* and *Scarascia*, 2018). Projections suggest that the most prominent decrease in precipitation will occur especially in the warm season (*Giorgi et al.*, 2019). Projections for Southeast Europe show that mean precipitation will decrease in the period 2021–2050 relative to the reference period 1961–1990, whereas mean air temperature, mean potential and actual evapotranspiration will increase between the two periods (*Cheval et al.*, 2017). Reduction in precipitation for the part of the Mediterranean region where Montenegro is located will be the largest in the summer season (*Lionello* and *Scarascia*, 2018), which is in concordance with the already observed trends. The Mediterranean region will be particularly vulnerable to future changes in extreme temperature and precipitation (*Paxian et al.*, 2015). Despite a decrease in mean precipitation, studies suggest that by the end of the century, heavy precipitation will show drastic increase across many areas (*Barcikowska et al.*, 2018; *Paxian et al.*, 2015; *Samuels et al.*, 2018; *Santos et al.*, 2019; *Tramblay* and *Somot*, 2018). Over this part of the Mediterranean region, besides total precipitation, consecutive wet days and number of wet days will decrease, whereas precipitation on extremely wet days are expected to increase (*Samuels et al.*, 2018). For the Balkan region, these changes are projected to be particularly strong during the summer season (*Paxian et al.*, 2015). Over the Balkans, positive trends in extreme precipitation could have strong impacts regarding flood hazards (*Tramblay* and *Somot*, 2018), whereas reducing total precipitation and increasing annual number of dry days, along with continued warming, could increase the susceptibility to droughts.

6. Conclusion

Principal component analysis and cluster analysis of seven precipitation-based input variables, calculated using data on mean monthly precipitation from 17 meteorological stations for the period 1961–2015, were used in order to achieve an eigenvector-based regionalization of Montenegro, i.e., to identify areas with similar spatial patterns of precipitation. In addition to the new regionalization, the study aims to contribute to the new knowledge on changes in precipitation over this part of the Mediterranean region during the last half century. The obtained results of precipitation trend analysis (primarily the reduction in annual and summer precipitations and an increase in the autumn season) confirm findings of the previous studies carried out for Montenegro and other parts of the Mediterranean region.

The observed changes in precipitation over Montenegro (as well as the changes projected by the end of the century) suggest that further analysis should be focused on adaptation and mitigation options in order to minimize the negative impacts of climate change and to achieve sustainable development of all of the most important socio-economic sectors and nature conservation in Montenegro.

References

Abbasnia, M. and *Toros, H.*, 2019: Analysis of Long-Term Changes in Extreme Climatic Indices: A Case Study of the Mediterranean Climate, Marmara Region, Turkey. In (Eds: *Vilibić, I., Horvath, K., Palau, J.*) Meteorology and Climatology of the Mediterranean and Black Seas. Pageoph Topical Volumes. Birkhäuser, Cham. 141–153.

Alexander, L.V., Zhang, X., Peterson, T.C., Caesar, J., Gleason, B., Klein Tank, A.M.G., Haylock, M., Collins, D., Trewin, B., Rahimzadeh, F., Tagipour, A., Rupa Kumar, K., Revadekar, J., Griffiths, G., Vincent, L., Stephenson, D.B., Burn, J., Aguilar, E., Brunet, M., Taylor, M., New, M., Zhai, P., Rusticucci, M. and *Vazquez-Aguirre, J.L.*, 2006: Global Observed Changes in Daily Climate Extremes of Temperature and Precipitation. *J. Geophys. Res. Atmos. 111*(*D5)*, D05109. https://doi.org/10.1029/2005JD006290

Almazroui, M., Dambul, R., Nazrul Islam, M. and *Jones, P.D.*, 2015: Principal Components-Based Regionalization of the Saudi Arabian Climate. *Int. J. Climatol. 35(9)*, 2555–2573. https://doi.org/10.1002/joc.4139

Barcikowska, M.J., Kapnick, S.B. and *Feser, F.*, 2018: Impact of Large-Scale Circulation Changes in the North Atlantic Sector on the Current and Future Mediterranean Winter Hydroclimate. *Clim. Dyn. 50(5-6)*, 2039–2059. https://doi.org/10.1007/s00382-017-3735-5

Bartholy, J. and *Pongrácz, R.*, 2010: Analysis of Precipitation Conditions for the Carpathian Basin Based on Extreme Indices in the 20th Century and Climate Simulations for 2050 and 2100. *Phys. Chem. Earth. 35(1-2)*, 43–51. https://doi.org/10.1016/j.pce.2010.03.011

Bravo Cabrera, J.L., Azpra Romero, E., Zarraluqui Such, V., Gay García, C. and *Estrada Porrúa, F.*, 2012: Cluster Analysis for Validated Climatology Stations Using Precipitation in Mexico. *Atmósfera 25(4)*, 339–354.

Burić, D., Ducić, V. and *Mihajlović, J., 2013:* The Climate of Montenegro: Modificators and Types – Part One. *Bull. Serbian Geogr. Soc. 93(4)*, 83–102. https://doi.org/10.2298/GSGD1304083B

Burić, D., Ducić, V. and Mihajlović, J., 2014: The Climate of Montenegro: Modificators and Types – Part Two. *Bull. Serbian Geogr. Soc. 94(1)*, 73–90. https://doi.org/10.2298/GSGD1401073B

Burić, D., Luković, J., Bajat, B., Kilibarda, M. and *Živković, N.*, 2015: Recent Trends in Daily Rainfall Extremes over Montenegro (1951–2010). *Nat. Hazard Earth. Sys. 15(9)*, 2069–2077. https://doi.org/10.5194/nhess-15-2069-2015

Caloiero, T., Caloiero, P. and *Frustaci, F.*, 2018: Long-Term Precipitation Trend Analysis in Europe and in the Mediterranean Basin. *Water Environ. J. 32*, 433–445. https://doi.org/10.1111/wej.12346

Cardoso Pereira, S., Marta-Almeida, M., Carvalho, A.C. and *Rocha, A.*, 2019: Extreme Precipitation Events under Climate Change in the Iberian Peninsula. *Int. J. Climatol. 40*, 1255–1278. https://doi.org/10.1002/joc.6269

Chen, D., Walther, A., Moberg, A., Jones, P., Jacobeit, J. and *Lister, D.*, 2015: European Trend Atlas of Extreme Temperature and Precipitation Records. Springer, Dordrecht.

Cheval, S., Dumitrescu, A. and *Birsan, M.V.*, 2017: Variability of the Aridity in the South-Eastern Europe over 1961–2050. *Catena 151*, 74–86. https://doi.org/10.1016/j.catena.2016.11.029

Çiçek, İ. and *Duman, N.*, 2015: Seasonal and Annual Precipitation Trends in Turkey. *Carpath. J. Earth Env. 10(2)*, 77–84.

Cook, B.I., Anchukaitis, K.J., Touchan, R., Meko, D.M. and *Cook, E.R.*, 2016: Spatiotemporal Drought Variability in the Mediterranean over the Last 900 Years. *J. Geophys. Res. Atmos. 121(5)*, 2060–2074. https://doi.org/10.1002/2015JD023929

Ćulafić, G., Mitrović, L., Ivanov, M. and *Golijanin, J.*, 2017: The Impact of Climate Change on the Water Regime of the Lim River. In (Ed: *Jojić, D.*) Proceedings of the 20th Anniversary of the Faculty of Natural Sciences and Mathematics at the University of Banja Luka. Faculty of Natural Sciences and Mathematics, University of Banja Luka, Banja Luka, 164–170. (in Serbian)

Dayon, G., Boé, J., Martin, É. and *Gailhard, J.*, 2018: Impacts of Climate Change on the Hydrological Cycle over France and Associated Uncertainties. *Cr. Geosci. 350(4)*, 141–153. https://doi.org/10.1016/j.crte.2018.03.001

Deitch, M.J., Sapundjieff, M.J. and *Feirer, S.T.*, 2017: Characterizing Precipitation Variability and Trends in the World's Mediterranean-Climate Areas. *Water 9*, 259. https://doi.org/10.3390/w9040259

Demšar, U., Harris, P., Brunsdon, C., Fotheringham, A.S. and *McLoone, S.*, 2013: Principal Component Analysis on Spatial Data: An Overview. *Ann. Am. Assoc. Geogr. 103(1)*, 106–128. https://doi.org/10.1080/00045608.2012.689236

D'Oria, M., Ferraresi, M. and *Tanda, M.G.*, 2017: Historical Trends and High-Resolution Future Climate Projections in Northern Tuscany (Italy). *J. Hydrol. 555*, 708–723. https://doi.org/10.1016/j.jhydrol.2017.10.054

Ducić, V., Luković, J., Burić, D., Stanojević, G. and *Mustafić, S.*, 2012: Precipitation Extremes in the Wettest Mediterranean Region (Krivošije) and Associated Atmospheric Circulation Types. *Nat. Hazard Earth. Sys. 12(3)*, 687–697. https://doi.org/10.5194/nhess-12-687-2012

Everitt, B.S., Landau, S., Leese, M. and *Stahl, D.*, 2011: Cluster Analysis (Fifth Edition). John Wiley & Sons, Chichester.

Gajić-Čapka, M. and *Cindrić, K.*, 2011: Secular Trends in Indices of Precipitation Extremes in Croatia, 1901–2008. *Geofizika 28*, 293–312.

Giorgi, F., Raffaele, F. and *Coppola, E.*, 2019: The Response of Precipitation Characteristics to Global Warming from Climate Projections. *Earth Syst. Dynam. 10(1)*, 73–89. https://doi.org/10.5194/esd-10-73-2019

Gocic, M. and *Trajkovic, S.*, 2014: Spatio-Temporal Patterns of Precipitation in Serbia. *Theor. Appl. Climatol. 117(3)*, 419–431. https://doi.org/10.1007/s00704-013-1017-7

Goossens, C.R., 1985: Principal Component Analysis of Mediterranean Rainfall. *J. Climate 5(4)*, 379–388. https://doi.org/10.1002/joc.3370050405

Guirguis, K.J. and *Avissar, R.*, 2008: A Precipitation Climatology and Dataset Intercomparison for the Western United States. *J. Hydrometeorol. 9(5)*, 825–841. https://doi.org/10.1175/2008JHM832.1

Hoerling, M., Eischeid, J., Perlwitz, J., Quan, X., Zhang, T. and *Pegion, P.*, 2012: On the Increased Frequency of Mediterranean Drought. *J. Clim. 25*, 2146–2161. https://doi.org/10.1175/JCLI-D-11-00296.1

Institute of Hydrometeorology and Seismology of Montenegro, 2006: Climatological Normals. Retrieved on April 17, 2018 from http://www.meteo.co.me/misc.php?text=126&sektor=1

Jolliffe, I.T., 1998: Principal Component Analysis (Springer Series in Statistics). Springer-Verlag, New York.

Journée, M., Delvaux, C. and *Bertrand, C.*, 2015: Precipitation Climate Maps of Belgium. *Adv. Sci. Res. 12*, 73–78. https://doi.org/10.5194/asr-12-73-2015

Kaiser, H., 1974: An Index of Factor Simplicity. *Psychometrika 39*, 31–36. https://doi.org/10.1007/BF02291575

Kendall, M.G., 1975: Rank Correlation Methods (Fourth Edition). Charles Griffin, London.

Kostopoulou, E. and *Jones, P.D.*, 2005: Assessment of Climate Extremes in the Eastern Mediterranean. *Meteorol. Atmos. Phys. 89(1–4)*, 69–85. https://doi.org/10.1007/s00703-005-0122-2

Lelieveld, J., Hadjinicolaou, P., Kostopoulou, E., Chenoweth, J., El Maayar, M., Giannakopoulos, C., Hannides, C., Lange, M.A., Tanarhte, M., Tyrlis, E. and *Xoplaki, E.*, 2012: Climate Change and Impacts in the Eastern Mediterranean and the Middle East. *Clim. Change 114(3–4)*, 667–687. https://doi.org/10.1007/s10584-012-0418-4

Lionello, P. and *Scarascia, L.*, 2018: The Relation between Climate Change in the Mediterranean Region and Global Warming. *Reg. Environ. Change 18(5)*, 1481–1493. https://doi.org/10.1007/s10113-018-1290-1

Lionello, P., Abrantes, F., Congedi, L., Dulac, F., Gacic, M., Gomis, D., Goodess, C., Hoff, H., Kutiel, H., Luterbacher, J., Planton, S., Reale, M., Schröder, K., Struglia, M. V., Toreti, A., Tsimplis, M., Ulbrich, U. and *Xoplaki, E.*, 2012: Introduction: Mediterranean Climate – Background Information. In (Ed: *Lionello, P.*) The Climate of the Mediterranean Region from the Past to the Future. Elsevier, Amsterdam. xxxv–xc.

Lovino, M., García, N.O. and *Baethgen, W.*, 2014: Spatiotemporal Analysis of Extreme Precipitation Events in the Northeast Region of Argentina (NEA). *J. Hydrol. Reg. Stud. 2*, 140–158. https://doi.org/10.1016/j.ejrh.2014.09.001

Lyra, G.B., Oliveira-Júnior, J.F. and *Zeri, M.*, 2014: Cluster Analysis Applied to the Spatial and Temporal Variability of Monthly Rainfall in Alagoas State, Northeast of Brazil. *Int. J. Climatol. 34(13)*, 3546–3558. https://doi.org/10.1002/joc.3926

Mann, H.B., 1945: Non-Parametric Tests Against Trend. *Econometrica 13*, 245–259. https://doi.org/10.2307/1907187

Markonis, Y., Batelis, S.C., Dimakos, Y., Moschou, E. and *Koutsoyiannis, D.*, 2017: Temporal and Spatial Variability of Rainfall over Greece. *Theor. Appl. Climatol. 130(1–2)*, 217–232. https://doi.org/10.1007/s00704-016-1878-7

Mills, G.F., 1995: Principal Component Analysis of Precipitation and Rainfall Regionalization in Spain. *Theor. Appl. Climatol. 50(3–4,)* 169–183. https://doi.org/10.1007/BF00866115

Muñoz-Díaz, D. and *Rodrigo, F.S.*, 2004: Spatio-Temporal Patterns of Seasonal Rainfall in Spain (1912–2000) Using Cluster and Principal Component Analysis: Comparison. *Ann. Geophys. 22*, 1435–1448. https://doi.org/10.5194/angeo-22-1435-2004

Napoli, A., Crespi, A., Ragone, F., Maugeri, M. and *Pasquero, C.*, 2019: Variability of Orographic Enhancement of Precipitation in the Alpine Region. *Sci. Rep. 9*, 13352. https://doi.org/10.1038/s41598-019-49974-5

Nastos, P.T. and *Zerefos, C.S.*, 2008: Decadal Changes in Extreme Daily Precipitation in Greece. *Adv. Geosci. 16*, 55–62. https://doi.org/10.5194/adgeo-16-55-2008

North, G.R, Bell, T.L., Cahalan, R.F. and *Moeng, F.J.*, 1982: Sampling Errors in the Estimation of Empirical Orthogonal Functions. *Mon. Weather Rev. 110*, 699–706. https://doi.org/10.1175/1520-0493(1982)110<0699:SEITEO>2.0.CO;2

Oliver, J.E., 1980: Monthly Precipitation Distribution: A Comparative Index. *Prof. Geogr. 32(3)*, 300–309. https://doi.org/10.1111/j.0033-0124.1980.00300.x

Paxian, A., Hertig, E., Seubert, S., Vogt, G., Jacobeit, J. and *Paeth, H.*, 2015: Present-Day and Future Mediterranean Precipitation Extremes Assessed by Different Statistical Approaches. *Clim. Dyn. 44(3–4)*, 845–860. https://doi.org/10.1007/s00382-014-2428-6

Piras, M., Mascaro, G., Deidda, R. and *Vivoni, E.R.*, 2016: Impacts of Climate Change on Precipitation and Discharge Extremes through the Use of Statistical Downscaling Approaches in a Mediterranean Basin. *Sci. Total Environ. 543(Part B)*, 952–964.

https://doi.org/10.1016/j.scitotenv.2015.06.088
Popov, T., Gnjato, S. and *Trbić, G.*, 2019a: Changes in Precipitation over the East Herzegovina Region. *Bull. Serbian Geogr. Soc. 99(1)*, 29–44. https://doi.org/10.2298/GSGD1901029P
Popov, T., Gnjato, S., Bajić, D. and *Trbić, G.*, 2019b: Spatial Patterns of Precipitation in Bosnia and Herzegovina. *J. Geogr. Inst. Jovan Cvijić SASA. 69(3)*, 185–195. https://doi.org/10.2298/IJGI1903185P
Ribes, A., Thao, S., Vautard, R., Dubuisson, B., Somot, S., Colin, J., Planton, S. and *Soubeyroux, J.M.*, 2019: Observed Increase in Extreme Daily Rainfall in the French Mediterranean. *Clim. Dyn. 52(1–2)*, 1095–1114. https://doi.org/10.1007/s00382-018-4179-2
Río, S.d., Herrero, L., Fraile, R. and *Penas, A.*, 2011: Spatial Distribution of Recent Rainfall Trends in Spain (1961–2006). *Int. J. Climatol. 31(5)*, 656–667. https://doi.org/10.1002/joc.2111
Rodrigo, F.S. and *Trigo, R.M.*, 2007: Trends in Daily Rainfall in the Iberian Peninsula from 1951 to 2002. *Int. J. Climatol. 27(4)*, 513–529. https://doi.org/10.1002/joc.1409
Samuels, R., Hochman, A., Baharad, A., Givati, A., Levi, Y., Yosef, Y., Saaroni, H., Ziv, B., Harpaz, T. and *Alpert, P.*, 2018: Evaluation and Projection of Extreme Precipitation Indices in the Eastern Mediterranean Based on CMIP5 Multi-Model Ensemble. *Int. J. Climatol. 38(5)*, 2280–2297. https://doi.org/10.1002/joc.5334
Santos, M., Fonseca, A., Fragoso, M. and *Santos, J.A.*, 2019: Recent and Future Changes of Precipitation Extremes in Mainland Portugal. *Theor. Appl. Climatol. 137(1–2)*, 1305–1319. https://doi.org/10.1007/s00704-018-2667-2
Sen, P.K., 1968: Estimates of the Regression Coefficient Based on Kendall's Tau. *J. Am. Stat. Assoc. 63*, 1379–1389. https://doi.org/10.2307/2285891
Singh, S.K., Lo, E.Y. and *Qin, X.*, 2017: Cluster Analysis of Monthly Precipitation over the Western Maritime Continent under Climate Change. *Climate 5(4)*, 84. https://doi.org/10.3390/cli5040084
Stathis, D. and *Myronidis, D.*, 2009: Principal Component Analysis of Precipitation in Thessaly Region (Central Greece). *Global Nest J. 11(4)*, 467–476. https://doi.org/10.30955/gnj.000534
Tošić, I., Zorn, M., Ortar, J., Unkašević, M., Gavrilov, M.B. and *Marković, S.B.*, 2016: Annual and Seasonal Variability of Precipitation and Temperatures in Slovenia from 1961 to 2011. *Atmos. Res. 168*, 220–233. https://doi.org/10.1016/j.atmosres.2015.09.014
Tramblay, Y. and *Somot, S.*, 2018: Future Evolution of Extreme Precipitation in the Mediterranean. *Clim. Change 151(2)*, 289–302. https://doi.org/10.1007/s10584-018-2300-5
Tu, K., Yan, Z.W. and *Wang, Y.*, 2011: A Spatial Cluster Analysis of Heavy Rains in China. *Atmos. Ocean Sci. Lett. 4(1)*, 36–40. https://doi.org/10.1080/16742834.2011.11446897
Türkeş, M., Koç, T. & Sariş, F., 2009: Spatiotemporal Variability of Precipitation Total Series over Turkey. *Int. J. Climatol. 29(8)*, 1056–1074. https://doi.org/10.1002/joc.1768
Van Rooy, M.P., 1965: A Rainfall Anomaly Index (RAI) Independent of Time and Space. *Notos 14*, 43–48.
Ward, J.H., 1963: Hierarchical Groupings to Optimize an Objective Function. *J. Am. Stat. Assoc. 58*, 236–244. https://doi.org/10.1080/01621459.1963.10500845
White, D., Richman, M. and *Yarnal, B.*, 1991: Climate Regionalization and Rotation of Principal Components. *Int. J. Climatol. 11(1)*, 1–25. https://doi.org/10.1002/joc.3370110102
Wigley, T.M.L., Lough, J.M. and *Jones, P.D.*, 1984: Spatial Patterns of Precipitation in England and Wales and Revised England and Wales Precipitation Time Series. *J. Climate. 4(1)*, 1–25, https://doi.org/10.1002/joc.3370040102
Yosef, Y, Aguilar, E. and *Alpert, P.*, 2019: Changes in Extreme Temperature and Precipitation Indices: Using an Innovative Daily Homogenized Database in Israel. *Int. J. Climatol. 39(13)*, 5022–5045. https://doi.org/10.1002/joc.6125

DOI:10.28974/idojaras.2020.4.6

IDŐJÁRÁS

Quarterly Journal of the Hungarian Meteorological Service
Vol. 124, No. 4, October – December, 2020, pp. 521–539

Estimation of Dew Point Temperature in Different Climates of Iran Using Support Vector Regression

Mohammad Nazeri-Tahroudi[1] and **Yousef Ramezani**[2,*]

[1] *Department of Water Engineering, University of Birjand, Birjand, Iran*

[2] *Department of Water Engineering, University of Birjand, Birjand, Iran*

**Corresponding author E-mail: y.ramezani@birjand.ac.ir*

(Manuscript received in final form November 11, 2019)

Abstract— The prediction of global climate change using the values recorded in a statistical period requires a precise method that can accurately identify the fluctuations of these changes. By patterning these changes, the parameter values for the years or future periods are predicted, or the statistical gap can be eliminated. In this research, meteorological data of six stations in different climates of Iran were used to model and estimate the values of the dew point temperature (DPT). The stations studied are Ahvaz, Urmia, Kerman, Gorgan, Rasht, and Babolsar. In order to estimate the DPT values, support vector regression was used, and to optimize the parameters of the support vector regression model, the ant colony algorithm was used. In this study, four different input patterns of meteorological data have been investigated as input of the support vector regression model. Pattern I with seven inputs (monthly minimum, maximum, and average air temperatures, monthly precipitation, saturation vapor pressure, actual vapor pressure and relative humidity), Pattern II with three inputs (monthly average air temperature, saturation vapor pressure, and actual vapor pressure), Pattern III with two inputs (monthly minimum and maximum air temperatures), and Pattern IV with an input (monthly average air temperature) were used. It is recommended that if the number of inputs in the model is small, the model will be more user-friendly. Based on the results of analyzing different patterns, it can be concluded, that Pattern III is the suitable pattern for estimating DPT values at the stations studied in different climates of Iran based on the three criteria of root mean square error (RMSE), Nash–Sutcliffe model efficiency coefficient (NSE), and coefficient of determination (R^2). Overall, the results showed that the selected pattern increases the accuracy of the model by up to 24% compared to the conventional model.

Key-words: Ant Colony Algorithm, FAO Penman – Monteith, Modeling, Nonlinear Regression.

1. Introduction

Dew occurs when the temperature is equal to the dew point temperature (DPT). These conditions occur on the ground for two important reasons. First, the propagation of longwave radiation makes the surface of the ground cool in the night. For condensation, temperature need to be reduced to DPT. Second, often the soil provides dew point moisture. That is, wet and warm soils can help to form dew. Cooling of wet soil during the night will cause condensation, especially in clear nights. Clear nights allow long wavelengths radiation have max propagation to space. The cloudy sky can absorb a portion of the longwave radiation and reflect the other part back to the ground, which prevents the surface from cooling too much. Calm wind prevents mixing of wet air and dry air above it. Heavy dew tends to happen when the wind is calm, not when the wind is strong. Especially, when the soil is wet, the density of the moisture is higher on the surface than on the top. Therefore, cooling of air with high moisture can make condensation. Soil moisture is very important for the production of dew (especially heavy dew). The probability of heavy dew formation in arid areas that do not receive rain during one or two weeks, is very low. When the soil gets wet well, it takes several days to lose its moisture through evaporation. If the night after the rain is clear, dew can be formed during next mornings (especially in areas with vegetation, clear sky, and calm winds). The difference between temperature and DPT is also important, because it determines how much temperature should be cooled to reach saturation. A low DPT, along with favorable factors for dew, is likely to cause heavy dew.

Access to accurate DPT data is of particular importance in various fields of science such as hydrology, climate, and agriculture. DPT is the temperature at which the air must reach its lowest point of saturation. In fact, it is the temperature at which water vapor turns into liquid. The exchange of radiation between the Earth's surface and the atmosphere, the vapor pressure, and the turbulent heat are the most important factors in the formation of dew (*Mohammadi et al*., 2016).

The climate change and the increasing need for water have made management planning more effective in controling water use in the future. With prediction and modeling of various hydrological parameters, in addition to managing the use of water resources, their behavior can be studied. The results of a simulation model can also be used to verify the accuracy of data, or to modify and complete them. According to *Govindaraju* (2000), models used today in hydrology include mathematical-physical, geomorphologic, and empirical models. The first set of models is based on the physical properties of the system, which are expressed in terms of differential equations. Meanwhile, the second group is based on the geomorphological characteristics of the hydrological system. Experimental models attempt to establish a relationship between input and output data regardless of parameters that, these models are

also known as average or black box models. So far, various researchers around the world have developed and modeling models for modeling and predicting various hydrological data in hourly, daily and monthly time scales. Genetic programming is a branch of evolutionary algorithms which is capable of modeling completely nonlinear and dynamic processes. The genetic programming method was first developed by *Koza* (1992). This method is considered as an evolutionary algorithm approach, based on Darwin's theory of evolution. The above algorithms attempt to define an objective function in the form of qualitative criteria then to use the above function to compare the various problem-solving solutions in a step-by-step process of data structure correction, and finally, they provide the suitable solution. Genetic programming is one method among evolutionary algorithm methods which is more suitable due to its precision (*Alvisi et al*., 2006).

The support vector machine (SVM) is also one of the supervised learning methods which can be used for both categorization and regression. This method has been developed by *Vapnik* (1998) on the basis of statistical learning theory. The support vector machine is a method for double-class classification in arbitrary features space, and therefore, it is a suitable method for prediction problems (*Pai* and *Hong* 2007). The support vector machine is basically a two-class classification which separates classes by a linear boundary. In this method, the closest examples to the decision boundary are called support vectors. These vectors determine the decision boundary equation. Classic intelligent simulation algorithms, such as artificial neural networks, usually minimize the mean absolute error or root mean square error of the training data, but SVM models use the principle of minimizing structural errors (*Hamel*, 2011). Recently, these models have been used in a wide range of hydrological problems, in particular, in the prediction of flow data.

The SVM model and the MLP (multi-layer perceptron) pattern of the artificial neural network were used to predict the monthly level of Eris Lake in North America by *Khan* and *Coulibaly* (2006). The results showed that the SVM model had a high performance in predicting the level of this lake. To predict Caspian Sea level changes, *Imani et al*. (2014) used SVM and GEP (gene expression programming) models with satellite data. The results showed that the SVM model with a root mean square error of 0.305 m and a coefficient of determination of 0.96 has a better performance than the GEP model.

Jeong et al. (2012) examined the monthly precipitation in Korea using the ANFIS model. They analyzed the correlation between climatic and hydrologic data and obtained three parameters for the development of the ANFIS model. *Citakoglu et al*. (2014) used an ANFIS and ANN method to investigate monthly evapotranspiration in Turkey. They surveyed various climatic data to obtain the appropriate fitness as input, and they concluded that the accuracy of both models is reasonable, but the accuracy of the ANN model is greater. *Cobaner et al*. (2014) have modeled the maximum, minimum, and average temperatures of

Turkey using the ANN, ANFIS, and MLR models. By examining these models, it was concluded that the ANFIS model has a higher accuracy than the other models. *Zounemat-Kermani* (2012) compared MLR models and the Levenberg-Marquardt (LM) model to estimate DPT data in Ontario, Canada. By examining these models, the results showed that the Levenberg-Marquardt (LM) algorithm yields better results than the MLR model. *Shiri et al.* (2014) examined the accuracy of two models, GP and ANN, to estimate the DPT data at two stations in Korea. Their research results showed that the accuracy of the GP model is better than that of the ANN. *Kim et al.* (2015) estimated daily DPT values using two soft computing techniques in California (USA). By comparing a conventional regression model, they found that the more advanced software computational models are more flexible in determining daily DPT estimates and have higher accuracy. *Mohammadi et al.* (2016) used the ANFIS model to select DPT-compatible data. They used minimum, maximum, and average temperatures, DPT, relative humidity, atmospheric vapor pressure, water vapor pressure, sunshine hours, and horizontal radiation data of two stations in Iran. The results of their research showed that the use of two time series of minimum temperature and water vapor pressure increases the accuracy of DPT data prediction. *Santamaría-Bonfil et al.* (2016) proposed a hybrid methodology for wind speed forecasting based on support vector regression using historical wind speed data from the Mexican Wind Energy Technology Center. They compared the hybrid model with autoregressive models. Results show, that forecasts made with our method are more accurate for medium (5–23 h ahead) short-term WSF (Wind Speed Forecasting) and WPF (Wind Power Forecasting) than those made with persistence and autoregressive models. *Ruan et al.* (2018) developed a model to estimate the temperature inside the three-core cable joint based on support vector regression (SVR). The results showed that the proposed model could accurately estimate the joint temperature, even though the thermal conductivity of armor wrap used in thermal analysis for model training differs from its real value.

Given the different climates of Iran, it will be difficult to provide a model that can be used for all regions. Different models in different climates of Iran should be checked and verified. Therefore, this research tried to evaluate the performance of the SVR model in DPT modeling using monthly minimum, maximum, and average air temperatures, saturation vapor pressure, actual vapor pressure, monthly precipitation, and relative humidity in five different climates of Iran.

2. *Material and methods*

2.1. Study area

Iran, with an area of over 1 648 000 square kilometers, is located in the Northern Hemisphere and on the Asian continent. Iran, with an average annual precipitation of 250 mm, is located between the two meridians of 44° and 64° East and two circuits 25° and 40° North. About 94.8 percent of the country's surface area is located in arid and semi-arid regions with low precipitation and high evapotranspiration (*Khalili et al*., 2016). In this study, monthly minimum, maximum, and average air temperatures, saturation vapor pressure, actual vapor pressure, monthly precipitation, dew point temperature, and relative humidity of Babolsar, Gorgan, Kerman, Rasht, Urmia, and Ahvaz stations were used in a 64-year-long statistical period (1951–2014). *Fig. 1* shows the studied area and the position of the stations. The characteristics of the meteorological stations were also described in *Table 1*.

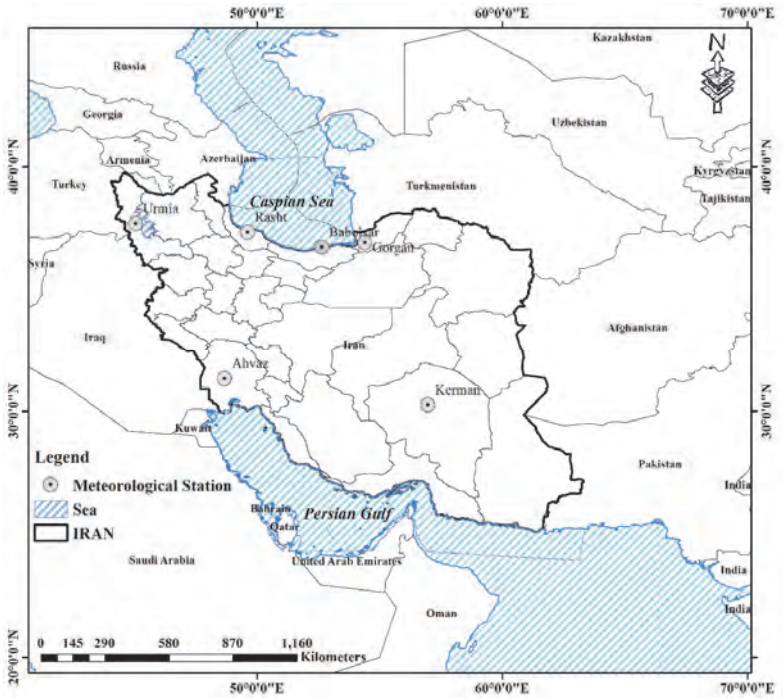

Fig. 1. Location map of the selected stations in Iran.

Table 1. Annual statistics of stations used in the period 1951–2014

Station	T_{min} (°C)	T_{avg}(°C)	T_{max} (°C)
Urmia	0.01	11.28	23.74
Ahvaz	13.41	26.10	37.91
Babolsar	8.71	16.80	26.85
Kerman	0.55	17.03	29.89
Gorgan	7.56	17.75	31.49
Rasht	6.04	16.22	23.97

2.2. De Martonne climate factor

De Martonne proposed the following formula in 1926 with variations in the relationship and the replacement of the evaporation with temperature (*Deer*, 1963):

$$I = \frac{P}{T + 10}, \tag{1}$$

whereI is the De Martonne aridity index, P is equal to the annual precipitation (mm), and T is equal to the average annual air temperature (°C). Although evaporation factor has been eliminated in De Martonne's relationship, evaporation has also been related to air temperature and rising temperature, increases evaporation. Therefore, the high value of I can be high due to low air temperature or high precipitation. Based on De Martonne's relationship, six types of climates have been classified in *Table 2*.

Table 2. Climatic classification based on the De Martonne index

Climate	I
Dry	I < 10
Moderately dry	10 < I < 19.9
Mediterranean	20 < I < 23.9
Moderately wet	24 < I < 27.9
Wet	28 < I < 34.9
Extremely wet	35 < I

2.3. Support vector regression (SVR)

The first use of this model in water issues was presented by *Dibike et al*. in 2001 by precipitation-runoff modeling (*Hofmann et al*., 2002). The support vector machine (SVM) of an efficient learning system based on a theory of optimization must use the principle of inductive minimization of structural error and leads to a general optimal solution. In the SVM regression model, the function related to the dependent variable *Y*, which itself is a function of several independent variables *x*, is estimated (Eq. 2). Similar to other regression issues, the relationship between independent and dependent variables is determined with algebraic function $f(x)$ (Eq. 3) plus allowed error ε:

$$y = f(x) + noise, \tag{2}$$

$$f(x) = W^T.\phi(x) + b \tag{3}$$

If W (vector of coefficients) and b (constant) are the characteristics of the regression function and ϕ is a kernel function, then the goal is to find a functional form for $f(x)$. This is accomplished by training SVM model by a set of samples (training set). Therefore, in order to calculate W and b, the error function must be optimized in the ε -SVM model, taking into account the conditions set out in Eqs. (4 and 5):

$$\frac{1}{2}W^T W + C\sum_{i=1}^{N}\xi_i + C\sum_{i=1}^{N}\xi_i^* \tag{4}$$

$$\begin{aligned} &W^T.\phi(x_i) + b - y_i \le \varepsilon + \xi_i^* \\ &y_i - W^T.\phi(x_i) - b \le \varepsilon + \xi_i \\ &\xi_i, \xi_i^* \ge 0 \quad , \quad i = 1,...,N \end{aligned} \tag{5}$$

In the above equations, C is a positive integer that determines the penalty when a model training error occurs, ϕ is the kernel function, N is the number of samples, and the two indices of ξ_i and ξ_i^* are the Slack variables, which determine the upper and lower limit of the training error associated with the allowed error value ε. In problems, it is predicted that the data is within the boundary range ε. Now, if the data is out of range ε, there will be an error equal to ξ_i and ξ_i^*. It is worth mentioning that the SVM model solves the problems

caused by the under fitting and over fitting by simultaneously minimizing two terms $W^T W/2$ and training errors, namely $C\sum_{i=1}^{N}(\xi_i+\xi_i^*)$, in. Therefore, by introducing the Lagrange coefficients a_i and a_i^*, the optimization problem will be solved with numerical maximization of the following quadratic function (Eqs. 6 and 7):

$$\sum_{i=1}^{N} y_i(a_i+a_i^*)-\varepsilon\sum_{i=1}^{N}(a_i+a_i^*)- 0.5\sum_{i,j=1}^{N}(a_i+a_i^*)(a_j+a_j^*)\phi(x_i)^T\phi(x_j) \quad , \tag{6}$$

$$\sum_{i=1}^{N}(a_i+a_i^*)=0 \qquad 0\le a_i\le C,\ 0\le a_i^*\le C,\ i=1,2,...,N \quad . \tag{7}$$

The above objective function is a convex function, and therefore, the solution would be unique and optimal. After defining the Lagrange coefficients, the characteristics *w* and *b* in the SVM regression model is calculated using the Karush-Kan-Tucker theory (Eq. 8):

$$W=\sum_{j=1}^{N}(a_i+a_i^*)\phi(x_i) \ . \tag{8}$$

As a result, the SVM regression model is:

$$W=\sum_{i=1}^{N}(a_i+a_i^*)\phi(x_i)^T\phi(\mathrm{x})+b \ . \tag{9}$$

It should be noted that the Lagrange terms $((a_i+a_i^*))$ can be zero or non-zero. Therefore, only data sets whose coefficients $\overline{a_i}$ are non-zero are entered in the final regression equation, and this data set is known as the support vectors. In simple terms, support vectors are data that help to create a regression function. Among the vectors mentioned, those whose $|\overline{a_i}|$ values are less than *C* are called margin support vectors. When the value $|\overline{a_i}|$ of the support vectors is equal to *C*, it is known as an error support vector or a bounded support vector. Margin support vectors are found on the margin of the insensitive boundary, while error support vectors are out of range. Finally, the regression SVM function can be rewritten in the following form:

$$f(x) = \sum_{i=1}^{N} a_i \phi(x_i)^T \phi(x_j) + b \,. \quad (10)$$

In Eq. (10), the calculation of $\phi(x)$ in its characteristic space may be very complicated. To solve this problem, the regular trend in the SVM regression model is the selection of a kernel function as $K(x_i, x) = \phi(x_i)^T \phi\sqrt{b^2 - 4ac}$. Various kernel functions can be used to construct different types of ε-SVM models. The most commonly used kernel functions available in the vector regression model are: (i) polynomial kernel with 3 target characteristics, (ii) a sigmoid kernel containing 2 target characteristics, and (iii) a kernel of radial base functions (RBF) with target characteristics.

2.4. Ant colony algorithm (ACO)

The ACO algorithm is a meta-exploration methodology that was proposed in 1992 by *Dorigo*. The ant colony algorithm was the first ACO algorithm proposed by *Colorni et al.* in 1991. One of the first applications of the ACO algorithm has been to solve the traveling salesman problem (*Dorigo*, 1992). Since the ACO algorithms depend on the type of use and similarity of the ants moving on the graph, the use of the traveling salesman problem to explain the basic principles of ant algorithms was highly logical, and it was originally a typical example for introducing this algorithm (*Akbarpour et al.*, 2020).

In this study, the ACO algorithm with 50 replicates and 50 members of the population was used to optimize the *ε*, sigma, and *C* parameters of the multivariate support vector regression (MSVR) model to develop the MSVR-ACO model. The objective function in the algorithm is to reduce the error rate in the estimated values using the root mean square error (RMSE).

In this study, different input patterns of meteorological data have been investigated as input of the MSVR-ACO model, and the superior model was determined at each meteorological station. The four patterns in this study are described in *Table 3*. The flowchart of the proposed methodology is demonstrated in *Fig. 2*.

Table 3. Patterns of the MSVR-ACO model

Pattern	Number of inputs	Input variables
I	seven parameters	monthly minimum, maximum, and average air temperatures, monthly precipitation, saturation vapor pressure, actual vapor pressure, and relative humidity
II	three parameters	monthly average air temperature, saturation vapor pressure, and actual vapor pressure
III	two parameters	monthly minimum and maximum air temperatures
IV	one parameter	monthly average air temperature

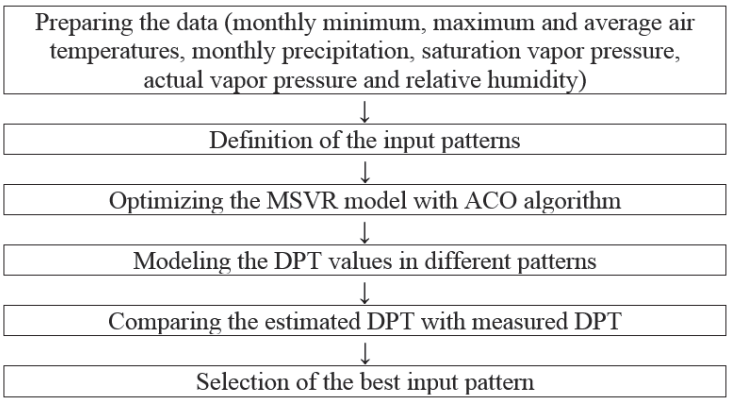

Fig. 2. Flowchart of the proposed methodology.

3. Results and discussion

As it was mentioned, the De Martonne's method was used to study the climate in the studied areas. Results of the study are presented in *Table 4*.

Table 4. Results of the study of the climate of the studied areas based on the De Martonne index

Station	Average annual air temperature (ºC)	Annual precipitation (mm)	De Martonne index	Climate
Urmia	11.28	337.33	15.85	Moderately dry
Ahvaz	26.10	234.40	6.49	Dry
Babolsar	16.80	890.88	33.24	Wet
Kerman	17.03	147.53	5.45	Dry
Gorgan	17.75	571.53	20.59	Mediterranean
Rasht	16.22	1334.51	50.89	Extremely wet

According to the results presented in *Table 4*, it can be seen that the stations studied have been selected from different climates. It should be noted that in this research the ACO algorithm was used to optimize the parameters of the MSVR model. The results of the evaluation of the performance of the ACO algorithm in estimating the DPT values of the Babolsar station were presented as an example in *Fig. 3*. Regarding *Fig. 3*, it can be seen that after 17 iterations, no improvement was achieved.

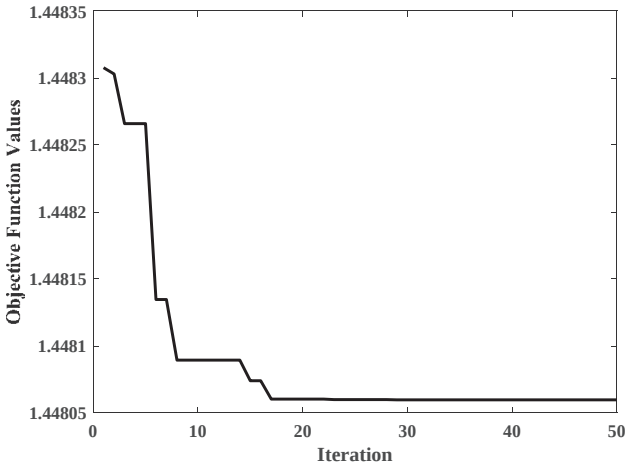

Fig. 3. Results of the performance of the ant colony algorithm in estimating DPT values at Babolsar station (Pattern *IV*).

The DPT values was simulated using the optimal values of the parameters of the MSVR model. The results of estimating the DPT values of Gorgan and Kerman stations are presented in *Figs. 4* and *5* (Pattern *I*)

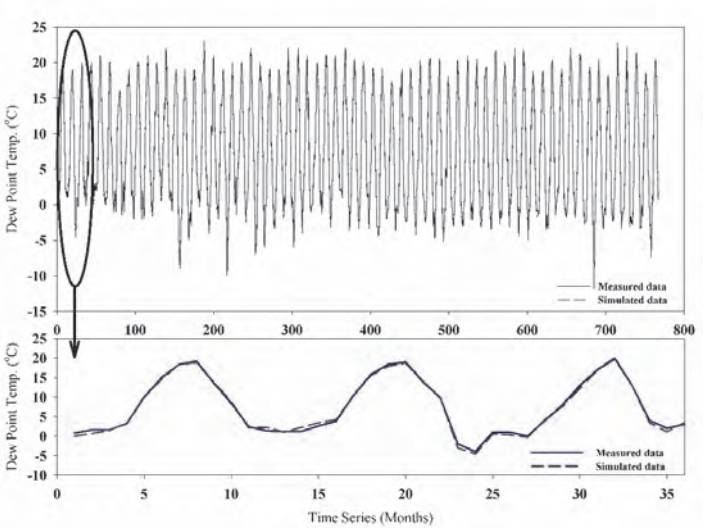

Fig. 4. Estimation of DPT values of Gorgan meteorological station using Pattern *I.*

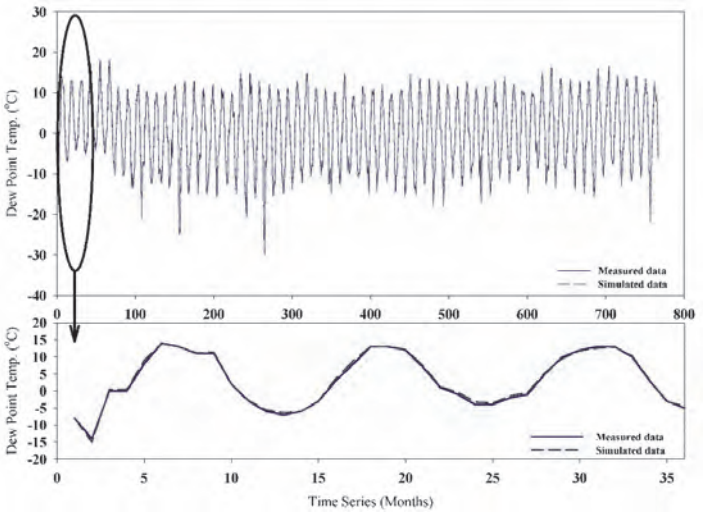

Fig. 5. Estimation of DPT values of Kerman meteorological station using Pattern *I.*

According to the results presented in *Figs. 4* and *5*, it can be seen that selection of seven parameters as inputs of the MSVR-ACO model will be able to model the DPT values of the studied stations. Also, the results indicate the DPT values with high accuracy, which have been derived from the integration of the MSVR model and the ACO algorithm. Other input patterns were also calculated, and the accuracy of different patterns were verified by three RMSE, coefficient of determination (R^2), and Nash–Sutcliffe model efficiency coefficient tests. The results of the investigation and verification of various patterns in the estimation of DPT values are presented in *Figs. 6*, *7*, and *8*.

The results of verification of MSVR-ACO model in examining different patterns indicated that in Gorgan meteorological station, Pattern *I* had the lowest RMSE (*Fig. 5*). At this station, Pattern *III* was ranked second. This pattern has an RMSE of 0.61 °C in estimating DPT values. Pattern *IV* has error almost identical to a high RMSE, Pattern *I*, Pattern *II*, and Pattern *III*. In general, based on the RMSE, Pattern *I* is the best pattern followed by Pattern *III*, Pattern *II*, and Pattern *IV* respectively. The NSE coefficient also indicated that Pattern *I* and Pattern *III* have higher efficiency than Pattern *II*, and Pattern *IV*. The NSE model efficiency coefficient, as well as the RMSE, identified Pattern *I*, Pattern *III*, Pattern *II*, and Pattern *IV* as better patterns, respectively (*Fig. 7*). However, the performance of Pattern *II* and Pattern *III* is very similar to each other. Based on the R^2 between estimated and measured values, it was found that all patterns are highly correlated (*Fig. 8*). The Gorgan meteorological station is located in the mediterranean climate in terms of the De Martonne index, with an average temperature of 17.75 °C.

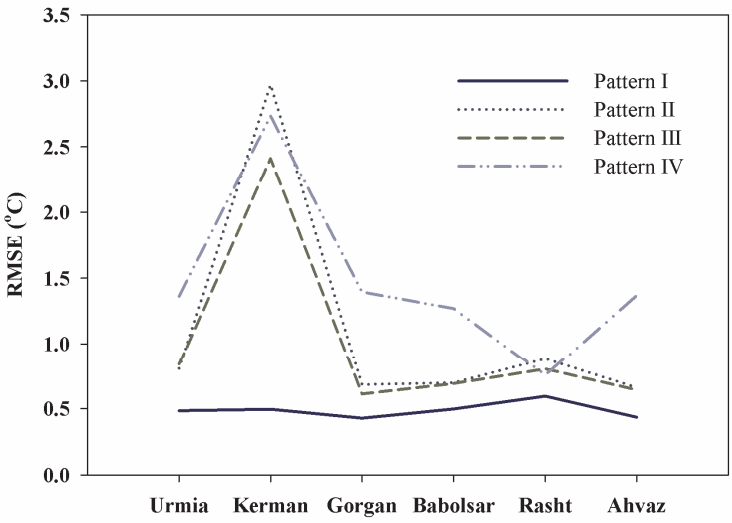

Fig. 6. Verification of different patterns in estimation of DPT values using RMSE.

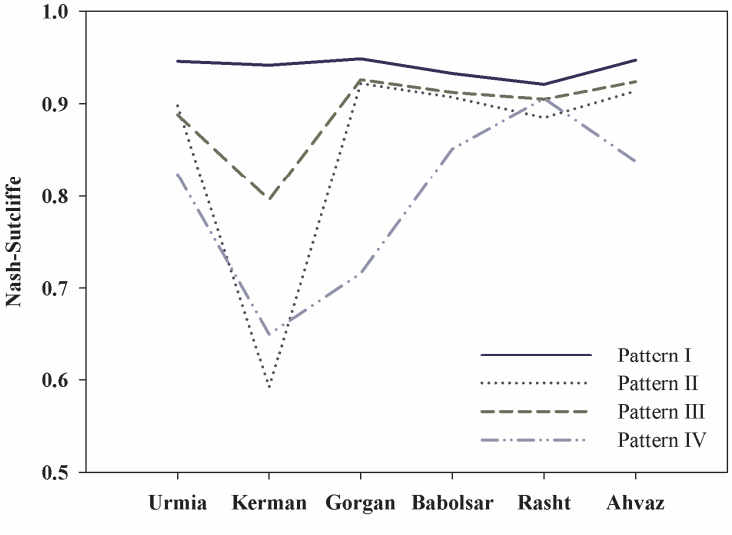

Fig. 7. Verification of different patterns in estimation of DPT values using NSE.

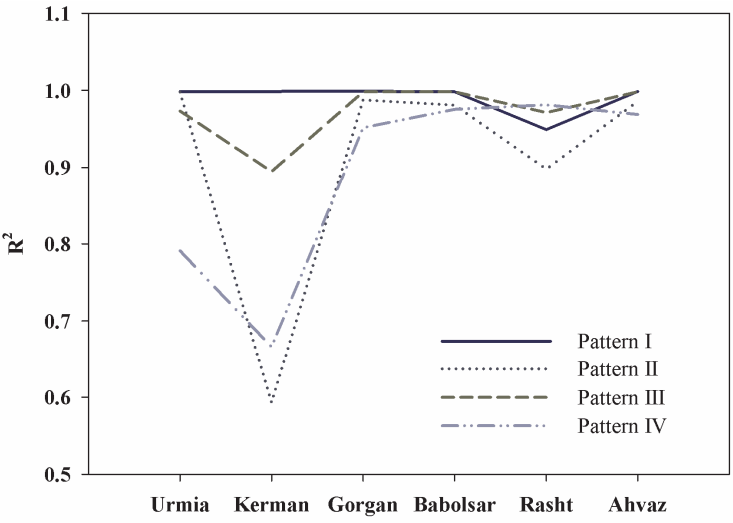

Fig. 8. Verification of different patterns in estimation of DPT values using R^2.

At the Kerman meteorological station, Pattern *I* was introduced as a top model in estimating DPT values. According to the RMSE, Pattern *I* is the best pattern for estimating the DPT values of this station, which includes an error equal to 0.49 °C. After Pattern *I*, Pattern *III* has the lowest RMSE. Pattern *II* has the highest RMSE the Kerman station. Based on the RMSE, Pattern *IV* and Pattern *II* are assigned the third and fourth ranks with an error value of 2.73 and 2.97 °C, respectively. The NSE model efficiency coefficient also introduced Pattern *I* as the best pattern for estimating DPT values, and based on this criterion, as well as the RMSE, Pattern *III* was ranked as the second. Pattern *IV* and Pattern *II* were introduced as the third and fourth ranks in estimation of the DPT values. The coefficient of R^2 also introduced Pattern *I* as the superior pattern and Pattern *II* as a worse pattern for estimating DPT values at Kerman station.

The Urmia meteorological station has a moderately dry climate with an average temperature of 11.28 °C. Based on the RMSE results in modeling the DPT values of this station, it was determined that Pattern *I* is the best pattern for estimating DPT values. Based on the RMSE values, Pattern *II* with an error value of 0.80 °C has the second rank. Patterns *III* and *IV* ranked as the third and fourth, respectively. The results show the same acceptable accuracy in Pattern *II* and Pattern *III*. In addition to the RMSE, the results of the NSE model efficiency coefficient showed that Pattern *I* and *II* are better. Based on the NSE model efficiency coefficient, Pattern *III* and *IV* were ranked as the third and fourth, respectively. The results of the coefficient of determination of the model also introduced Patterns *I* and *II* as superior patterns, which expresses the high accuracy of Patterns *I* and *II* compared to Patterns *III* and *IV*.

The wet station in this study is Babolsar station with an average temperature of 16.8 °C. Based on the RMSE, Pattern *I* was identified as the best. The RMSE value of Pattern *I* in the estimation of DPT values in Babolsar station is about 0.49 ° C. Pattern *III* with the lowest RMSE has the second rank followed by Patterns *II* and *IV*. There is not much difference between Pattern *II* and Pattern *III*. The NSE model efficiency coefficient also showed that Pattern *IV* has weak efficiency in modeling the DPT values of the Babolsar station, while Patterns *III* and *II* have a good performance in estimating DPT values. The accuracy of Patterns *III* and *II* was also confirmed according to the R^2 between measured and simulated data.

The meteorological station of Rasht with an average temperature of 16.22 °C is considered to be in the extremely wet regions of Iran in terms of the De Martonne climate index. Verification of DPT values at this station based on the RMSE showed that Pattern *I* is the best pattern for estimating DPT values and has the lowest RMSE (0.59 °C). The RMSE value in Pattern *III* is equal to 0.80 °C, and in Patterns *II* and *IV* it is 0.87 and 0.75 °C, respectively. The NSE model efficiency coefficient also considered the efficiency of Pattern *I* to be excellent in estimating DPT values. According to the NSE model efficiency coefficient, Pattern *II* was the worst. Patterns *I*, *III*, and *IV* have good efficiency.

At Ahvaz meteorological station, Pattern *I* was introduced as the best pattern according to the three criteria of RMSE, NSE, and R^2. The RMSE ranked Pattern *III* as the second pattern. Patterns *III* and *II* have the same RMSE, approximately. The NSE model efficiency coefficient is also obtained with the values obtained from Patterns *I*, *III*, and *II*. These three patterns are presented as superior patterns in terms of efficiency. The coefficient of determination of the estimation of all patterns is high. In general, the results indicated that Pattern *I* was better at most stations as this has been confirmed by *Mohammadi et al.* (2016). According to the studies done on this topic in different regions, a comparison between the results of the models and the number of inputs has been made, and the results are presented in *Table 5*. The results of checking the RMSE values compared with the results of other researchers using two input parameters showed that, compared to *Mohammadi et al*. (2016), the accuracy of the ANFIS model was same as the MSVR model in the study area. Meanwhile, in other parts of the world, the accuracy of the MSVR-ACO model is proven to be higher than that of the other models.

4. Conclusion

One of the problems with estimating DPT values is the availability of many parameters. Therefore, the use of a model that can accurately estimate these (DPT) values with lower parameters is of great importance. Today, with the development of computer softwares and powerful processors, there are several methods and softwares available for estimating unavailable data and prediction. These models include black box models of artificial neural network, ANFIS models, various algorithms, linear time series models, nonlinear models, and so on. Nevertheless, each of these types of models requires their own assumptions or is not suitable for any type of data. Also, the type of data input and the number of inputs are different for the models. In addition to the foregoing, a selection of data should also be made before modeling or predictions, so that better inputs with high correlation can be selected as inputs. In this study, meteorological data from six stations from different climates of Iran were used to estimate DPT values. To estimate DPT values, four patterns were used as inputs. Pattern *I* was selected with seven inputs, Pattern *II* with three inputs, Pattern *III* with two inputs, and Pattern *IV* with one input as study patterns. As it was mentioned above, non-linear MSVR-ACO model was used to estimate DPT values. Also, to optimize the parameters of the mentioned model, the ACO algorithm was used. In fact, in this study, DPT values were estimated using the MSVR-ACO combined model. The precision of estimated values at each station was investigated by the RMSE, NSE model efficiency coefficient, and R^2 methods.

Table 5. Comparison of the results of the present study with some existing researches

Reference	Studied model	Number of inputs	Region	RMSE (^{o} C)
Mohammadi et al. (2016)	ANFIS	2	Iran (Kerman)	0.833
Mohammadi et al. (2016)	ANFIS	2	Iran (Tabas)	0.544
Hubbard et al. (2003)	Regression based	2	USA (six stations)	3.22
Zounemat-Kermani (2012)	MLR	4	Canada (Geraldton)	0.931
Zounemat-Kermani (2012)	ANN	4	Canada (Geraldton)	0.904
Kim et al. (2014)	GRNN	2	USA (U.C. Riverside)	1.20
Kim et al. (2014)	GRNN	2	USA (Durham)	1.84
Kim et al. (2014)	MLP	2	USA (U.C. Riverside)	1.29
Kim et al. (2014)	MLP	2	USA (Durham)	1.89
Present study	MSVR-ACO	7	Iran (Urmia)	0.485
			Iran (Kerman)	0.495
			Iran (Gorgan)	0.428
			Iran (Bobolsar)	0.497
			Iran (Rashat)	0.594
			Iran (Ahvaz)	0.435
Present study	MSVR-ACO	3	Iran (Urmia)	0.805
			Iran (Kerman)	2.971
			Iran (Gorgan)	0.682
			Iran (Bobolsar)	0.696
			Iran (Rashat)	0.878
			Iran (Ahvaz)	0.660
Present study	MSVR-ACO	2	Iran (Urmia)	0.838
			Iran (Kerman)	2.412
			Iran (Gorgan)	0.611
			Iran (Bobolsar)	0.690
			Iran (Rashat)	0.801
			Iran (Ahvaz)	0.642
Present study	MSVR-ACO	1	Iran (Urmia)	1.362
			Iran (Kerman)	2.734
			Iran (Gorgan)	1.394
			Iran (Bobolsar)	1.268
			Iran (Rashat)	0.757
			Iran (Ahvaz)	1.369

The results showed that at almost all stations Pattern *I* was ranked first. In general, stations of Urmia, Kerman, Gorgan, Babolsar, Rasht, and Ahvaz, Pattern *II* has about 66, 500, 59, 40, 48, and 52 percent increased RMSE, respectively. Pattern *III* was recognized as a suitable pattern at all meteorological stations. The use of all of the seven parameters in the investigation and estimation of the DPT values of the stations under consideration will be highly accurate. However, the problem with the use of seven parameters will be as follows:

a) Receiving and collecting all the required informations is difficult and requires a lot of time.

b) Using all parameters in estimating DPT values reduces the computational speed and adjusts the computations to the algorithms to be considered.

c) Despite the availability of all the existing parameters, there is no need to use different models to estimate DPT values.

Therefore, the use of all of the seven parameters in the estimation of DPT values, which increases the accuracy of modeling, is not recommended. Based on the above mentioned results, it can be concluded that for each stations Pattern *III* (using the parameters of the monthly minimum and maximum air temperatures as model inputs), is a suitable pattern to estimate the monthly DPT values.

Acknowledgements: Authors are thankful to the University of Birjand, Birjand, Iran.

References

Akbarpour, A., Zeynali, M.J., and Tahroudi, M.N., 2020: Locating optimal position of pumping Wells in aquifer using meta-heuristic algorithms and finite element method. *Water Resources Management. 34(1),* 21-34.

Alvisi, S., Mascellani, G., Franchini, M., and *Bardossy, A.*, 2006: Water level forecasting through fuzzy logic and artificial neural network approaches. *Hydrol. Earth Syst. Sci. Discuss.10*, 1–17. https://doi.org/10.5194/hess-10-1-2006.

Citakoglu, H., Cobaner, M., Haktanir, T., and *Kisi, O., 2014:* Estimation of monthly mean reference evapotranspiration in Turkey. *Water Res. Manage. 28,* 99–113. https://doi.org/10.1007/s11269-013-0474-1

Cobaner, M., Citakoglu, H., Kisi, O., and *Haktanir, T.*, 2014: Estimation of mean monthly air temperatures in Turkey. *Comput. Electron. Agricult.109*, 71–79. https://doi.org/10.1016/j.compag.2014.09.007

C*olorni, A., Dorigo, M.,* and *Maniezzo, V.*, 1991: Ant system: An autocatalytic optimizing process. Dipartimento Di Elet-tronica, Politecnico Di Milano, Milan, Italy.

Doerr, A.H., 1963: De Martonne's Index of Aridity and Oklahoma's Climate. *Proc. Oklahoma Acad. Sci. 43*, 211–213.

Dibike, Y.B., Velickov, S., Solomatine, D., and *Abbott, M.B., 2001:* Model induction with support vector machines: introduction and applications. *J. Comput. Civil Engin.. 15*, 208–216. https://doi.org/10.1061/(ASCE)0887-3801(2001)15:3(208)

Dorigo, M., 1992: Optimization, learning and natural algorithms. PhD Thesis, Politecnico di Milano.

Dorigo, M., Maniezzo, V., and *Colorni, A.*, 1991: Ant System: An Autocatalytic Optimizing Process Dip. Elettronica, Politecnico di Milano, Technical Report 91-016REV.

Govindaraju, R.S., 2000: Artificial neural networks in hydrology. I: Preliminary concepts. *J. Hydrol. Engin. 5*, 115–123. https://doi.org/10.1007/978-94-015-9341-0

Hamel, L.H., 2011: Knowledge discovery with support vector machines. Vol 3. John Wiley & Sons.

Hofmann, T., Tsochantaridis, I., and *Altun, Y.*, 2002: Learning over structured output spaces via joint kernel functions. In: Proceedings of the Sixth Kernel Workshop.

Hubbard, K.G., Mahmood, R.,and *Carlson, C.*, 2003: Estimating daily dew point temperature for the northern Great Plains using maximum and minimum temperature. *Agronomy J. 95*,323–328. https://doi.org/10.2134/agronj2003.3230

Imani, M., You, R.J., and *Kuo, C.Y.*, 2014: Forecasting Caspian Sea level changes using satellite altimetry data (June 1992–December 2013) based on evolutionary support vector regression algorithms and gene expression programming. *Glob. Planet. Change 121*, 53–63. https://doi.org/10.1016/j.gloplacha.2014.07.002

Jeong, C., Shin, J.Y., Kim, T., and *Heo, J.H.*, 2012: Monthly precipitation forecasting with a neuro-fuzzy model. *Water Res. Manage. 26*, 4467–4483. https://doi.org/10.1007/s11269-012-0157-3

Khalili, K., Tahoudi, M.N., Mirabbasi, R., and *Ahmadi, F.*, 2016: Investigation of spatial and temporal variability of precipitation in Iran over the last half century. Stoch. Environ. Res. Risk Assess. 30,1205–1221. https://doi.org/10.1007/s00477-015-1095-4

Khan, M.S. and *Coulibaly, P.*, 2006: Application of support vector machine in lake water level prediction. *J. Hydrol. Engin. 11*, 199–205. https://doi.org/10.1061/(ASCE)1084-0699(2006)11:3(199)

Kim, S., Singh, V., Lee, C., and *Seo, Y.*, 2015: Modeling the physical dynamics of daily dew point temperature using soft computing techniques. *KSCE J. Civil Engin. 19*, 1930–1940. https://doi.org/10.1007/s12205-014-1197-4

Koza, J.R., 1992: Genetic Programming II, Automatic Discovery of Reusable Subprograms. MIT Press, Cambridge, MA.

Mohammadi, K., Shamshirband, S., Petković, D., Yee, L., and *Mansor, Z.*, 2016: Using ANFIS for selection of more relevant parameters to predict dew point temperature. Appl. Thermal Engin. 96, 311–319. https://doi.org/10.1016/j.applthermaleng.2015.11.081

Pai, P.F. and *Hong, W.C.*, 2007: A recurrent support vector regression model in rainfall forecasting. *Hydrol. Proc. 21*, 819–827. https://doi.org/10.1002/hyp.6323

Ruan, J., Zhan, Q., Tang, L., and *Tang, K.*, 2018: Real-Time Temperature Estimation of Three-Core Medium-Voltage Cable Joint Based on Support Vector Regression. *Energies 11(6)*, 1405. https://doi.org/10.3390/en11061405

Santamaría-Bonfil, G., Reyes-Ballesteros, A., and *Gershenson, C.*, 2016: Wind speed forecasting for wind farms: A method based on support vector regression. *Renew. Energy 85*, 790–809. https://doi.org/10.1016/j.renene.2015.07.004

Shiri, J., Kim, S., and *Kisi, O.*, 2014: Estimation of daily dew point temperature using genetic programming and neural networks approaches. *Hydrol. Res. 45*,165–181. https://doi.org/10.2166/nh.2013.229

Vapnik, V., 1998: Statistical learning theory Wiley, New York.

Zounemat-Kermani, M., 2012: Hourly predictive Levenberg–Marquardt ANN and multi linear regression models for predicting of dew point temperature. *Meteorol. Atmosph. Phys. 117*, 181–192. https://doi.org/10.1007/s00703-012-0192-x

DOI:10.28974/idojaras.2020.4.7

IDŐJÁRÁS

Quarterly Journal of the Hungarian Meteorological Service
Vol. 124, No. 4, October – December, 2020, pp. 541–560

The future of edible crops in Europe and their maximum point of resistance in temperature increase

Aleksandar Valjarević [1,2,] *, **Miško Milanović** [3], **Jelena Golijanin** [4], **Miroljub Milinčić** [3], and **Tin Lukić** [5]

[1] *Department for Management of Science and Technology Development, Ton Duc Thang University,Ho Chi Minh City, Vietnam*

[2] *Faculty of Environment and Labour Safety, Ton Duc Thang University, Ho Chi Minh City, Vietnam*

[3]*Faculty of GeographyUniversity of Belgrade Studentski trg 3/III, 11000 Belgrade, Serbia*

[4] *University of East Sarajevo Faculty of Philosophy, Department of Geography Sarajevo, Bosnia and Herzegovina*

[5]*University of Novi Sad,Faculty of Sciences Department of Geography, Tourism and Hotel Management Trg Dositeja Obradovića 3, 21000 Novi Sad, Serbia*

* *Corresponding author Email:* aleksandar.valjarevic@tdtu.edu.vn

(Manuscript received in final form July 24, 2020)

Abstract— In the last decades, knowledge about the climate has increased significantly. Climate change today is the subject of many sciences, including meteorology, climatology, geology, geography, geophysics, astronomy, etc. The present predictions with updated meteorological data and with data of the number of particles of CO_2 in the troposphere may give satisfying results. Forecasting for industrial grains such as maize, soybean, and wheat will be essential for industry and everyday life. Within the last agreement of climate change in Paris, global temperatures will continuously be increasing by 2100. In this research, we used a synthetic grid with agroclimatological data which comprises predictions until 2100. These data were found in the sub-section called World Clim Version 1 or in the CMIP5 database. After numerical and geospatial GIS analysis, we got the following predictions: (i) slight- no temperature changes or changes including the increase of temperature by 0.5 °C, (ii) moderate- temperature increases by 2.0 °C, (iii) severe- temperature increases by 5.0 °C, and (iv) incredible- temperature increases to extreme values, incase of which the survival of plants will be endangered.

Key-words: plants, Europe, GIS, geospatial, agroclimatology, predictions, future

1. Introduction

Wheat, corn, and soybean are the most widespread edible plants in the world. The same edible plants are present in Europe's temperate zones (Food and Agricultural Organization of the United Nations, 2016). For this study, we used the physical and geographical properties of Europe, covering 13,460,990 km^2 (*Rumford*, 2007; *Newman*, 2006).

Climate change has an enormous influence on the population, future migration, dispersion of goods, and economic growth, not only in Europe but also throughout the world (*Kottek et al.*, 2006). The consequence may also be the changing of land fertility and land quality. With the constant increase of temperatures, we may expect the expansion of non-fertile soils, especially in arid areas (*Perry et al*., 2004 *Lenihan et al.*, 2003).

The harmful effect of climate change can put to risk agricultural production and sustainable development. The influence of such climate parameters was successfully included in the modelling of soybean and maize during their early growth phase, in the territory of the United States of America (*Liheng et al*., 2016).

Specific climate models are necessary for oil palm growth, to which authors applied 2.7 °C – 4.0 °C temperature increase until 2100. Recently, many types of researches have been predicting surface and sea-surface temperatures at a global scale (*Köppen*, 1900). Using different kinds of simulations, including sea-ice concentration and sea-surface temperatures, the authors gave a new perspective of global circulation and climate change. In this research, many relation models of temperature-precipitation were tested (*Dittus et al.*, 2018; *Gouda, et al.*, 2017). For this purpose, the authors used the CLIMEX software modelling (*Paterson et al.*, 2015).

With the prediction of low precipitation and extreme weather conditions to 2050, the modelling of wheat was performed, along with the display of its vulnerability (*Beck et al.*, 2005). The damage of some species of grain would be 30%, especially in the vegetative period (*Semenov* and *Shewry*, 2011). The relationship between edible grains and meteorological measurements was successfully established and studied on new resistant species of grains. These new species could be adapted to extreme temperatures and extreme meteorological parameters to a great extent. For example, newly modified grains may grow at higher altitudes or in hotter regions and semi-arid and arid areas (*Challinor et al*., 2009.)

According to the estimation of the influence of climate changes on the food production and food reserves, in the case of doubling the CO_2 level, the food production, especially the production of grains, can become minimal in developing countries, which would have fatal consequences for their economies (*Rosenzweig* and *Parry*, 1994).

Climate change has already affected the southern part of California, where regional increases in temperature and vegetation may be destructive for some plants. The data of these effects have been observed and estimated for a long term period. In this research, CMIP5 temperature projection was used with the parameters of particularly extreme conditions. Researchers used a vegetation model to illustrate temporal and spatial shifts in land cover, in response to changes in environmental conditions (*Bachelet et al.,* 2016). In the study of land use and land cover changes in eastern Sudan, researchers investigated the changes of land cover with the help of the aridity index, temperature, and rainfall changes of land cover. In this research, soil erosion effects and agricultural influence on new lands were used (*Suleiman* and *Elagib*, 2012).

Similar predictions based on numerical simulations and geographical parameters showed that some grains might survive, even if temperature increases by more than 3.0 °C. This study presupposes that the bad influence of climate change will not be manifested equally in different places, while the temperatures will be the same everywhere (*Asseng et al.,* 2013). Temperature extremes' influence on the growth was successfully tested on some plants with different phonological characteristics. Temperature is a primary factor affecting the rate of plant development. Warmer temperatures expected with climate change, and the potential for more extreme temperature events will impact plant productivity (*Hatfield* and *Prueger*, 2015; *Ayal* and *Filho,* 2017).

Each of the seven continents has its climate properties, and therefore, the effect of climate change will not be the same for all of them. Many researchers have studied the influence of climate change on local, regional, and global scales. *Barrow* (1993) analyzed the effects of climate change using a generalized circulation model (GCM) applied in the territory of Europe.

By studying the spatial aggregation between crops and climate, it is possible to adapt to the plants' productivity with the help of digital analysis. In the territory of Ethiopia, in the area of highlights, researchers applied climate variability effect on agricultural production. They concluded that humanity must use the adaptive capacity to climate change in many aspects, including tourism and suitability (*Kovacs et al.,* 2017; *Vukoičić et al.,* 2018). The analyzed winter species of wheat crops and the effect of climatic variability in Canada's territory for 30 years showed better results than the summer species of wheat (*Qian et al.,* 2009).

Climate modeling of various zones was applied by (*Zhang et al*., 2012). In this research, the authors compared the phenology of rice with the phenology of wheat and with a large number of different climate parameters. A particular influence of climate change and the vulnerability of corn have been applied to the crops in Slovenia using modern phenology methods (*Ceglar et al*., 2011). Global warming also influences the energy, which is necessary for better crop growing. Thus, high energy imposed on plants during their growth may produce irretrievable damage (*Sanderson*, 1999*; Mohareb et al.,* 2017).

These authors introduced a particular statistic emulator, which was presented by dynamical model of crops. Some authors meticulously presented food security challenges with the influence of climate change in the territory of Malaysia. This research included adaptations of the plants in case of temperature increase and variable precipitations (*Al-Amin* and *Ahmed*, 2016). Climate changes can produce significant consequences for crops productivity and food security at a global scale (*Lobell* and *Field*, 2007). Other researchers included plants diversity in the area of Europe when temperatures increase (*Lazzerini et al.*, 2015).

Other authors described future climate changes in the Apennine Mountains to find the connection between crops and climate (*Dibari et al.*, 2015). Most of the adaptation strategies included a large number of climate and water management scenarios. This water variability always included deficits of precipitations and a high rate of temperatures. Two climate change scenarios (CMP5 and GCMs models) were used in this research (*Huang et al.*, 2018; *He et al.*, 2018; *Fraga et al.*, 2018). There is also a research investigating post-Soviet cotton cultivation and integrated irrigation or non-irrigation parameters in Central Asia. The data downloaded from the Landsat satellite Modis (Modis Resolution Imaging Spectroradiometer) may help determine the mean value of the forest belt (*Conrad et al.*, 2016). In Spain, a researcher adapted a unique AdaptaOlive model to establish simulation for future climate change. This model may show a deficit of precipitation and irrigation and predict future strategies (*Lorite et al.*, 2018). All of the investigations must be delegated to better prediction of climate risk management. The climate risk management may be addressed and applied to plants, since the climate is always interacting with plants (*Araya et al.*, 2017; *Pramanik et al.*, 2018).

2. Physical geography of Europe

European geospace, including its borders, was the subject of this study. Some of the authors have used Europe independently, while others have been conducting their research on Eurasia (*Thuiller et al.*, 2004). Europe, including the European part of the Russian Federation, has an area of 13,460,990 km^2. The border between Asia and Europe is on the Ural Mountains at 67°E. In the south, the bordering point is Cape Litinon at 34.55° S, and in the north, it is Cape Nordkap in Norway at 71.21° N. In the west, this point is Cape Dunmore Head in Ireland, at 10.30° W. The main climatological advantage of Europe is its position in the northern temperate zone. The relief of Europe near the coastline is lower than 3° of the angle of slope. The other advantage could be that Europe has a long and indented coastline, with the average indent ratio of 4.1 km^2. A large number of islands and the indented coastline may be the advantage because of different climate variables. In the territory of Europe, there are three different coastal belts: the Atlantic, the Arctic, and the Mediterranean.

The Atlantic coast is located in Western Europe, and it reaches the shores of Norway in the northwest. The Arctic coast is located in Northern Europe. Northern Europe, in terms of region, belongs to the polar Arctic region. The Mediterranean coast is the third specific region of Europe. The Mediterranean belt has the Iberian, Apennine, and Balkan Peninsulas. The coastlines of Europe reach the seas of Africa. The relief in Europe does not abound in very high mountains. Furthermore, the energy of relief is low in comparison with other continents. Accordingly, Europe has excellent possibilities for plants' growth, especially for grains. The most dominant mountain system is the Alps (4807 m), the following is Ural, which presents the border between Europe and Asia with a length of 2500 km.

The essential plains in Europe present the most significant agricultural areas. These plains are located in East Europe, Central Europe, the Netherlands, and Pannonian Basin. The average production in the countries which belong to European plains is between 3,500,000 and 7,000,000 tons. The total area of plains is 4,000,000 km^2 (*Cocks,* 2000). In the east, the East European plain reaches the Ural. The Central European plain covers the northern parts of Germany and Poland.

In the north, Europe is open until the Baltic and North Seas, in the south its boundary is in central Germany, i.e., the Sudetes and the Beskids. The Pannonian plain's length is 1,000 km, whereas the average height is between 200 and 400 km. Its lowest parts are characterized by very fertile soils, covering the area of 125,000 km^2. The Pannonian plain is surrounded by the Alps, the Carpathians, and the Dinarides.

3. Methods and data

The CO_2 concentration is assumed following the estimate of the fifth Assessment Report AR5. This assessment is also used and implemented in the CMIP5 model. The potential scenario is divided into four categories; all scenes are connected with the concentration of particles in the lower belts of the atmosphere. The concentration of the pre-industrial level of CO2 was near 0 levels. After the industrial revolution, this concentration increased to +2.6, +4.5, +6.0, and to 8.5 in recent times (*Weyant et al.*, 2009; *Moss et al.*, 2008). In this study, we used a specially created algorithm and procedures in the Geo-Python code. This code is implemented in the architecture of the QGIS software. Using georeferencing, interpolation, semi-kriging, kriging, and sub-kriging, we studied the dispersion and properties of three grains (wheat, corn, soybean) using GIS software DIVA and QGIS. After a successful georeferencing of the European border, we continued with the process of downloading data from the DIVA-GIS database. Four kinds of data were downloaded: maximum, minimum, and average annual temperatures, and average annual precipitations (*Table 1*).

Table 1. Physical properties of plants following the change of precipitation and temperature

Sp.	Length of growing season in days			Temperature variables in C°					Precipitation in mm/m^2			
	Gm	Gmix	Gu	Ktmp	Tmi	Tomi	Tomx	Tmax	Pmin	Pmx	Pomi	Pomx
Z.M	65	100	82	0	12	16	24	38	600	1800	800	1500
T.A	120	180	150	0	6	17	25	30	400	800	500	700
G.M	75	180	128	0	10	20	33	38	450	1800	600	1500

Abbreviations: Gm-Growing season minimal, Ga-Growing season maximal, Gu-Growing used, Ktmp-Killing temperature, Tmi-Temperature minimal, Tomi-Temperature optimal minimal, Tomx-Temperature optimal maximal, Pmin-Precipitation minimal, Pmx-Precipitation maximal, Pomi-Precipitation optimal minimal, Pomx-Precipitation optimal maximal, Z.M-Zea Mays, T.A-Triticum Aestivum, G.M-Glycine Max. (Source: Food and Crop UN organization)

All of these data are for the period between 2000 and 2100. The obtained results of GIS analysis after numerical analysis are divided into six classes. These classes are excellent, very suitable, suitable, marginal, very marginal, not situated. After in-depth analysis of plants, we obtained the areas of their dispersion. The properties of plants were used from the database Eco-crop, in which we found all the phenomenological data for investigated grains. This base belongs to the official plants support of the United Nations. In this database, we found 2568 common plants with complete physical and biological properties such as growth period in total, killing temperature of the root, minimal temperature for the proposed plant. These physiological properties, combined with climatological features, may give excellent results for dispersion of plants and prediction of growth in the future.

Further, considering the temperature changes, we performed the analysis of the areas for soybean (*Glycine*), maize (*Zea Mays*), and wheat (*Triticum aestivum*). All of the plants are very important not only for Europe but also for the whole world when it comes to the production of food and energy. The following features are the export capacity of Europe and the assessments of what would happen if temperatures increase to incredible condition.

If Europe became semi-arid and arid land with some agrotechnological support, it could be a leader in grains production. The data for the prediction were given in raster or Geo-tiff extension. This raster is very precise, and it was downloaded from the official web page DIVA at the free data of climate (http://www.worldclim.org/). This service includes free, simple, and effective climatological data from the past, present, and future. We used old version 1.4 of data, because all the data in this version were given in a couple of extensions. The extension used is Geo-tiff in the resolution of 10, 5, 2.5 minutes, and 30 seconds. Continuation of 30 seconds is exact and useful for climatological data predictions, giving prediction to the year 2100.

This year presents long-term analyses, and it is the right prediction for potential adapting (*Zabel et al.*, 2014). Long-term climatological data can be successfully changed and used to map and spatial modelling of bioclimatological data and properties (*New et al.*, 2000; *Saha* and *Khan*, 2000; Mitchell and Jones, 2005). Other data were used from the downloaded pages at the Davis University of California and the Stockholm Institute of Environment for the comparison (*Vicuna et al.*, 2007).

The first grid of precipitation is analyzed within nine classes. Average precipitations in Europe were presented by using QGIS, for the period between 1960 and 2000. Average temperatures are presented in *Figs. 1* and *2* between the same periods in the same territory. This grid is used for in-depth agroclimatological forecasting of three researched grains. After exporting grid data, we inserted this grid on the map. After that, we started with the analysis of data and their modelling (*Ward*, 2007; *Li et al.*, 2015). The predictions were also divided into four classes. When the temperature increases by 0.5 °C up to 2100, it presents optimistic scenarios and is strongly connected with the Paris agreement.

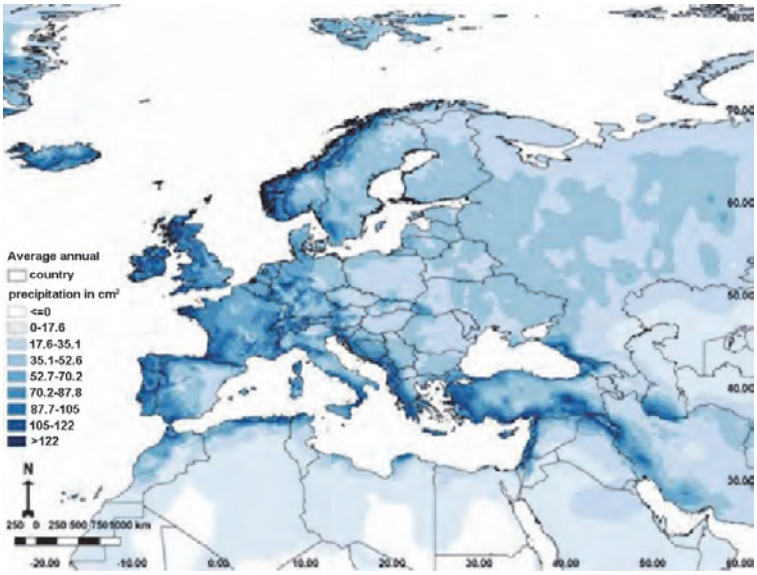

Fig. 1. Average annual precipitation in Europe within the period of 1960–2000.

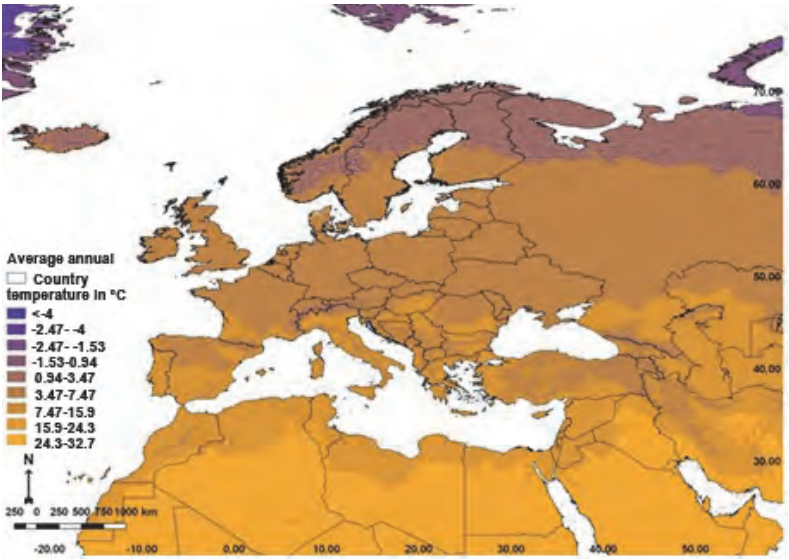

Fig. 2. Average annual temperature in Europe within the period of 1960–2000.

In the second class, we may expect 2.0 °C increase in temperature. This prediction shows that the Paris agreement is fulfilled but not in all countries. The third class shows the rise in temperature by 5.0 °C and the rejection of the Paris agreement by 60% of countries. Finally, the last fourth class presents catastrophic, devastating temperatures for the survival of plants.

In case of corn, the most optimal growth temperatures are between 16 °C and 24 °C, but for wheat, these temperatures are between 15 °C and 23 °C; soybean is more resistant, and its maximal point of resistance is between 20 °C and 33 °C. After setting the European border, we included all European countries according to the EU base. These countries are Albania, Andorra, Austria, Azerbaijan, Belarus, Belgium, Bosnia and Herzegovina, Bulgaria, Croatia, Cyprus, Czech Republic, Denmark, Estonia, Finland, Georgia, Germany, Greece, Hungary, Iceland, Ireland, Italy, Kazakhstan, Latvia, Lichtenstein, Lithuania, Luxemburg, Macedonia, Malta, Moldova, Monaco, Montenegro, The Netherlands, Norway, Poland, Portugal, Romania, Russia, San Marino, Serbia, Slovakia, Slovenia, Spain, Sweden, Switzerland, Turkey, Ukraine, United Kingdom, Vatican City, Cyprus. Between 1960 and 2000, the average and yearly precipitation over the territory of Europe was between 702 and 878 mm (*Fig. 1*). The average temperature in Europe within the 40 years was between 7.5 °C and 15.9 °C (*Fig. 2*).

4. GIS agroclimatological and numerical data analysis

Geographic Information System (GIS) and the modelling of agroclimatological data, as well as the plant distribution and properties, are fundamental approaches that can be used for presenting the spatial features of climate and climate changes. Climate modelling based on agroclimatological data may show the present condition and predict the future of plants. Ordinary kriging and semi-kriging methods were employed through QGIS and DIVA software. This algorithm was used to estimate plant properties called spatial analysis. Although there are many other algorithms, this algorithm is beneficial, because it is precise and fast in calculating the data. The kriging method was used as one of the most standard methods in interpolation and clustering. Also, this method reduced the errors of geostatistical analysis. By using the grid analysis, we estimated two cycles of 40 years.

In this way, we established a long-term analysis of meteorological data. The agroclimatological properties and plant distribution were obtained by applying open-source software DIVA-GIS for mapping and geographic data analysis. This software is robust with very high accuracy. The derived raster has a resolution of 1 km^2. After determining the grid, we inputted shape files extension. The advantage of DIVA-GIS software is that it can read many types of input files such as CSV, Excel, ESRI shape file, and KLM.

5. Results and discussion

After modelling the agroclimatological data, we used the interaction between average annual temperature and precipitation. The first prediction concerns a temperature increase of 0.5 °C until 2100. The second prediction, which would be more realistic, presupposes temperature increase of 2.0 °C. The third prediction included a 5.0 °C increase of temperature, and the fourth presents the ultimate limit for the survival of plants, thus presenting catastrophic scenarios.

After complete geospatial analysis for corn, the minimum temperature is 24.0 °C and the maximum is 50.0 °C. The condition for wheat is somewhat different, where the minimum temperature is 19.0 °C and the peak is 40.0 °C.

In contrast, for soybean, the minimum temperature is 26.0 °C and the maximum is 54.0 °C. This analysis gives novel results for the maximum resistance for the three investigated plants in Europe. All results are classified into six classes (excellent, very suitable, suitable, marginal, and very marginal, not situated).

The first three classes correspond to excellent and optimal conditions for the plant growth; the fourth and fifth classes correspond to the minimum requirements for the growth, whereas the sixth one corresponds to the impossibility of plants' growing. Since GIS analyses were exact, we estimated areas for all European countries. According to the data from 2014, the total number of inhabitants in Europe is 853,215,836.

For corn, if the average annual temperature increases by 0.5 °C, the ratio of area classes in Europe will be the following: (excellent: 20.6%, very suitable: 6.4%, suitable: 6.7%, marginal: 8.9%, very marginal: 14.7%, and not situated: 42.7%). For the class marginal and very marginal, the possibility of growth of plants is minimal. If the temperature increases by 2.0 °C , the areas would be as follows: excellent: 14.3% , very suitable: 7.6%, suitable: 4.2%, marginal: 7.8%, very marginal: 13.7%, not situated: 52.4%. If the average annual temperature increases by 5.0 °C, the distribution of classes will be- excellent: 10.3%, very suitable: 2.8%, suitable: 2.1%, marginal: 5.1%, very marginal: 5.3%, and not situated: 74.4%. In the case of devastating temperatures, we got the following results for the territory of Europe- excellent: 0.3%, very suitable: 0.3%, suitable 0.34%, marginal: 0.02%, very marginal: 0.04%, not situated: 99%. For the areas of wheat, when temperature increases by 0.5 °C, classes will be distributed in the following way: excellent: 4.4%, very suitable: 9.1%, suitable: 15.9%, marginal: 21.2%, very marginal: 8.6%, not situated: 40.8%. In case of temperature increase of 2.0 °C, we may expect the following dispersion: excellent: 3.78%, very suitable: 5.04%, suitable: 10.7%, marginal: 20.47%, very marginal: 15.22%, not situated: 45.42%.

If temperature increases by incredible 5.0 °C, distribution is -excellent: 4.7%, very suitable: 3.87%, suitable: 2.78%, marginal: 10.35%, very marginal: 14.7%, and not situated: 63.6%. When the temperature reaches the highest value, distribution of wheat areas will be -excellent: 0.013%, very suitable: 0.008%, suitable: 0.82%, marginal: 1.54%, very marginal: 1.35%, not situated: 96.2%. The situation for soybean if temperature increases by 0.5 °C is excellent: 10.16%, very suitable: 10.1%, suitable: 16.28%, marginal: 2.,2%, very marginal: 9.22%, not situated: 30.04%.

If temperature increases by 2.0 °C, we have excellent: 8.16%, very suitable: 9.1%, suitable: 15.28%, marginal: 28.2%, very marginal: 11.22%, not situated: 28.04%. If temperature increases by 5.0 °C, we have the following classes: excellent: 2.16%, very suitable: 4.9%, suitable: 12.88%, marginal: 20.2%, and very marginal: 19.22, and not situated: 40.64%. If temperature increases to devastating rate we, may expect the areas as follows: excellent: 0,012%, very suitable: 0.002%, suitable: 0.004%, marginal: 0.005%, very marginal: 0.077%, and not situated 99.9%. In the interval between 0.5 °C and 5.0 °C, we have the increase of the class not situated for wheat by 9.7%, for corn by 4.62%, for soybean by 11.13%.

When we established the estimation country by country, the results were calculated in the following way: if temperature increases by 0.5 °C, France has 234,500 km^2, Italy has 150,040 km^2, Spain has 79,400 km^2 in the exellent class. If temperature increases by 0.5 °C, the class not situated will cover the territory of 2,718,450 km^2 in the Russian Federation, 660,450 km^2in Turkey, 400,661 km^2 in Ukraine. If temperature increases by 2.0 °C, we have the following results for excellent class: France: 198,600 km^2, Italy: 116,630 km^2,

Turkey: 100,900 km^2. Countries in the not situated class are the Russian Federation with 2,866,470 km^2, Kazakhstan with 2,720,770, km^2, Ukraine with 412,196 km^2.

If temperature increases by 5.0 °C, we may expect an excellent area in the following countries: Italy: 131,100 km^2, France: 105,230 km^2, Turkey: 52,700 km^2. In the class not situated, we have the Russian Federation with 3,732,190 km^2, Kazakhstan with 2,726,060 km^2, Turkey with 697,760 km^2. For wheat, we have somewhat different situations. If temperature increases by 0.5 °C, excellent class will be distributed in Italy on 64,700 km^2, in Turkey on 52,100 km^2, in Portugal on 26,350 km^2. Not situated class will be distributed in Russia on 3,487,600 km^2, in Kazakhstan on 2,686,670 km^2, and in Turkey on 398,920 km^2. If temperature increases by 2.0 °C within excellent class, we have areas in Italy 76,910 km^2, in France 35,300 km^2, in Portugal 34,100 km^2. In not situated class, we have 3,554,470 km^2 in the Russian Federation, 2,666,210 km^2 in Kazakhstan, 481,380 km^2 in Turkey. If temperature increases by 5.0°C, we have in excellent class 38,600 km^2 in Italy, 24,400 km^2 in Portugal, 21,590 km^2. In the class not situated, we have 3,624,500 km^2 in the Russian Federation, 2,680,940 km^2 in Kazakhstan, and 587,940 km^2 in Turkey. The results are somewhat different for soybean, especially those concerning the temperature increase by 2.0 °C to 5.0 °C.

If temperature increases by 0.5 °C, we have the excellent class in the following countries: Turkey: 160,170 km^2, Italy: 119,300 km^2, Greece: 57,200 km^2. In the class not situated we have Kazakhstan with 2,710,250 km^2, Russia with 1,568,177 km^2, Turkey with 457,400 km^2. If temperature increases by 2.0 °C, in the excellent class, Turkey will have 91,500 km^2, Italy 80,000 km^2, Spain 47,300 km^2. For class not situated, we have the following countries: Russia with 2,753,900 km^2, Kazakhstan with 2,715,440 km^2, Turkey with 530,060 km^2. If temperature increases by 5.0°C, we have in the excellent class Italy with 89,200 km^2, Turkey with 34,200 km^2. For class not Situated, we have Russia with 3,234,560 km^2 and Kazakhstan with 2,900,400 km^2 (*Figs. 3–5*).

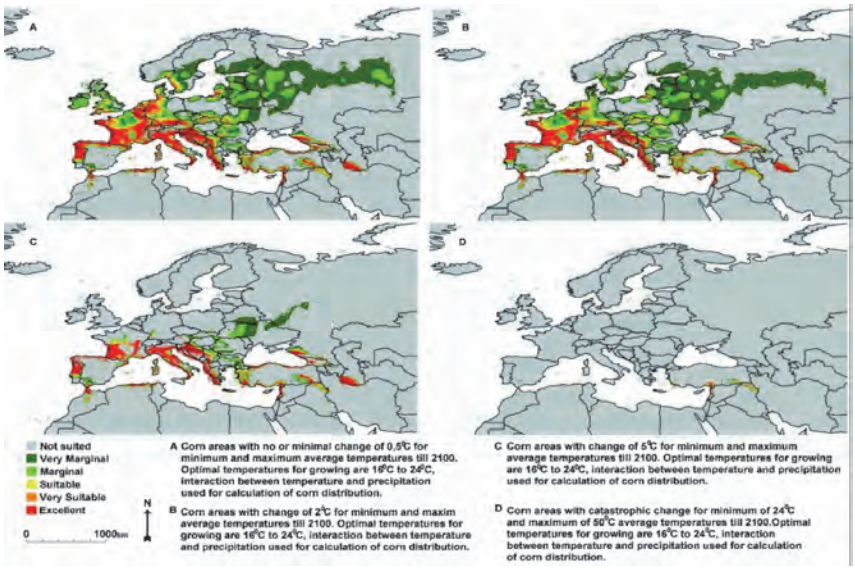

Fig. 3. Distribution of corn areas in different climate predictions (slight- there is no change of climate or maximum temperature increases by 0.5°C, moderate –maximum temperature increases by 2.0°C, severe –maximum temperature increases by 5.0°C, and incredible – the temperature further increases, and we may expect the disappearance of all plants.

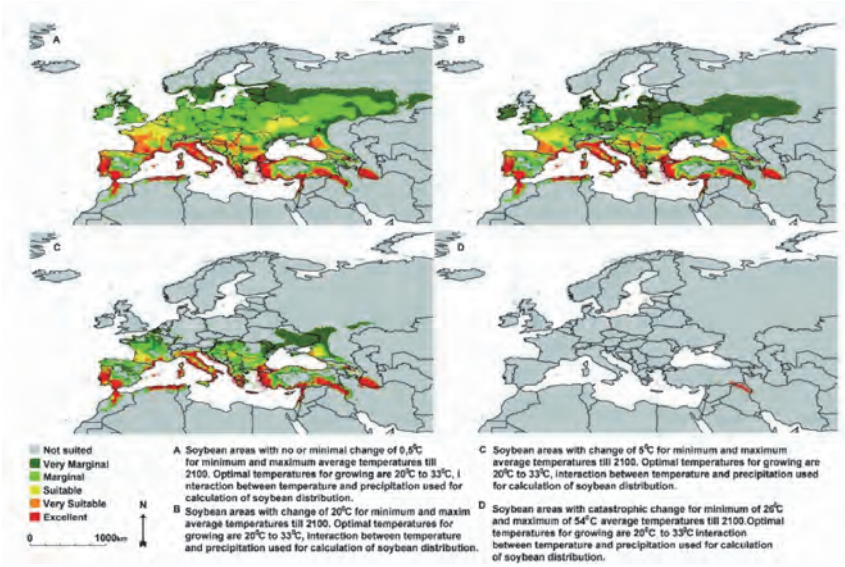

Fig. 4. Distribution of wheat areas in different climate (slight- there is no change of climate or maximum temperature increases by 0.5°C, moderate –maximum temperature increases by 2.0°C, severe –maximum temperature increases by 5.0°C, and incredible – the temperature further increases, and we may expect the disappearance of all plants.

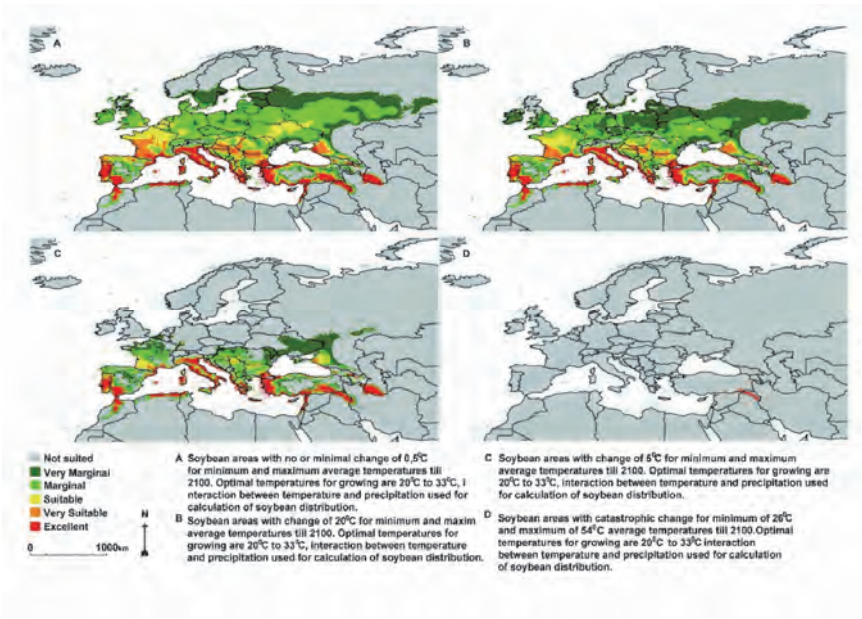

Fig. 5. Distribution of soybean areas in different climate predictions (slight- there is no change of climate or maximum temperature increases by 0.5°C, moderate –maximum temperature increases by 2.0°C, severe –maximum temperature increases by 5.0°C, and incredible – the temperature further increases, and we may expect the disappearance of all plants.

With the help of agroclimatological modelling, we gave geographical and climatological predictions for the future existence of the three plants (corn, wheat, and soybean) in the territory of Europe. After the complete analysis, we concluded that corn and wheat have very similar properties, especially in the dispersion after the increase of temperature. Meanwhile, wheat is slightly different if temperature increases by 0.5 °C, the difference in the territory covered across European countries. 3.5% of European countries have more substantial areas under wheat than under corn. If temperature changes by 2.0 °C, we can expect a similar dispersion of wheat and corn in the territory of Europe. If the temperature increases by 2.0 °C, for soybean we have 5% greater area than for wheat and corn; even if the temperature increased by 5.0 °C, soybean might cover some territories in Europe (*Fig. 6*).

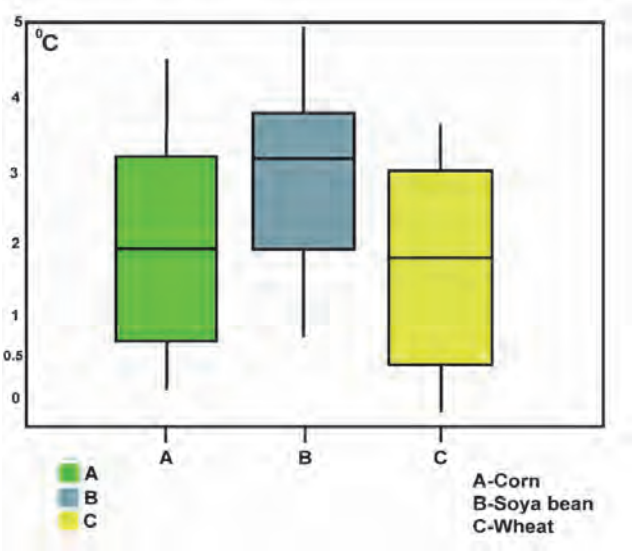

Fig. 6. The resistance of corn, wheat, and soybean by the increase of temperature in Europe per hectare.

However, even if temperature increases by 2.0 °C, the dispersion of three listed plants will be very similar, especially in the southern and south eastern part of Europe. The main changes will be in the territory of East Europe, the Russian Federation, and Scandinavia. The plants may survive on higher lands or under the mountains' basins. Some mountains could be the most resistant areas, and under them, at the elevation higher than 1200 m, there might be possibilities for wheat, corn, and soybean growing. These mountains are Prokletije Mountains, the Alps, the Central Massif, the Pyrenees, etc.

Also, one small area near the Sea of Azov with the line of 200 km, and line near the Caspian Basin may be useful even if the temperature increases. Along the frontier between France and Belgium, there will be a sufficiently broad belt in the Ardennes, under the mountains of Dinarides in Bosnia and Herzegovina and Croatia, and Throdos Mountains in Cyprus, Gascogne in France, and the Massif Central. Under the Eifel mountain range and the Black Forest, Bavarian Forest, and the whole sub-alpine zone, we may expect isolated but resistant zones. The entire sub-alpine area, the Balkan Peninsula, Mount Olympus in Greece, the Pindus Mountains, and the Arachova Mountains are expected to be more resistant, too.

Other resistant areas are in the Apennine Peninsula under the east Apennines, in the part of the Pannonian Basin that belongs slightly to Hungary,

Serbia, and Romania. In western Poland, some parts of the Iberian Peninsula in the regions of Estremadura Alentejo in Portugal and Spain, an area under the Pyrenees, as well as the Sierra Nevada and Aragon may be resistant even if temperature increases by 5.0 °C. In the territory of the Russian Federation, a suitable area would be 300 km from the Sea of Azov, between Rostov-on-Don and Krasnodar, and in the Kazakhstan Atyrau Region 150 km from the Sea of Azov.

In Turkey, similar zones may be found under the Taurus Mountains, Pontic, and Ararat. But, all of these areas would be converted into more isolated islands. 70% of those areas may survive even in temperatures between 24.0 °C and 50.0 °C. Corn areas would be reduced by 40%. The maximum threshold for soybean is between 26.0 °C and 54.0 °C, which shows that soybean is more resistant than wheat and corn. For wheat, we concluded that in the territory of Europe, this plant might survive the increase of 4.0 °C, while corn might survive 3.0 °C increase and soybean might survive 5.0 °C increase. The dispersion of these plants depends on geographical coordinates, longitude, and latitude (*Fig. 7)*

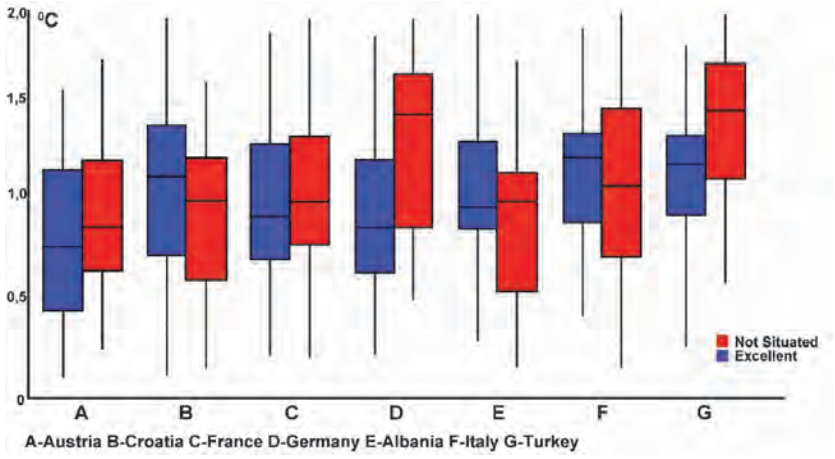

Fig. 7. Dispersion of the suitable and not suitable crop areas if temperature increases between 0.5 °C and 2.0 °C, an example of some countries used in this research.

6. Conclusions and possibilities

The first estimation stated that all three researched plants (wheat, corn, soybean) might resist the increase of temperature by 2.0 °C to a maximum of 4.0 °C. The crops of these species will be moved to a higher elevation, from 400 m to 1000 m. Some researches stated that if the temperature increases by 4.0 °C, a large part of the European continent would become desert and arid area. In other studies, some predictions included the rise of sea level, in case of which many fertile lands would disappear. Meanwhile, areas such as the Scandinavian Peninsula, Greenland, and Iceland could not become new fertile areas for plants, because of the high concentrations of ice in the permafrost. Many European countries, such as Austria, Germany, Hungary, all Balkan countries, also Spain and Portugal, would become inhabitable deserts. According to our results, in the case of temperature increase by 5.0 °C, potential areas within the classes (excellent, very suitable, suitable) would become smaller by 85%, or they would be islands (isolated areas), which may grow and give sufficient goods, with watering. Our model included the connection between precipitation and temperature and the growing period of plants. Plant analysis included the average elevation of all countries, according to which we obtained results in three dimensions (height, geographical latitude, and geographic longitude). Finally, our research gave an optimistic picture of European countries, namely, the list of European countries that may become resistant even with the increase of temperature by 4.0 °C.

As previously mentioned, Russia, Scandinavia, and Iceland will not become countries with fertile soils. When the ice starts melting, it may produce a large number of muddy rivers. The new species of investigated grains may adapt to high altitudes or with a new volume of precipitation. These new sorts can live with a smaller amount of water. In our study, the relationship between temperature and water is also taken into account. What would happen if the number of days with precipitation became significantly smaller or we did not have watering? These results may be very worrying. In this research, the areas investigated are those which could be suitable for new crops. As a positive result of our modelling, we can mention that appropriate zones would be located within urban and sub-urban zones after the climate changes. Therefore, a new urban policy would be required, which should be directed against the inevitable conversion of agricultural lands into urban ones.

For our climatological prediction, we used a moderate scenario made according to current data chosen from the official web page of open source GIS portal DIVA-GIS. These data were found in the sub-section called (WorldClim Version 1) or in the CMIP5 database. In this database, variables are monthly average minimum temperature, monthly average maximum temperature, and total monthly precipitation. CMIP5 database parameters include greenhouse gas scenarios, which included representative concentration pathways (rcp60 or

moderate prediction). This grid is exact and presents a distance of 900 m from the equator in longitude and latitude. After numerical and geospatial GIS analysis, we got the following predictions: (i) slight- no temperature changes or changes including the increase of temperature by 0.5 °C, (ii) moderate- temperature increases by 2.0 °C, (iii) severe- temperature increases by 5.0 °C, and (iv) incredible- temperature increases to extreme values, in case of which the survival of plants will be endangered. The last climate properties present the devastation model of climate, and in that case, all plants will be destroyed. At the end of this research, this modelling of climate parameters was mapped, analyzed, and the optimal patterns between climate change and plants' growth were found.

Alternative solutions could be informing ecological zones and vertical farms within urban settlements. In the suburban and open areas, in such situations, new parcels would be formed that would be near significant accumulations, even at higher altitudes. Any future climate model is an essential prerequisite to reach local, regional, and global climate predictions as pleasant as possible. Only sufficiently good predictions offer possibilities to be successfully prepared and adapted for future climate changes. This research can be extended with new and precise data and applied to all countries in the world.

References

Araya, A., Kisekka, I., Lin, X., Vara Prasad, V., Gowda, P., Rice, C., and *Andales, A.,* 2017: Evaluating the impact of future climate change on irrigated maize production in Kansas. *Climate Risk Manage. 17*, 139–154. https://doi.org/10.1016/j.crm.2017.08.001

Al-Amin, A. and *Ahmed, F., 2016:* Food Security Challenge of Climate Change: An Analysis for Policy Selection. *Future 83*, 50–63. https://doi.org/10.1016/j.futures.2016.04.002

Asseng, S., Ewert, F., Rosenzweig, C., Jones, J., Hatfield, J., Ruane, A., Boote, J., Thorburn, J., Rötter, P., Cammarano, D., Brisson, N., Basso, B., Martre, P., Aggarwal, K., Angulo, C., Bertuzzi, P., Biernath, C., Challinor, J., Doltra, J., Gayler, S., Goldberg, R., Grant, R., Heng, L., Hooker, J., Hunt, A., Ingwersen, J., Izaurralde, C., Kersebaum, C., Müller, C., Naresh, S., Nendel, C., O'Leary, G., Olesen, E., Osborne, M., Palosuo, T., Priesack, E., Ripoche, D., Semenov, A., Shcherbak, I., Steduto, P., Stöckle, C., Stratonovitch, P., Streck, T., Supit, I., Tao, F., Travasso, M., Waha, K., Wallach, D., White, W., Williams, R., and *Wolf, J., 2013:* Uncertainty in simulating wheat yields under climate change. *Nat. Climate Change 9*, 827–832. https://doi.org/10.1038/nclimate1916

Ayal, D. and *Filho, L.,* 2017: Farmers perceptions of climate variability and its adverse impacts on crop and livestock production in Ethiopia. *J. Arid Environ. 140*, 20–28. https://doi.org/10.1016/j.jaridenv.2017.01.007

Barrow, M., 1993: Scenarios of climate change for the European Community. *Eur. J. Agronomy 4*, 247–260. https://doi.org/10.1016/S1161-0301(14)80174-3

Bachelet, D., Ferschweiler, K., Sheehan, T., and Strittholt, *J., 2016*: Climate change effects on southern California deserts. *J. Arid Environ. 127*, 17–29. https://doi.org/10.1016/j.jaridenv.2015.10.003

Beck, C., Grieser, J., and *Rudolf, B.,* 2005*:* New Monthly Precipitation Climatology for the Global Land Areas for the Period 1951 to 2000. Climate status report, German Weather Service, Offenbach, *181–190.* Reprint available at http://gpcc.dwd.de

Conrad, C., Lamers. A., Ibragimov, N., Low, F., and *Martius., 2016:* Analysing irrigated crop rotation patterns in arid Uzbekistan by the means of remote sensing: A case study on post-Soviet agricultural land use. *J. Arid Environ. 124*, 150–159. https://doi.org/10.1016/j.jaridenv.2015.08.008

Ceglar, A., Črepinšek, Z., Kajfež-Bogataj, L., and *Pogačar, T.,* 2011: The simulation of phenological development in dynamic crop model: The Bayesian comparison of different methods. *Agric. Forest Meteorol. 151*, 101–115. doi: https://doi.org/10.1016/j.agrformet.2010.09.007

Cocks, M., 2000: The Early Paleozoic geography of Europe. *J. Geol. Soc. 157*, 1–10. https://doi.org/10.1144/jgs.157.1.1

Challinor, J., Ewert, F., Arnold, S., Simelton, E., and *Fraser, E.,* 2009: Crops and climate change: progress, trends, and challenges in simulating impacts and informing adaptation. *J. Exp. Botany 60*, 2775–2789. https://doi.org/10.1093/jxb/erp062

Dibari, C., Argenti, G., Catolfi, F., Moriondo, M., Stagliano, N., and *Bindi. M., 2015:* Pastoral suitability driven by future climate change along the Apennines. *Italian J. Agronomy 10 (676)*, 109–116. https://doi.org/10.4081/ija.2015.659

Dittus, A., Karoly, J., Donat, G., Lewis, C., and *Alexander, L., 2018:* Understanding the role of sea surface temperature-forcing for variability in global temperature and precipitation extremes. *Weather Climate Extr. 21*, 1–9. https://doi.org/10.1016/j.wace.2018.06.002

Food and Agricultural Organization at the United Nations, 2016:[retrieved at 12.11.2018] http://faostat.fao.org/. Index Mundi [retrieved at 04.04.2019], http://www.indexmundi.com/

Fraga, H., García de Cortázar Atauri, I.. and *Santos, J.,* 2018: Viticultural irrigation demands under climate change scenarios in Portugal. *Water Agric. Manage. 196*, 66–74. https://doi.org/10.1016/j.agwat.2017.10.023

Gouda, C., Sahoo, K., Samantray, P., and *Himesh, S.,* 2017: Simulation of extreme temperature over Odisha during May 2015. *Weather Climate Ext. 17*, 17–28. https://doi.org/10.1016/j.wace.2017.07.001

Hatfield, L. and *Prueger, H.,* 2015: Temperature extremes: Effect on plant growth and development. *Weather Climate Ext. 10*, 4–10. https://doi.org/10.1016/j.wace.2015.08.001

Huang, S., Wortmann, M., Deuthmann, D., Menz, C., Shi, F., Zhao, C., Su, B., and Krysanova, V., 2018: Adaptation strategies of agriculture and water management to climate change in the Upper Tarim River basin, NW China. *Agric. Water Manage. 203*, 207–224. https://doi.org/10.1016/j.agwat.2018.03.004

He, Y., Liang, H., Wang, H., and *Hou, L., 2018:* Modeling nitrogen leaching in a spring maize system under changing climate and genotype scenarios in arid Inner Mongolia, China. *Agric. Water Manage. 210*, 316–323. https://doi.org/10.1016/j.agwat.2018.08.017

Kottek, M., Grieser, C., Beck, B., Rudolf, F., and *Rubel, F., 2006:* World Map of the Köppen-Geiger climate classification updated. *Met. Zeitsch. 15*, 259–263. https://doi.org/10.1127/0941-2948/2006/0130

Kovacs, A., Nemeth, A., Unger J., and *Kantor, N.,* 2017: Tourism climatic conditions of Hungary – present situation and assessment of future changes. *Időjárás 121*, 79–99.

Köppen, W., 1900: Versuch einer Klassifikation der Klimate, vorzugsweise nach ihren Beziehungen zur Pflanzenwelt. *Geogr. Zeitsc. 6*, 593–611. (In German)

Lazzerini, G., Dibari, C., Merante, M., Pacini, G., Moschini, V., Migliorin, P., and *Vazzana, C.,* 2015: Identification and mapping the high nature value farmland by the comparison of a combined and species approaches in Tuscany, Italy. *Italian J. Agronomy 10 (676)*, 132–143. https://doi.org/10.4081/ija.2015.676

Li, S., An, P., Pan, Z., Wang, F., Li, X., and *Liy, Y., 2015:* Farmers' initiative on adaptation to climate change in the Northern Agro-pastoral Ecotone. *Int. J. Disaster Risk Reduc. 12*, 278–284. https://doi.org/10.1016/j.ijdrr.2015.02.002

Liheng, Z., Le, Yu., Xuecao, Li., Lina, Hu., and *Peng, G., 2016:* Rapid corn and soybean mapping in US Corn Belt and neighboring areas. *Sci. Reports 6, 36240*. https://doi.org/10.1038/srep36240

Lenihan, M.J., Drapek, R., Bachelet, D., and Neilson, R., 2003. Climate Change Effects on Vegetation Distribution, Carbon, and Fire in California. *Ecol. Appl. 13, 1667–1681.* https://doi.org/10.1890/025295

Lobell, D. and *Field, C., 2007:* Global scale climate–crop yield relationships and the impacts of recent warming. Environ. *Res. Letter 2*, 014002. https://doi.org/10.1088/1748-9326/2/1/014002

Lorite, I., Gabaldón-Leal, C., Ruiz-Ramos, M., Belaj, A., De la Rosa, R., León, L., and *Santos, C., 2018:* Evaluation of olive response and adaptation strategies to climate change under semi-arid conditions. *Agric. Water Manage. 204*, 247–261. https://doi.org/10.1016/j.agwat.2018.04.008

Mitchell, D. and *Jones, D.*, 2005: An improved method of constructing a database of monthly climate observations and associated high-resolution grids. *Int. J. Climatol. 25*, 693–712. https://doi.org/10.1002/joc.1181

Mohareb, E., Heller, M., Novak, P., Goldstein, B., Fonoll, X., and *Raskin, L.*, 2017: Considerations for reducing food system energy demand while scaling up urban agriculture. *Environ. Res. Lett. 12, 125004.*

Moss, R., Babiker, M., Brinkman, S., Calvo, E., Carter, T., Edmonds, E., Elgizouli, I., Emori, *S., Erda, L., Hibbard, K., Jones, R., Kainuma, M., Kelleher, J., Francois-Lamarque, J., Manning, M., Matthews, B., Meehl, J., Meyer, L., Mitchell, J., Nakicenovic, N., O'Neill, B., Pichs, R., Riahi, K., Rose, S., Runci, P., Stouffer, R., Van Vuuren, D., Weyant, J., Wilbanks, T., Van Ypersele, J.,* and *Zurek, M., 2008.* Towards New Scenarious for Analysis of Emissions, Climate Change, Impacts and Response Strategies Geneva. *Intergov. Panel Climate Change 132.*

New, M., Hulme, M., and *Jones, P.*, 2000: Representing Twentieth-Century Space–Time Climate Variability. Part II: Development of 1901–96 Monthly Grids of Terrestrial Surface Climate. *J. Climate 13*, 2217–2238. https://doi.org/10.1175/1520-0442(2000)013<2217:RTCSTC>2.0.CO;2

Newman, D., 2006: The lines that continue to separate us: borders in our 'borderless' world. *Prog. Human Geogr. 30*, 143–161. https://doi.org/10.1191/0309132506ph599xx

Paterson, R., Kumar, L., Taylor, S., and *Lima, N., 2015:* Future climate effects on suitability for growth of oil palms in Malaysia and Indonesia. *Sci. Reports 5*, 14457. https://doi.org/10.1038/srep14457

Perry, L., Rosenzweig, C., Iglesias, A., Livermore, M., and *Fischer, G.*, 2004: Effects of climate change on global food production under SRES emissions and socio-economic scenarios. *Glob. Environ. Change 14*, 53–67. https://doi.org/10.1016/j.gloenvcha.2003.10.008

Pramanik, M., Paudel, U., Mondal, B., Chakraborti, S., and *Deb, P.*, 2018: Predicting climate change impacts on the distribution of the threatened Garcinia indica in the Western Ghats, India. *Climate Risk Manage. 19*, 94–105. https://doi.org/10.1016/j.crm.2017.11.002

Qian, B., De Jong, R., and *Gameda, S., 2009.* Multivariate analysis of water-related agroclimatic factors limiting spring wheat yields on the Canadian prairies. *Eur. J. Agronomy 30*, 140–150. https://doi.org/10.1016/j.eja.2008.09.003

Rosenzweig, C. and *Parry, M., 1994:* Potential impact of climate change on world food supply. *Nature 360*, 133–138. https://doi.org/10.1038/367133a0

Rumford, C., 2007: Does Europe Have Cosmopolitan Borders. *Globalizations 4*, 327–339. https://doi.org/10.1080/14747730701532419

Saha, A. and *Khan, S.*, 2000: Use long-term meteorological data for estimation of irrigation requirement of wheat (Triticum aestivum) at different risk level. *Indian J. Agric. Sci. 70*, 177–180.

Sanderson, M., 1999. The classification of climates from Pythagoras to Koppen. *Bull. Amer. Meteorol. Soc. 80*, 669–673. https://doi.org/10.1175/1520-0477(1999)080<0669:TCOCFP>2.0.CO;2

Seidler, R., Dietrich, K., Schweizer, S., Bawa, K.S., Chopde, S., Zaman, F., Sharma, A., Bhattacharya, S., Devkota, P., and *Khaling, S., 2018.* Progress on integrating climate change adaptation and disaster risk reduction for sustainable development pathways in South Asia: Evidence from six research projects. *Int. J. Disaster Risk Reduc. 31*, 92–101. https://doi.org/10.1016/j.ijdrr.2018.04.023

Semenov, M.A., and *Shewry, P.R.*, 2011: Modelling predicts that heat stress, not drought, will increase vulnerability of wheat in Europe. *Sci. Reports 1*, 66–71. https://doi.org/10.1038/srep00066

Suleiman, M. and *Elaqib, A.*, 2012*:* Implications of climate, land-use and land-cover changes for pastoralism in eastern Sudan. *J. Arid Environment 85*, 132–141. https://doi.org/10.1016/j.jaridenv.2012.05.001

Thuiller, W., Lavorel, S., Araújo, B., Sykes, T., and *Prentice, C., 2004:* Climate change threats to plant diversity in Europe. *Proc. of the Nat. Academy of Science of the U.S.A. 102*, 8245–8250. https://doi.org/10.1073/pnas.0409902102

Vacca, A., Loddo, S, Melis, T., Funedda, A., Puddu, R., Verona, M., Fanni, S., Fantola, F., Madrau, S., Marrone, A., Serra, G., Tore, G., Manca, C., Pasci, S., Puddu, M.R., and *Schirru, P.*, 2013: A GIS based method for soil mapping in Sardinia, Italy: A geomatic approach. *J. Environ. Manage. 138*, 87–96. https://doi.org/10.1016/j.jenvman.2013.11.018

Valjarević, A., Djekić, T., Stevanović, V., Ivanović, R., and *Jandziković, B., 2018a:* GIS Numerical and remote sensing analyses of forest changes in the Toplica region for the period of 1953–2013. *Appl. Geogr. 92*, 131–139. https://doi.org/10.1016/j.apgeog.2018.01.016

Valjarević, A., Srećković-Batoćanin, D., Valjarević, D, and *Matović, V., 2018b.* A GIS- based method for analysis of a better utilization of thermal-mineral springs in the municipality of Kursumlija (Serbia). *Renew. Sust. Energy Rev. 92*, 948–957. https://doi.org/10.1016/j.rser.2018.05.005

Vicuna, S., Maurer, E, Joyce, B., Dracup, A., and *Purkey, D., 2007:* The Sensitivity of California Water Resources to Climate Change Scenarios. *J. Amer. Water Res. Assoc. 43*, 482–492. https://doi.org/10.1111/j.1752-1688.2007.00038.x

Vukoičić, D., Milosavljević, S., Penjišević, I., Bačević, N., Nikolić, M., Ivković, R., and *Jandžiković B.*, 2018: Spatial analysis of air temperature and its impact on the sustainable development of mountain tourism in Central and Western Serbia. *Időjárás 122*, 259–283. https://doi.org/10.28974/idojaras.2018.3.3

Ward, D., 2007: Modelling the potential geographic distribution of invasive and species in New Zealand. *Biol. Invasions 9*, 723–735. https://doi.org/10.1007/s10530-006-9072-y

Weyant, J., Azar, C., Kainuma, M., Kejun, J., Nakicenovic, N., Shukla, R, La Rovere, R., and *Yohe, G.*, 2009*:* Report of 2.6 Versus 2.9 Watts/m^2 RCPP Evaluation Panel Geneva, Switzerland: IPCC Secretariat.

Zabel, F., Putzenlechner, B., and *Mauser, W., 2014:* Global Agricultural Land Resources – A High Resolution Suitability Evaluation and Its Perspectives until 2100 under Climate Change Conditions. PLOS ONE 9. e114980. https://doi.org/10.1371/journal.pone.0114980

Zhang, W., Jiang, Y., Dong, M., and *Yang, H., 2012:* Relationship between the radial growth of Picea meyeri and climate along elevations of the Luyashan Mountain in North-Central China. *For. Ecol. Manag. 265*, 142-149. https://doi.org/10.1016/j.foreco.2011.10.017.

Zhang, S. and *Fulu, T.*, 2013: Modeling the response of rice phenology to climate change and variability in different climatic zones: Comparisons of five models. *Eur. J. Agronomy 45*, 165–176. https://doi.org/10.1016/j.eja.2012.10.005

IDŐJÁRÁS

VOLUME 124 * 2020

BUDAPEST, HUNGARY

AUTHOR INDEX

TABLE OF CONTENTS

I. Papers

SUBJECT INDEX

D

E

F

G

H

Q

R

S

T

U

V

W

X

Y

Z

INSTRUCTIONS TO AUTHORS OF *IDŐJÁRÁS*

The purpose of the journal is to publish papers in any field of meteorology and atmosphere related scientific areas. These may be

- research papers on new results of scientific investigations,
- critical review articles summarizing the current state of art of a certain topic,
- short contributions dealing with a particular question.

Some issues contain "News" and "Book review", therefore, such contributions are also welcome. The papers must be in American English and should be checked by a native speaker if necessary.

Authors are requested to send their manuscripts to

Editor-in Chief of IDŐJÁRÁS
P.O. Box 38, H-1525 Budapest, Hungary
E-mail: journal.idojaras@met.hu

including all illustrations. MS Word format is preferred in electronic submission. Papers will then be reviewed normally by two independent referees, who remain unidentified for the author(s). The Editor-in-Chief will inform the author(s) whether or not the paper is acceptable for publication, and what modifications, if any, are necessary.

Please, follow the order given below when typing manuscripts.

Title page should consist of the title, the name(s) of the author(s), their affiliation(s) including full postal and e-mail address(es). In case of more than one author, the corresponding author must be identified.

Abstract: should contain the purpose, the applied data and methods as well as the basic conclusion(s) of the paper.

Key-words: must be included (from 5 to 10) to help to classify the topic.

Text: has to be typed in single spacing on an A4 size paper using 14 pt Times New Roman font if possible. Use of S.I. units are expected, and the use of negative exponent is preferred to fractional sign. Mathematical formulae are expected to be as simple as possible and numbered in parentheses at the right margin.

All publications cited in the text should be presented in the *list of references*, arranged in alphabetical order. For an article: name(s) of author(s) in Italics, year, title of article, name of journal, volume, number (the latter two in Italics) and pages. E.g., *Nathan, K.K.,* 1986: A note on the relationship between photosynthetically active radiation and cloud amount. *Időjárás 90,* 10–13. For a book: name(s) of author(s), year, title of the book (all in Italics except the year), publisher and place of publication. E.g., *Junge, C.E.,* 1963: *Air Chemistry and Radioactivity*. Academic Press, New York and London. Reference in the text should contain the name(s) of the author(s) in Italics and year of publication. E.g., in the case of one author: *Miller* (1989); in the case of two authors: *Gamov* and *Cleveland* (1973); and if there are more than two authors: *Smith et al.* (1990). If the name of the author cannot be fitted into the text: *(Miller,* 1989); etc. When referring papers published in the same year by the same author, letters a, b, c, etc. should follow the year of publication. DOI numbers of references should be provided if applicable.

Tables should be marked by Arabic numbers and printed in separate sheets with their numbers and legends given below them. Avoid too lengthy or complicated tables, or tables duplicating results given in other form in the manuscript (e.g., graphs). *Figures* should also be marked with Arabic numbers and printed in black and white or color (under special arrangement) in separate sheets with their numbers and captions given below them. JPG, TIF, GIF, BMP or PNG formats should be used for electronic artwork submission.

More information for authors is available: journal.idojaras@met.hu

Published by the Hungarian Meteorological Service

Budapest, Hungary

ISSN 0324-6329 (Print)

ISSN 2677-187X (Online)